VOL.107 NO.EM2. APRIL 1981

JOURNAL OF THE ENGINEERING MECHANICS DIVISION

PROCEEDINGS OF
THE AMERICAN SOCIETY
OF CIVIL ENGINEERS

VOL.107 NO.EM2. APRIL 1981

JOURNAL OF THE ENGINEERING MECHANICS DIVISION

PROCEEDINGS OF
THE AMERICAN SOCIETY
OF CIVIL ENGINEERS

ISSN 0044-7951

AMERICAN SOCIETY OF CIVIL ENGINEERS

CONTENTS

This Journal is published bimonthly by the American Society of Civil Engineers. Publications office is at 345 East 47th Street, New York, N.Y. 10017. Address all ASCE correspondence to the Editorial and General Offices at 345 East 47th Street, New York, N.Y. 10017. Allow six weeks for change of address to become effective. Subscription price to members is $14.00. Nonmember subscriptions available; prices obtainable on request. Second-class postage paid at New York, N.Y. and at additional mailing offices. EE, EM.

TECHNICAL NOTES

Proc. Paper 16157

DISCUSSION

Proc. Paper 16149

[a]Discussion period closed for this paper. Any other discussion received during this discussion period will be published in subsequent Journals.

16170 ALONG-WIND MOTION OF MULTISTORY BUILDING

KEY WORDS: Frequency analysis; **Random vibration; Structural analysis; Tall buildings;** Wind direction; **Wind forces; Wind loads**

ABSTRACT: Treating the wind-excited motion of a multistory building as a random vibration problem, the input-output spectral density relationships are derived using a transfer matrix formulation. In this analysis the motion of the building is restricted to the direction parallel to the average wind flow, the along-wind direction; and the structural response is represented by a displacement variable and a force variable in each story unit. A 40-story building is used as a numerical example.

REFERENCE: Yang, J. N., and Lin, Y. K., "Along-Wind Motion of Multistory Building," *Journal of the Engineering Mechanics Division,* ASCE, Vol. 107, No. EM2, **Proc. Paper 16170**, April, 1981, pp. 295-307

16172 BUILDING INTERNAL PRESSURE: SUDDEN CHANGE

KEY WORDS: Acoustics; Aerodynamic forces; Aerodynamic loads; **Aerodynamics; Buildings; Internal pressure;** Pressure measurement; Transient response; Unsteady state; **Wind forces;** Wind loads; **Wind pressure**

ABSTRACT: The change of the internal pressure of a building caused by the sudden opening of a window or door under the action of wind is analyzed using the Bernoulli equation of fluid mechanics. The problem is treated at several levels of sophistication, from the simplest quasi-steady isothermal incompressible solution to the most complex solution assuming unsteady isentropic compressible flow with due regards to the inertia effect. Following the break of a window or door by wind, the internal pressure reaches the external pressure at the opening rather rapidly. After the internal pressure has reached the external pressure, there is an overshoot and subsequent oscillation of the internal pressure, in spite of the constancy of the external pressure under a steady wind. The results are compared to solutions obtained from the Helmholtz resonator model of acoustics.

REFERENCE: Liu, Henry, and Saathoff, Patrick J., "Building Internal Pressure: Sudden Change," *Journal of the Engineering Mechanics Division,* ASCE, Vol. 107, No. EM2, **Proc. Paper 16172**, April, 1981, pp. 309-321

16192 TORTIONAL VIBRATION OF EXCITED STRUCTURES

KEY WORDS: Aerodynamic forces; **Aeroelasticity;** Dynamic response; Random vibration; Random vibration analysis; **Structural dynamics; Torsion; Torsional vibration;** Wind direction; **Wind forces**

ABSTRACT: A method for analyzing the torsional vibration of along-wind excited structures is presented. The method is based on random vibration concepts and yields the expected maximum translational and torsional responses of a single-mass structure. The approach is similar to the gust factor method. Aerodynamic admittance functions are derived which are used to estimate the spectral density function of the random torque and the cross-spectral density function of the force and torque acting on the structure. These are required for estimating the structure's translational and torsional mean square responses. Results for several examples indicate that the dynamic torsional response increases as follows: as the width of the structure's exposed face increases, as the structural or geometric eccentricity increases, and as torsional natural frequency decreases.

REFERENCE: Foutch, D. A., and Safak, E., "Tortional Vibration of Along-Wind Excited Structures," *Journal of the Engineering Mechanics Division,* ASCE, Vol. 107, No. EM2, **Proc. Paper 16192**, April, 1981, pp. 323-337

16177 NATURAL FREQUENCIES OF CURVED GIRDERS

KEY WORDS: **Bridges (girder); Curved beams; Finite element method;** Flexural strength; Inertia; **Natural frequency;** Stiffness; Structural engineering; Torsion; **Vibration**

ABSTRACT: A general finite element displacement formulation is presented to determine the natural frequencies of spatial thin-walled curved girders including the warping contribution. Also included are the rotatory inertia effects with respect to flexure and torsion, and the effects of antisymmetry of cross section (found to be significant). The stiffness and inertia properties of the finite element are obtained using the solutions of homogeneous differential equations governing the static problem as deformation modes. The obtained element relationships were programmed for use in digital computers, and a few example problems were analyzed. Some charts are given to expedite the determination of natural frequencies of horizontally curved girders.

REFERENCE: Yoo, Chai Hong, and Fehrenbach, Jon P., "Natural Frequencies of Curved Girders," *Journal of the Engineering Mechanics Division,* ASCE, Vol. 107, No. EM2, **Proc. Paper 16177**, April, 1981, pp. 339-354

16193 LOGICAL ANALYSIS OF STRUCTURAL FAILURE

KEY WORDS: Bridge failures; **Failure (mechanics); Human factors;** Logical elements; **Logic design;** Random error; **Safety; Safety design;** Structural behavior

ABSTRACT: In engineering only the product, the hardware, is a physical system; the system which designs it, produces it and uses it is human and therefore complex and vulnerable. Human error of one form or another is a major cause of failures. One way of attempting to reduce this is to find ways of distilling conclusions from past performance by a logical analysis of available information. This analysis may then be stored as a computer data structure and used as a basis for predictions regarding future projects. The vehicle for this process, the handling of rather imprecise information, is fuzzy logic. A logical hierarchy of simple deductions has been set up to represent the three main influences on structural safety—human error, random hazards as well as the system uncertainty of reliability theory. The hierarchy is used to obtain measures of safety for two famous bridge failures.

REFERENCE: Blockley, David I., "Logical Analysis of Structural Failure," *Journal of the Engineering Mechanics Division,* ASCE, Vol. 107, No. EM2, **Proc. Paper 16193**, April, 1981, pp. 355-365

16200 ULTIMATE LOAD BEHAVIOR OF CURVED I-BEAMS

KEY WORDS: **Curved beams; Deflection; I beams;** Load bearing capacity; **Loading tests;** Load limits; Mathematical models; Matrices (mathematics); **Plastics; Stability;** Tests

ABSTRACT: A method of analyzing the large-deflection behavior of the horizontally curved I-beam, in both elastic and inelastic regions, by using the transfer matrix method is presented. Three kinds of separate loading (e.g., equal end moments, a concentrated load at the midspan, and uniformly distributed load) are considered for this analysis. The ultimate strength is determined for several given curvatures. Experimental studies are also made for six supported I-beams to determine the effect of curvature on the behavior of ultimate load-deformation. Finally, a formula is also deduced to predict the approximate ultimate strength of the curved I-beams.

REFERENCE: Fukumoto, Yuhshi, and Nishida, Susumu, "Ultimate Load Behavior of Curved I-Beams," *Journal of the Engineering Mechanics Division,* ASCE, Vol. 107, No. EM2, **Proc. Paper 16200**, April, 1981, pp. 367-385

16208 ELASTIC STRESSES IN FRETTING FATIGUE

KEY WORDS: **Elasticity (mechanical); Fatigue (materials); Fracture mechanics; Fractures (materials);** Fracture strength; **Fretting;** Mathematical models; **Stress (mechanics)**

ABSTRACT: The distribution of stresses in a typical two-dimensional fretting-fatigue problem has been analyzed by assuming homogeneous, isotropic and linearly elastic material. "Closed type" solutions have been obtained that are "exact" within the assumptions used. According to the numerical results presented, a small region of the plate immediately outside the contact area would appear to be most critical from the viewpoint of crack initiation. However, under certain conditions (e.g., in the presence of micropores or other types of discontinuities) cracks could also initiate at some subsurface sites.

REFERENCE: Chung, Jung S., Oran, Cenap, and Hoeppner, David W., "Elastic Stresses in Fretting Fatigue," *Journal of the Engineering Mechanics Division,* ASCE, Vol. 107, No. EM2, **Proc. Paper 16208**, April, 1981, pp. 387-403

16183 UNBALANCED ANISOTROPIC SANDWICH PLATES

KEY WORDS: Anisotropy; **Composite structures; Dynamic structural analysis;** Fourier series; **Laminates;** Orthotropism; **Plates (structural members); Sandwich laminates;** Stiffness; **Vibration**

ABSTRACT: The modified stiffness method of unbalanced anisotropic sandwich plates is extended and applied to the dynamic analysis of sandwich plates consisting of an orthotropic core and two equal thickness anisotropic face plates. The formulation allows for the dynamic analysis of certain types of sandwich plates that were not amenable to rigorous solutions due to the existence of anisotropic coupling stiffnesses, such as those with inbalanced angle-ply faces. The method is independent of the boundary conditions and can be combined with a variety of analysis techniques. Using a series solution, results are generated for simply-supported sandwich plates with unbalanced cross-ply and angle-ply face plates. In addition, the effect of coupling in the static and dynamic responses is presented. Coupling can influence the structural response significantly.

REFERENCE: Ibrahim, Ibrahim M., Farah, Anis, and Rizk, M. Nabil F., "Dynamic Analysis of Unbalanced Anisotropic Sandwich Plates," *Journal of the Engineering Mechanics Division,* ASCE, Vol. 107, No. EM2, **Proc. Paper 16183**, April, 1981, pp. 405-418

U.S. Customary-SI Conversion Factors

In accordance with the October, 1970 action of the ASCE Board of Direction, which stated that all publications of the Society should list all measurements in both U.S. Customary and SI (International System) units, the following list contains conversion factors to enable readers to compute the SI unit values of measurements. A complete guide to the SI system and its use has been published by the American Society for Testing and Materials. Copies of this publication (ASTM E-380) can be purchased from ASCE at a price of $3.00 each; orders must be prepaid.

All authors of *Journal* papers are being asked to prepare their papers in this dual-unit format. To provide preliminary assistance to authors, the following list of conversion factors and guides are recommended by the ASCE Committee on Metrication.

To convert	To	Multiply by
inches (in.)	millimeters (mm)	25.4
feet (ft)	meters (m)	0.305
yards (yd)	meters (m)	0.914
miles (miles)	kilometers (km)	1.61
square inches (sq in.)	square millimeters (mm^2)	645
square feet (sq ft)	square meters (m^2)	0.093
square yards (sq yd)	square meters (m^2)	0.836
square miles (sq miles)	square kilometers (km^2)	2.59
acres (acre)	hectares (ha)	0.405
cubic inches (cu in.)	cubic millimeters (mm^3)	16,400
cubic feet (cu ft)	cubic meters (m^3)	0.028
cubic yards (cu yd)	cubic meters (m^3)	0.765
pounds (lb) mass	kilograms (kg)	0.453
tons (ton) mass	kilograms (kg)	907
pound force (lbf)	newtons (N)	4.45
kilogram force (kgf)	newtons (N)	9.81
pounds per square foot (psf)	pascals (Pa)	47.9
pounds per square inch (psi)	kilopascals (kPa)	6.89
U.S. gallons (gal)	liters (L)	3.79
acre-feet (acre-ft)	cubic meters (m^3)	1,233

JOURNAL OF
THE ENGINEERING
MECHANICS DIVISION

ALONG-WIND MOTION OF MULTISTORY BUILDING

By J. N. Yang[1] and Y. K. Lin,[2] M. ASCE

INTRODUCTION

Wind excited vibrations of a building can cause failures of structural members, discomfort of its occupants, unsightly cracks on the interior claddings, etc.; therefore, it is important to provide adequate design to minimize the chance of excessive stresses and excessive displacements. Since all natural strong winds are turbulent with randomly fluctuating wind velocities, a probabilistic approach is most suitable for the analysis of such problems. The pioneer work of Davenport (4) made use of the general methodology of random vibration which was becoming increasingly more popular during the 1950s and 1960s primarily in aeronautical engineering applications. Since then, numerous papers have been published on the subject (e.g., Refs. 7, 9–12). Typically in these previous works, the motion of a building is expressed in terms of normal modes, the obvious advantage being that the solution to a complicated multi-mode system is an immediate extension of that of a single-degree-of-freedom system. However, several practical shortcomings remain, including the following.

For a complicated structure, the determination of normal modes can be difficult or extremely time consuming; therefore, the true advantage of a normal mode formulation depends on whether or not it is adequate to represent the structural response by only the first very few modes. This implies that the normal mode approach may be suitable for the analysis of wind-induced displacements, but it may not be so for wind-induced internal forces. The forces are obtained from differentiation (or its equivalent) of the displacements, thus a higher accuracy is required for their computation. Secondly, the normal modes are, by definition, associated with an undamped system. The magnitude of damping in each mode must be assumed rather arbitrarily by lumping together various contributions

[1]Prof., Dept. of Civ., Mech. and Environmental Engrg., George Washington Univ., Washington, D.C. 20052.

[2]Prof., Dept. of Aeronautical and Astronautical Engrg., Univ. of Illinois, Urbana, Ill.

Note.—Discussion open until September 1, 1981. To extend the closing date one month, a written request must be filed with the Manager of Technical and Professional Publications, ASCE. Manuscript was submitted for review for possible publication on March 11, 1980. This paper is part of the Journal of the Engineering Mechanics Division, Proceedings of the American Society of Civil Engineers, ©ASCE, Vol. 107, No. EM2, April, 1981. ISSN 0044-7951/81/0002-0295/$01.00.

which occur at different parts of the building based largely on the experience of the analyst. This may lead to errors, since damping has an over-riding effect on the structural response.

In the present paper, an alternate formulation is used which dispenses of the intermediate step of computing the normal modes and deals directly with both displacement and force types of structural response. Making use of the concept of transfer matrix (8), the approach allows a realistic representation of the interaction between various parts within the system. In particular, it is possible to assign appropriate damping coefficients associated with various structural members or joints between members, or both. The approach is especially suitable for tall buildings having many stories in the construction. Additional simplification is achieved under an assumption that every story in the building is identically constructed, although this assumption is not required for the validity of a transfer matrix approach. The application of the methodology is illustrated by an example of a 40-story building under the excitation of a wind turbulence field which is statistically stationary in time but nonhomogeneous in space.

Formulation

The structural model chosen for the present study is an N-story building shown in Fig. 1(a). The following assumptions are made to simplify the analysis:

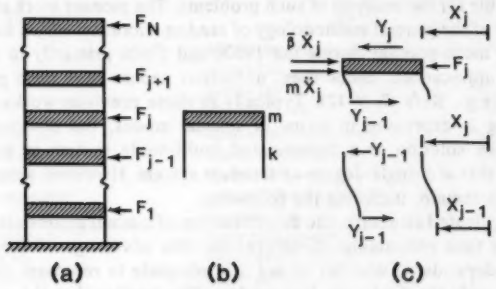

FIG. 1.—Structural Model: (*a*) N-Story Building under Wind Loads; (*b*) Construction Unit; (*c*) External and Internal Forces on jth Unit

(1) The Building structure is composed of N identical construction units typified by the one shown in Fig. 1(b); (2) the mass of each unit is concentrated at the floor level; (3) linear elasticity is provided by massless columns or shear walls between neighboring floors; (4) wind excitations are applied at discrete floor levels; and (5) the response of the structure to external excitations can be described by a displacement variable and a force variable in each construction unit.

Referring to Fig. 1(c), let X_j and Y_{j-1} be, respectively, the displacement at the floor and the shear force in the column or shear wall of the jth unit. It is seen that

$$Y_j = Y_{j-1} + m\ddot{X}_j + \bar{\beta}\dot{X}_j - F_j \quad \ldots \quad (1)$$

$$Y_{j-1} = K(X_j - X_{j-1}) \quad \ldots \quad (2)$$

in which m = the mass of the jth floor; $\bar{\beta}$ = damping coefficient; and K = the stiffness.

Taking the Fourier transform and rearranging terms, these two equations may be cast in a matrix form as follows:

$$\begin{Bmatrix} \bar{X}_j \\ \bar{Y}_j \end{Bmatrix} = \begin{bmatrix} 1 & K^{-1} \\ (-m\omega^2 + i\bar{\beta}\omega) & K^{-1}(-m\omega^2 + i\bar{\beta}\omega) + 1 \end{bmatrix} \begin{Bmatrix} \bar{X}_{j-1} \\ \bar{Y}_{j-1} \end{Bmatrix} - \begin{Bmatrix} 0 \\ \bar{F}_j \end{Bmatrix} \quad (3)$$

or, more simply:

$$\{Z\}_j = [T]\{Z\}_{j-1} - \begin{Bmatrix} 0 \\ \bar{F}_j \end{Bmatrix} \quad \ldots\ldots\ldots\ldots\ldots\ldots\ldots\ldots\ldots\ldots\ldots\ldots (4)$$

in which $\{Z\}_j = \{\bar{X}_j, \bar{Y}_j\}'$ = a state vector; an over bar denotes the Fourier transform; $i = (-1)^{1/2}$; and $[T]$ is known as a transfer matrix. In Eq. 3 the stiffness K is complex-valued if the structural damping or viscous damping between floors are taken into consideration. The physical meaning of matrix $[T]$ is clear; it represents the transfer mechanism of a construction unit. If the excitation F_j is absent, state vector $\{Z\}_{j-1}$ is transfered to state vector $\{Z\}_j$ through $[T]$.

Eq. 4 can be applied repeatedly to obtain a relation between $\{Z\}_0$ and $\{Z\}_N$; namely:

$$\{Z\}_N = [T]^N\{Z\}_0 - \sum_{j=1}^{N} [T]^{N-j} \begin{Bmatrix} 0 \\ \bar{F}_j \end{Bmatrix} \quad \ldots\ldots\ldots\ldots\ldots\ldots\ldots\ldots\ldots\ldots (5)$$

The boundary conditions at the base and at the top floor of the building dictate that

$$\{Z\}_N = \begin{Bmatrix} \bar{X}_N \\ 0 \end{Bmatrix}, \quad \{Z\}_0 = \begin{Bmatrix} 0 \\ \bar{Y}_0 \end{Bmatrix} \quad \ldots\ldots\ldots\ldots\ldots\ldots\ldots\ldots\ldots\ldots (6)$$

Substituting Eq. 6 into Eq. 5, we obtain from the second row

$$0 = \tau_{22}(N)\bar{Y}_0 - \sum_{j=1}^{N} \tau_{22}(N-j)\bar{F}_j \quad \ldots\ldots\ldots\ldots\ldots\ldots\ldots\ldots\ldots\ldots (7)$$

in which $\tau_{22}(N)$ = the (2,2) element of $[T]^N$; and $\tau_{22}(N-j)$ = the (2,2) element of $[T]^{N-j}$. It follows from Eq. 7 that

$$\bar{Y}_0 = \sum_{j=1}^{N} \frac{\tau_{22}(N-j)\bar{F}_j}{\tau_{22}(N)} \quad \ldots\ldots\ldots\ldots\ldots\ldots\ldots\ldots\ldots\ldots\ldots\ldots (8)$$

Thus the vector $\{Z\}_0$ (Eq. 6) is expressible in terms of the random excitations $\bar{F}_j$ and the elements of transfer matrix $[T]$.

The Fourier transforms of the displacement at the mth floor and the shear force immediately above the mth floor, $\bar{X}_m$ and $\bar{Y}_m$, which constitute the response vector $\{Z\}_m$, can be calculated in the same manner as in Eq. 5. With N being replaced by m, Eq. 5 becomes

$$\{Z\}_m = [T]^m\{Z\}_0 - \sum_{j=1}^{m} [T]^{m-j} \begin{Bmatrix} 0 \\ \bar{F}_j \end{Bmatrix} \quad \ldots\ldots\ldots\ldots\ldots\ldots\ldots\ldots\ldots\ldots (9)$$

Substituting $\{Z\}_0 = \{0, \bar{Y}_0\}'$ and using Eq. 8, we obtain

$$\{Z\}_m = \frac{1}{\tau_{22}(N)} \begin{Bmatrix} \tau_{12}(m) \\ \tau_{22}(m) \end{Bmatrix} \sum_{j=1}^{N} \tau_{22}(N-j)\bar{F}_j - \sum_{j=1}^{m} \begin{Bmatrix} \tau_{12}(m-j) \\ \tau_{22}(m-j) \end{Bmatrix} \bar{F}_j \quad \ldots \quad (10)$$

Eq. 10 is an input-output relation in the (transformed) frequency domain in which the $\bar{F}_j (j = 1, 2, \ldots N)$ are the inputs and $\{Z\}_m$ the outputs. The various $\tau_{kl}(n)$ elements characterize the structural model.

Spectral Relationship

When wind loads on a building are modeled as stochastic processes, the inputs $\bar{F}_j (j = 1, 2, \ldots, N)$ in Eq. 10 are Fourier transforms of stochastic processes. If the wind loads are assumed to be statistically stationary in time, then their Fourier transforms do not exist in the sense of mean-square integrals. In this case, the $\bar{F}$s are merely formal representations; however, Eq. 10 can still be used conveniently to construct spectral relationships between inputs and outputs. For example, the spectral density of the random displacement X_m at the mth floor, denoted by $\Phi_{X_m X_m}(\omega)$, can be obtained by multiplying the first row in Eq. 10 by its complex conjugate, and replacing each product $\bar{F}_i \bar{F}_j^*$ by the cross-spectral density $\Phi_{F_i F_j}(\omega)$, namely:

$$\Phi_{X_m X_m}(\omega) = |\tau_{12}(m)|^2 |\tau_{22}(N)|^{-2} \sum_{i=1}^{N} \sum_{j=1}^{N} \tau_{22}(N-i)\tau_{22}^*(N-j)\Phi_{F_i F_j}(\omega)$$

$$+ \sum_{k=1}^{m} \sum_{l=1}^{m} \tau_{12}(m-k)\tau_{12}^*(m-l)\Phi_{F_k F_l}(\omega)$$

$$- 2\,\mathrm{Re}\left[\tau_{12}(m)\tau_{22}^{-1}(N) \sum_{i=1}^{N} \sum_{k=1}^{m} \tau_{22}(N-i)\tau_{12}^*(m-k)\Phi_{F_i F_k}(\omega) \right] \quad \ldots \ldots \quad (11)$$

in which Re{ } signifies the real part of a complex expression. Similarly, the spectral density of the shear force Y_n can be obtained from the second row of Eq. 10:

$$\Phi_{Y_m Y_m}(\omega) = |\tau_{22}(m)|^2 |\tau_{22}(N)|^{-2} \sum_{i=1}^{N} \sum_{j=1}^{N} \tau_{22}(N-i)\tau_{22}^*(N-j)\Phi_{F_i F_j}(\omega)$$

$$+ \sum_{k=1}^{m} \sum_{l=1}^{m} \tau_{22}(m-k)\tau_{22}^*(m-l)\Phi_{F_k F_l}(\omega)$$

$$- 2\,\mathrm{Re}\left[\tau_{22}(m)\tau_{22}^{-1}(N) \sum_{i=1}^{N} \sum_{k=1}^{m} \tau_{22}(N-i)\tau_{22}^*(m-k)\Phi_{F_i F_k}(\omega) \right] \quad \ldots \ldots \quad (12)$$

Cross-spectral densities of the outputs such as $\Phi_{X_m Y_m}(\omega)$ can also be obtained if desired.

As seen from the preceding equations the computation of output spectral and cross-spectral densities requires the knowledge of $\Phi_{F_i F_j}(\omega)$ and $\tau_{kl}(n)$. The former are the cross-spectral densities of the wind loads, and the latter are the elements of $[T]^n$. These will be considered in the subsequent sections.

Wind Load Model

Analogous to the case of an airfoil, both drag and lift forces are generated due to relative motion between air particles and a building. The drag forces, however, are responsible for the along wind motion of the building. Since most buildings are not streamlined, the actual force-generation mechanism is complicated and is not fully understood at the present time. For lack of better representations, the common practice has been the use of a rather simple analytical form for the drag forces as follows:

$$F_j(t) = \frac{1}{2} \rho A_j C_D V_j^2 \quad \text{. . . . .} \quad (13)$$

in which ρ = air density; A_j = tributary area of the jth floor; V_j = wind velocity relative to the structure; and C_D = drag coefficient which can be different for different structural forms and should be experimentally determined, at least, for each category of buildings.

The velocity of the building itself is generally low. Thus V_j can be taken to be just the wind velocity, which may be decomposed into a mean velocity and a random fluctuation about the mean. Let

$$V_j = u_j [1 + \xi_j(t)] \quad \text{. . . . .} \quad (14)$$

in which $\xi_j(t)$ is assumed to be a stationary random process with zero mean. Then $E[V_j] = u_j$ where $E[\ ]$ denotes an ensemble average. It is reasonable to assume further than $|\xi_j(t)| << 1$ and to replace V_j^2 by $u_j^2 [1 + 2\xi_j(t)]$ in Eq. 13. Thus

$$F_j(t) = \nu_j [1 + 2\xi_j(t)] \quad \text{. . . . .} \quad (15)$$

$$\text{in which} \quad \nu_j = E[F_j(t)] = \frac{1}{2} \rho A_j C_D u_j^2 \quad \text{. . . . .} \quad (16)$$

It has been found (1) that the mean wind velocity u_j varies with the height from the ground according to a power law

$$u_j = u_g \left(\frac{z_j}{z_g} \right)^{\alpha} \quad \text{. . . . .} \quad (17)$$

in which z_j = the height of the jth floor; z_g = a reference height called the gradient height; u_g = the wind velocity at the gradient height; and α = a constant between 0.15 and 0.5. Roughly speaking, the gradient height is one beyond which the mean wind velocity becomes nearly independent of the distance from the ground. This parameter, as well as the exponent α in Eq. 17, is related to the ground roughness, characterized by the so-called roughness length which is better known to the fluid dynamicists. Davenport (3) has provided a chart where z_g and α can be found from the roughness length.

It should be noted that we have identified the mean wind velocity as being the same as the ensemble average which is a constant for a stationary random process. Several writers have taken, perhaps, a broader point of view by treating the mean wind velocity as a random variable. In particular, Davenport (5) has suggested that the mean wind is nearly Rayleigh distributed, and that the extreme

value of the mean wind at a given location follows the Type 1 extreme value distribution. However, for structural response calculations, the two approaches lead to the same results for structural response statistics.

The autocorrelation function of $F_j(t)$ is given by

$$E[F_j(t)F_j(t+\tau)] = R_{F_jF_j}(\tau) = \nu_j^2[1 + 4R_{\xi_j\xi_j}(\tau)] \quad \ldots\ldots\ldots\ldots\ldots\ldots \quad (18)$$

in which $R_{\xi_j\xi_j}(\tau)$ = the autocorrelation function for $\xi_j(t)$. In terms of spectral densities, Eq. 18 is equivalent to

$$\Phi_{F_jF_j}(\omega) = \nu_j^2[\delta(\omega) + 4\Phi_{\xi_j\xi_j}(\omega)] \quad \ldots\ldots\ldots\ldots\ldots\ldots\ldots\ldots \quad (19)$$

in which $\delta(\ )$ denotes the Dirac delta function. Following Davenport (4), the power spectrum of the fluctuating part of the wind, $y_j\xi_j(t)$ has a nearly universal expression

$$S(n) = \frac{4k_0u_r^2}{n}\frac{x^2}{(1+x^2)^{4/3}} \quad \ldots\ldots\ldots\ldots\ldots\ldots\ldots\ldots\ldots \quad (20)$$

in which n = frequency, in hertz (cycles per second); u_r = reference mean wind velocity, in meters per second at 10 m above the ground; k_0 = a constant; and $x = 1{,}200\,n/u_r$, in cycles.

Equation 20 is a one-sided spectrum in the positive frequency domain. When converted to correspond to the nondimensional $\xi_j(t)$ and to a two-sided spectral density in ω, Eq. 20 becomes

$$\Phi_{\xi_j\xi_j}(\omega) = \frac{2k_0}{|\omega|}\left(\frac{u_r}{y_j}\right)^2\left(\frac{600\,\omega}{\pi u_r}\right)^2\left[1 + \left(\frac{600\,\omega}{\pi u_r}\right)^2\right]^{-4/3} \quad \ldots\ldots\ldots\ldots \quad (21)$$

It is of interest to note that the Davenport spectrum tends to zero as $\omega^{-5/3}$ for large ω similar to the well-known von Karman spectrum, but they differ in the low-frequency region. The von Karman spectrum becomes rather flat (a zero-power law) as ω diminishes, whereas the Davenport spectrum tends linearly to zero with ω. Furthermore, the Davenport spectrum implies that the scale of turbulence is independent of height, as similarly proposed by Berman (2), although intuition would suggest that the turbulence scale should grow with height. The preceding brief description is to bring out subtle implications in Eq. 21 which has been used in our numerical calculations. The methodology presented in this paper is not restricted to any specific input spectra. It is not our intention to make an exhaustive comparison of suggested spectra in the literature, some of which have not been cited herein.

Analogous to Eqs. 18 and 19, the cross-correlation function and the cross-spectral density of $F_i(t)$ and $F_j(t)$ are, respectively:

$$R_{F_iF_j}(\tau) = \nu_i\nu_j[1 + 4R_{\xi_i\xi_j}(\tau)] \quad \ldots\ldots\ldots\ldots\ldots\ldots\ldots\ldots \quad (22)$$

$$\Phi_{F_iF_j}(\omega) = \nu_i\nu_j[\delta(\omega) + 4\Phi_{\xi_i\xi_j}(\omega)] \quad \ldots\ldots\ldots\ldots\ldots\ldots\ldots \quad (23)$$

Following Davenport (4), the one-sided cross-power spectrum for $u_i\xi_i(t)$ and $u_j\xi_j(t)$ defined on the positive domain in n (in cycles per second) may be expressed as

$$S(n)\exp\left(\frac{-c_1n|\Delta z|}{u_r}\right) \quad \ldots\ldots\ldots\ldots\ldots\ldots\ldots\ldots\ldots \quad (24)$$

in which $c_1 = 7.7$ (a constant); Δz = height separation $(i - j)h$; and h = story height. Converting Eq. 24 for the nondimensional $\xi_i(t)$ and $\xi_j(t)$, and for a two-sided cross-spectral density in ω, we obtain

$$\Phi_{\xi_i\xi_j}(\omega) = \frac{2K_0 u_r^2}{u_i u_j |\omega|} \left\{ \frac{\left(\frac{600\,\omega}{\pi\, u_r}\right)^2}{\left[1 + \left(\frac{600\,\omega}{\pi\, u_r}\right)^2\right]^{4/3}} \right\} \exp\left[\left(-\frac{c_1|\omega|}{2\pi}\right)\left(\frac{|i-j|h}{u_r}\right)\right] \quad . \quad . \quad . \quad (25)$$

Equation 25 reduces to Eq. 21 when $i = j$. Equations 16, 17, 19, 21, 23, and 25 provide the required statistical information of the wind loads for computing the first and the second statistical properties of the structural response.

Computation of $[T]^n$ for Large n

Functions $\tau_{kl}(n)$ appearing in Eqs. 11, 12, etc. for the spectral and cross-spectral densities of structural response are the elements of $[T]^n$; $n = 1, 2, \ldots, N$. Their computation by the obvious chain multiplication of the $[T]$ matrix $n - 1$ times can become very tedious when n is large, and the result can be inaccurate due to accumulated roundoff errors. In such a case, it is advantageous to use the following alternate computational scheme which is based on some special properties common to all transfer matrices (6).

Recall that

$$[T] = \begin{bmatrix} 1 & K^{-1} \\ -m\omega^2 + j\bar{\beta}\omega & 1 + K^{-1}(-m\omega^2 + j\bar{\beta}\omega) \end{bmatrix} \quad . \quad . \quad . \quad . \quad . \quad . \quad . \quad . \quad . \quad . \quad . \quad . \quad (26)$$

It can easily be shown that $|T| = 1$, and that the characteristic equation for either the eigenvalues of $[T]$ or the eigenvalues of $[T]^{-1}$ is the same

$$\lambda^2 - [k^{-1}(-m\omega^2 + j\bar{\beta}\omega) + 2]\lambda + 1 = 0 \quad . \quad . \quad . \quad . \quad . \quad . \quad . \quad . \quad . \quad . \quad . \quad . \quad . \quad . \quad . \quad . \quad (27)$$

Therefore, the roots of Eq. 27 are a reciprocal pair which may be expressed conveniently as $\lambda_{1,2} = \exp(\pm j\psi)$ where ψ may be obtained from

$$\cos\psi = 1 + \frac{1}{2}(-m\omega^2 + j\bar{\beta}\omega)K^{-1} \quad . \quad . \quad . \quad . \quad . \quad . \quad . \quad . \quad . \quad . \quad . \quad . \quad . \quad . \quad . \quad . \quad . \quad . \quad (28)$$

or, denoting $\omega_0^2 = K/m$ and $\zeta = \bar{\beta}/(2m\omega_0)$:

$$\cos\psi = 1 - \frac{1}{2}\left(\frac{\omega}{\omega_0}\right)^2 + j\zeta\left(\frac{\omega}{\omega_0}\right) \quad . \quad . \quad . \quad . \quad . \quad . \quad . \quad . \quad . \quad . \quad . \quad . \quad . \quad . \quad . \quad . \quad . \quad . \quad (29)$$

It is known that any analytic function of an $n \times n$ matrix may be expressed as a linear combination of any linearly independent analytic functions of the same matrix. By choosing the form

$$[T]^n = \frac{a_n}{2}([T] + [T]^{-1}) + \frac{b_n}{2}([T] - [T]^{-1}) \quad . \quad . \quad . \quad . \quad . \quad . \quad . \quad . \quad . \quad . \quad . \quad . \quad . \quad . \quad . \quad (30)$$

the coefficients a_n and b_n can be determined using the fact that Eq. 30 holds when the matrix $[T]$ is replaced by any eigenvalue of $[T]$. The two relationships

resulting from substituting $[T]$ by $\exp(\pm i\psi)$ lead to

$$a_n = \frac{\cos n\psi}{\cos \psi}, \quad b_n = \frac{\sin n\psi}{\sin \psi} \quad \ldots\ldots\ldots\ldots\ldots\ldots\ldots\ldots\ldots\ldots \quad (31)$$

which, in turn, lead to

$$[T]^n = \cos n\psi \begin{bmatrix} 1 & 0 \\ 0 & 1 \end{bmatrix} + \frac{\sin n\psi}{\sin \psi} \begin{bmatrix} 1 - \cos \psi & K^{-1} \\ -2K(1 - \cos \psi) & -(1 - \cos \psi) \end{bmatrix} \quad (31)$$

The elements $\tau_{22}(n)$ and $\tau_{12}(n)$ appearing in Eqs. 11 and 12 are given specifically:

$$\tau_{22}(n) = \cos n\psi - \left[\frac{\sin n\psi (1 - \cos \psi)}{\sin \psi} \right] \quad \ldots\ldots\ldots\ldots\ldots\ldots\ldots\ldots \quad (32)$$

$$\tau_{12}(n) = \frac{K^{-1} \sin n\psi}{\sin \psi} \quad \ldots\ldots\ldots\ldots\ldots\ldots\ldots\ldots\ldots\ldots\ldots\ldots \quad (33)$$

It should be noted that the value for ψ is complex for a damped system, or when the system is undamped where $|\omega/\omega_0| > 2$, as can be seen from Eq. 29. In these cases, ψ can be computed from

$$\psi = -j \ln(\gamma + \sqrt{\gamma^2 - 1}) \quad \ldots\ldots\ldots\ldots\ldots\ldots\ldots\ldots\ldots\ldots\ldots\ldots \quad (34)$$

in which γ is the right hand side of Eq. 29.

Numerical Examples.—To illustrate the application of the present methodology, Eqs. 23 and 25 are used in Eqs. 11 and 12 to compute the spectral densities for displacement response and shear force response. In each case, the result can be separated into two parts; i.e.:

$$\Phi_{x_m x_m}(\omega) = n_{11}^2 \delta(\omega) + n_{12}(\omega) \quad \ldots\ldots\ldots\ldots\ldots\ldots\ldots\ldots\ldots\ldots \quad (35)$$

$$\Phi_{y_m y_m}(\omega) = n_{21}^2 \delta(\omega) + n_{22}(\omega) \quad \ldots\ldots\ldots\ldots\ldots\ldots\ldots\ldots\ldots\ldots \quad (36)$$

in which

$$n_{11} = \left\{ \tau_{12}(m)\, \tau_{22}^{-1}(N) \sum_{j=1}^{N} \nu_j \tau_{22}(N - j) - \sum_{j=1}^{m} \nu_j \tau_{12}(m - j) \right\}_{\omega=0} \quad \ldots\ldots\ldots \quad (37)$$

$$n_{12}(\omega) = \left\{ |\tau_{12}(m)|^2 |\tau_{22}(N)|^{-2} \sum_{i=1}^{N} \sum_{j=1}^{N} \left(\frac{\nu_i \nu_j}{y_i y_j} \right) \tau_{22}(N - i) \tau_{22}^*(N - j) \right.$$

$$\cdot \exp\left(\frac{-c_1 |\omega| |i - j| h}{2\pi u_r} \right) + \sum_{k=1}^{m} \sum_{l=1}^{m} \left(\frac{\nu_k \nu_l}{y_k y_l} \right) \tau_{12}(m - k) \tau_{12}^*(m - l)$$

$$\cdot \exp\left(\frac{-c_1 |\omega| |k - l| h}{2\pi u_r} \right) - 2 \operatorname{Re}\left[\tau_{12}(m) \tau_{22}^{-1}(N) \sum_{i=1}^{N} \sum_{k=1}^{m} \left(\frac{\nu_i \nu_k}{y_i y_k} \right) \right.$$

$$\left.\left. \cdot \tau_{22}(N - i) \tau_{12}^*(m - k) \exp\left(\frac{-c_1 |\omega| |i - k| h}{2\pi u_r} \right) \right] \right\} \left(\frac{8 k_0 u_r^2}{|\omega|} \right)$$

$$\cdot \left(\frac{600\, \omega}{\pi\, u_r} \right)^2 \left[1 + \left(\frac{600\, \omega}{\pi\, u_r} \right)^2 \right]^{-4/3} \quad \ldots\ldots\ldots\ldots\ldots\ldots\ldots\ldots \quad (38)$$

$$n_{21} = \left\{ \tau_{22}(m)\tau_{22}^{-1}(N) \sum_{j=1}^{N} v_j \tau_{22}(N-j) - \sum_{j=1}^{m} v_j \tau_{22}(m-j) \right\}_{\omega=0} \quad \ldots\ldots (39)$$

$$n_{22}(\omega) = \left\{ |\tau_{22}(m)|^2 |\tau_{22}(N)|^{-2} \sum_{i=1}^{N} \sum_{j=1}^{N} \left(\frac{v_i v_j}{\bar{u}_i \bar{u}_j} \right) \tau_{22}(N-i)\tau_{22}^*(N-j) \right.$$

$$\cdot \exp\left(\frac{-c_1 |\omega| |i-j| h}{2\pi u_r} \right) + \sum_{k=1}^{m} \sum_{l=1}^{m} \left(\frac{v_k v_l}{\bar{u}_k \bar{u}_l} \right) \tau_{22}(m-k)\tau_{22}^*(m-l)$$

$$\cdot \exp\left(\frac{-c_1 |\omega| |k-l| h}{2\pi u_r} \right) - 2 \operatorname{Re}\left[\tau_{22}(m)\tau_{22}^{-1}(N) \sum_{i=1}^{N} \sum_{k=1}^{M} \left(\frac{v_i v_k}{\bar{u}_i \bar{u}_k} \right) \right.$$

$$\left. \left. \cdot \tau_{22}(N-i)\tau_{22}^*(m-k) \exp\left(\frac{-c_1 |\omega| |i-k| h}{2\pi u_r} \right) \right] \right\} \left(\frac{8k_0 u_r^2}{|\omega|} \right) \left(\frac{600\,\omega}{\pi u_r} \right)^2$$

$$\cdot \left[1 + \left(\frac{600\,\omega}{\pi u_r} \right)^2 \right]^{-4/3} \quad \ldots\ldots\ldots\ldots\ldots\ldots\ldots\ldots\ldots\ldots (40)$$

It is clear from Eqs. 35 and 36 that n_{11} and n_{21} are the average displacement and average shear force

$$E[X_m] = n_{11}, \quad E[Y_m] = n_{21} \quad \ldots\ldots\ldots\ldots\ldots\ldots\ldots\ldots (41)$$

whereas $n_{12}(\omega)$ and $n_{22}(\omega)$ gives the frequency distribution of the variances; i.e.:

$$\sigma_{X_m}^2 = E[X_m^2] - (E[X_m])^2 = \int_{-\infty}^{\infty} n_{12}(\omega)\, d\omega \quad \ldots\ldots\ldots\ldots\ldots (42)$$

$$\sigma_{Y_m}^2 = E[Y_m^2] - (E[Y_m])^2 = \int_{-\infty}^{\infty} n_{22}(\omega)\, d\omega \quad \ldots\ldots\ldots\ldots\ldots (43)$$

A 40-story building model has been chosen for the numerical example. The structural and aerodynamic physical data used in the computation are as follows: Number of stories $N = 40$; individual story height $h = 4$ m; lumped mass at individual floor $m = 1{,}290{,}000$ kg; elastic stiffness in each story $K = 10^9$ N/m; damping coefficient $\bar{\beta} = 21{,}550$ N/m/sec; wind-load tributary area for each story $A = 192$ m^2; gradient height $z_g = 300$ m; gradient wind velocity $\bar{u}_g = 44.69$ m/sec; reference mean wind velocity at 10 m height $u_r = 11.46$ m/sec; drag coefficient $C_D = 1.2$; air density $\rho = 1.23$ kg/m^3; ground surface drag coefficient $k_0 = 0.03$; exponent for the mean-wind-profile power law $\alpha = 0.4$; and $c_1 = 7.7$.

Figure 2 shows the computed spectral density for the displacement at the top floor, X_{40}, without the dirac delta function at $\omega = 0$. Therefore, this figure is actually a graph of the frequency distribution of the variance, i.e., the $n_{12}(\omega)$ function given by Eq. 38 for the special case $m = N = 40$. It is expected that the greatest displacement excursion occurs at the top floor. On the other hand, the maximum shear force occurs most likely in the bottom story. Thus, to illustrate the nature of the shear force response, the frequency distribution of the variance of Y_0 is plotted in Fig. 3. This is the $n_{22}(\omega)$ function given

by Eq. 40, computed for the special case $m = 0$ and $N = 40$. Only the positive ω domains are shown in Figs. 2 and 3; the graphs for the negative ω domains can be obtained as their mirror images. Two peaks are seen in both figures. The first peak at 0.04 rad/sec is due to the maximum in the wind spectrum, whereas the second peak at 1.02 rad/sec coincides with the fundamental natural frequency of the structural model. This means that both X_{40} and Y_0 are dominated

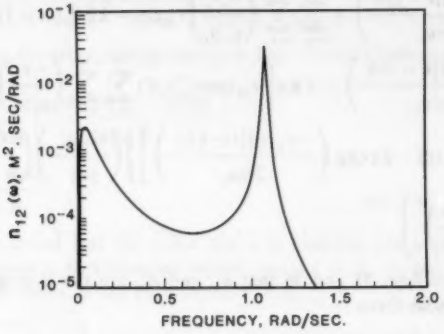

FIG. 2.—Frequency Distribution of Variance of Displacement at Top Floor of 40-Story Building

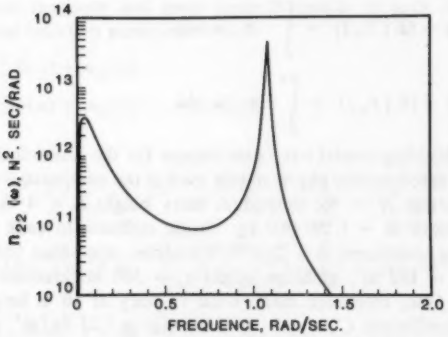

FIG. 3.—Frequency Distribution of Variance of Base Shear Force of 40-Story Building

by the fundamental mode; however, higher modes may have a greater contribution toward the displacement or force response at different locations of the structure.

Variances of X_{40} and Y_0 were obtained by integrating numerically their frequency distributions (Eqs. 42 and 43). Upon taking the squareroots, the standard deviations were found to be $\sigma_{X_{40}} = 0.0465m$ and $\sigma_{Y_0} = 0.182 \times 10^7\ N$. These can be compared with the respective mean values $E[X_{40}] = 0.1013$ m and $E[Y_0] = 0.389 \times 10^7\ N$ obtained, respectively, from Eqs. 37, 39, and 41.

Concluding Remarks

A number of simplifications have been used in this initial attempt at analyzing the wind-induced vibrations of a multi-story building with a transfer matrix formulation. By restricting the building motion to the along wind direction and by considering only one displacement variable and one force variable in each story unit, only 2×2 transfer matrices are required to represent the structural model, permitting closed form solutions for some of the results. The order of the transfer matrices will be increased when the torsional and the cross-wind motions are taken into account, a subject which will be dealt with in a paper to appear later.

The assumption that every story of the building is identically constructed has resulted in substantial saving in computer time. Specifically, a long chain product of transfer matrices is replaced by the basic transfer matrix raised to a high power, and a simple scheme has been devised to facilitate the computation. The use of essentially identical construction for every story is actually a rather common practice in the building industry because of the overall cost effectiveness, at least for moderately tall buildings. For very tall buildings, it may be more economical to divide the whole building into several groups, each of which consists of an array of identically constructed units. In the latter case, the method described herein for computing an arbitrary power of a transfer matrix can still be used to advantage.

Acknowledgment

The research is supported by the National Science Foundation Grant number NSF-PFR-78-24553. The writers are grateful for this support. The writers would like to thank B. Samali, graduate student of the George Washington University, for helping on numerical computations.

Appendix I.—References

1. Archibald, E. D., "Some Results of Observations with Kite-Wire Suspended Anemometers up to 1,300 Feet above the Ground in 1883–1885," *Nature*, Vol. 33, 1886, p. 593.
2. Berman, S., "Estimating the Longitudinal Wind Spectrum Near the Ground," *Quarterly Journal of the Royal Meteorological Society*, Vol. 91, 1965, p. 302–317.
3. Davenport, A. G., "A Rationale for Determination of Design Wind Velocities," *Journal of the Structural Division*, ASCE, Vol. 86, No. ST5, Proc. Paper 2476, May 1960, pp. 39–68.
4. Davenport, A. G., "The Application of Statistical Concepts to the Wind Loading of Structures," *Proceedings of the Institution of Civil Engineers*, Vol. 19, Aug., 1961, pp. 449–472.
5. Davenport, A. G., "The Treatment of Wind Loading on Tall Buildings," *Proceedings of the Symposium on Tall Buildings*, University of Southampton, Pergamon Press, London, England, 1966.
6. Lin, Y. K., and McDaniel, "Dynamics of Beam-Type Periodic Structures," *Journal of Engineering for Industry*, Vol. 91, Series B, No. 4, Nov., 1969, pp. 1133–1141.
7. Patrickson, C. P., and Friedman, P., "A Study of the Coupled Lateral and Torsional Response of Tall Buildings to Wind Loadings," *Technical Report UCLA-ENG-76126*, University of California at Los Angeles, Los Angeles, Calif., Dec., 1976.

8. Pestel, E. C., and Leckie, F. A., *Matrix Methods in Elasto-Mechanics*, McGraw-Hill Book Co., Inc., New York, N.Y., 1963.
9. Simiu, E., "Wind Spectra and Dynamic Alongwind Response," *Journal of the Structural Division*, ASCE, Vol. 100, No. ST9, Proc. Paper 10815, Sept., 1974, pp. 1897–1910.
10. Simiu, E., and Scanlan, R. H., *Wind Effects on Structures*, John Wiley and Sons, Inc., New York, N.Y., 1978.
11. Solnes, J., and Sigbjornsson, R., "Along-Wind Response of Large Bluff Buildings," *Journal of the Structural Division*, ASCE, Vol. 99, No. ST3, Proc. Paper 9585, Mar., 1973, pp. 381–398.
12. Vaicaitis, R., Shinozuka, M., and Takeno, M., "Response Analysis of Tall Buildings to Wind Loadings," *Journal of the Structural Division*, ASCE, Vol. 101, No. ST3, Proc. Paper 11194, Mar., 1975, pp. 585–600.

Appendix II.—Notation

The following symbols are used in this paper:

A_j = tributary area of jth floor;
C_D = drag coefficient;
C_1 = constant appearing in Eq. 24;
F_j = wind force applied to jth floor;
h = story height;
K = stiffness of one story;
K_0 = constant appearing in Eq. 20;
m = mass of jth floor;
n_{11} = average value of X_m, Eq. 41;
n_{21} = average value of Y_m, Eq. 41;
$n_{12}(\omega)$ = frequency distribution of variance of X_m;
$n_{22}(\omega)$ = frequency distribution of variance of Y_m;
$R_{\xi_j\xi_j}(\tau)$ = autocorrelation function of $\xi_j(t)$;
$R_{F_jF_j}(\tau)$ = autocorrelation function of $F_j(t)$;
$\text{Re}(\ )$ = real part of complex expression;
$S(n)$ = one-sided spectrum of fluctuating part of wind velocity;
$[T]$ = transfer matrix;
u_r = reference mean wind velocity in meter at 10 m above ground;
u_j = mean wind velocity at jth floor;
u_g = wind velocity at gradient height;
V_j = relative wind velocity at jth floor;
X_j = displacement of jth floor;
Y_j = shear force above jth floor;
Z_j = height of jth floor;
Z_g = reference height;
$\{Z\}_j$ = jth state vector;
Δz = height separation $(i - j)h$;
$\bar{\beta}$ = damping coefficient;
ω = frequency, in radians per second;
ρ = air density;
α = constant appearing in Eq. 17;
$\delta(\ )$ = dirac delta function;
ν_j = mean wind force applied to jth floor;
λ = eigen value of $[T]$;

ψ = exponent of λ;
$\xi_j(t)$ = random fluctuation of wind velocity about mean;
$\tau_{ij}(n)$ = (i, j) element of $[T]^n$;
$\Phi_{X_m X_m}(\omega)$ = spectral density of X_m;
$\Phi_{F_j F_j}(\omega)$ = spectral density of F_j; and
$\bar{}$ = an over-bar of quantity, indicates Fourier transform.

JOURNAL OF
THE ENGINEERING
MECHANICS DIVISION

BUILDING INTERNAL PRESSURE: SUDDEN CHANGE

By Henry Liu,[1] M. ASCE and Patrick J. Saathoff[2]

INTRODUCTION

The safety of buildings under the action of strong wind often depends as much on the building internal pressure as on the external pressure. Internal pressure also affects air infiltration and heat loss through buildings, indoor air pollution, occupant comfort, spread of fire and smoke in buildings, rain penetration into buildings, proper operation of certain mechanical equipment in buildings, and the accuracy of indoor barometric measurements. Despite all these implications, internal pressure has received far less attention than external pressure by researchers, and consequently, the subject is usually poorly understood. This paper seeks to clarify the nature of internal pressure variations, and to provide a rigorous theory on the subject based on fluid mechanics.

When an aperture of a building, such as a window or door, is opened suddenly in wind, a rapid change in pressure happens inside the building, causing the internal pressure to reach an equilibrium or steady-state value within a short period. The equilibrium internal pressure may be predicted in the manner considered by the first writer (4), and by Newberry and Eaton (7). The transient response of the internal pressure which happens before the pressure reaches equilibrium has been considered briefly by Euteneuer (1) and the first writer (5). It is the intent of the present paper to provide a more complete treatment and analysis of this problem. A related problem, namely, the fluctuations of building internal pressure induced by wind turbulence, has been treated recently by Holmes (2).

It is believed that a correct prediction of the transient response of the internal pressure is essential to many facets of wind engineering, such as the analysis

[1]Prof. of Civ. Engrg., Dept. of Civ. Engrg., Univ. of Missouri-Columbia, Columbia, Mo. 65211.

[2]Grad. Student, Dept. of Civ. Engrg., Univ. of Missouri-Columbia, Columbia, Mo. 65211.

Note.—Discussion open until September 1, 1981. To extend the closing date one month, a written request must be filed with the Manager of Technical and Professional Publications, ASCE. Manuscript was submitted for review for possible publication on January 17, 1980. This paper is part of the Journal of the Engineering Mechanics Division, Proceedings of the American Society of Civil Engineers, ©ASCE, Vol. 107, No. EM2, April, 1981. ISSN 0044-7951/81/0002-0309/$01.00.

of the dynamic windload on buildings—especially on claddings. Questions such as whether a gust factor should be used in building codes to determine internal pressure also can be answered more intelligently when this transient response problem is clearly understood.

Treatments of Problem

The problem to be treated is the transient response of the pressure inside a building following the breakage of a window or door during a wind storm. The window or door may be broken either by the inequilibrium in the internal and external pressures, by wind-generated missiles, or by any other cause.

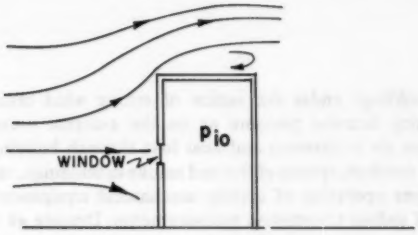

(a) BEFORE WINDOW BREAKAGE ($t < 0$)

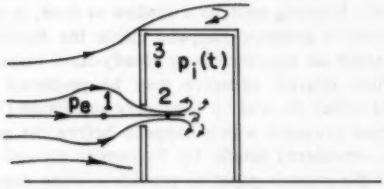

(b) AFTER WINDOW BREAKAGE ($t > 0$)

FIG. 1.—Change of Flow Pattern and Internal Pressure Due to Window Breakage

Referring to Fig. 1, suppose a window on the windward side is broken at time $t = 0$ and suppose the wind speed is V. The external and internal pressures at $t = 0$ are respective p_e and p_{io}. As soon as the window is broken, the internal pressure will rise, whereas the external pressure will remain constant. It will take a short while before the internal pressure $p_i(t)$ will reach its equilibrium value which is the same as the external pressure p_e. The problem can be solved by assuming either an isothermal or adiabatic condition, with the latter being more realistic.

Isothermal Quasi-Steady Solution.—Perhaps the simplest solution to the previously mentioned problem is to use the Bernoulli equation for steady incompressible flow:

$$\frac{V_1^2}{2}+\frac{p_1}{\rho_e}=\frac{V_2^2}{2}+\frac{p_2}{\rho_e} \quad \ldots\ldots\ldots\ldots\ldots\ldots\ldots\ldots\ldots\ldots\ldots\ldots\ldots\ldots (1)$$

in which V = velocity; p = pressure; and ρ_e = external air density. Subscripts 1 and 2 refer to respectively points 1 and 2 in Fig. 1(*b*). Note that $p_1 = p_e$ and $p_2 = p_i$. Also note that for simplicity, the density of the air inside the building has been assumed to be the same as outside. Since V_1 is much smaller than V_2, and since the volumetric discharge is $Q = AV_2$, where A is the effective area of the opening

$$Q = AV_2 = A\sqrt{\frac{2(p_e - p_i)}{\rho_e}} \quad \ldots\ldots\ldots\ldots\ldots\ldots\ldots\ldots\ldots\ldots\ldots\ldots\ldots\ldots (2)$$

From the conservation of mass

$$\rho_e Q = \frac{dM}{dt} = V_o\frac{d\rho_i}{dt} \quad \ldots\ldots\ldots\ldots\ldots\ldots\ldots\ldots\ldots\ldots\ldots\ldots\ldots\ldots (3)$$

in which M = the total mass of the air in the building; V_o = the volume of the building; and ρ_i = the density of the internal air.

Eliminating Q from Eqs. 2 and 3, using the equation of state of perfect gas, and assuming constant temperature

$$\frac{p_i}{p_e} = 1 - \left(\sqrt{1-\frac{p_{io}}{p_e}} - \frac{1}{2}\sqrt{\frac{p_a}{p_s}}\frac{t}{t_o}\right)^2 \quad \ldots\ldots\ldots\ldots\ldots\ldots\ldots\ldots\ldots\ldots (4)$$

in which p_a = the ambient pressure; p_s = the stagnation pressure $\rho_a V^2/2$; and $t_o = V_o/AV$ is a time constant.

From Eq. 4, the equilibrium condition is reached when

$$T_{eq} = \left(\frac{t}{t_o}\right)_{eq} = 2\sqrt{\frac{p_s}{p_a}\left(1-\frac{p_{io}}{p_e}\right)} \quad \ldots\ldots\ldots\ldots\ldots\ldots\ldots\ldots\ldots\ldots (5)$$

Isentropic Quasi-Steady Solution.—A more refined approach is to assume an isentropic, i.e., adiabatic and frictionless, flow and to give due regards to the variation of density from 1–2. The Bernoulli equation for this case is (6):

$$\frac{V_2^2}{2}+\frac{k}{k-1}\frac{p_2}{\rho_2}=\frac{V_1^2}{2}+\frac{k}{k-1}\frac{p_1}{\rho_1} \quad \ldots\ldots\ldots\ldots\ldots\ldots\ldots\ldots\ldots\ldots\ldots\ldots\ldots\ldots (6)$$

in which k = the ratio of the specific heat capacity at constant pressure and at constant volume, i.e., $k = C_p/C_v$. The continuity equation is

$$\rho_2 V_2 A = V_o\frac{d\rho_2}{dt} \quad \ldots\ldots\ldots\ldots\ldots\ldots\ldots\ldots\ldots\ldots\ldots\ldots\ldots\ldots\ldots\ldots (7)$$

The equation of adiabatic gas is

$$\frac{p_1}{\rho_1^k}=\frac{p_2}{\rho_2^k}=\frac{p_a}{\rho_a^k}=\text{constant} \quad \ldots\ldots\ldots\ldots\ldots\ldots\ldots\ldots\ldots\ldots\ldots\ldots\ldots\ldots (8)$$

in which the subscript "*a*" refers to the "atmospheric" or "ambient" condition.

Assuming $V_2 >> V_1$ in Eq. 6, the elimination of V_2 from Eqs. 6 and 7 yields

$$\frac{d\rho_2}{dt} = \frac{A\rho_2}{V_o}\sqrt{\frac{2k}{(k-1)}\left(\frac{p_1}{\rho_1} - \frac{p_2}{\rho_2}\right)} \quad \ldots\ldots\ldots\ldots\ldots\ldots\ldots\ldots (9)$$

Substituting Eq. 8 into Eq. 9 and rearranging terms yields

$$dt = \frac{t_o}{B}\frac{dx}{x\sqrt{1-x^{k-1}}} \quad \ldots\ldots\ldots\ldots\ldots\ldots\ldots\ldots (10)$$

in which $t_o = \frac{V_o}{AV}$, $B = \sqrt{\frac{k}{(k-1)}\frac{p_e}{p_s}\left(\frac{p_a}{p_e}\right)^{1/k}}$, $x = \frac{\rho_i}{\rho_e} = \left(\frac{p_i}{p_e}\right)^{1/k}$ (11)

Using the transformation $Y = X^{k-1}$ and $t/t_o = T$, Eq. 10 is changed to:

$$dT = \frac{1}{B}\frac{1}{(k-1)}\frac{dY}{Y\sqrt{1-Y}} \quad \ldots\ldots\ldots\ldots\ldots\ldots\ldots\ldots (12)$$

Integrating Eq. 12 and using the initial condition $Y = Y_o$ when $T = 0$ yields

$$T = \frac{t}{t_o} = \frac{1}{\sqrt{k(k-1)\frac{p_e}{p_s}\left(\frac{p_a}{p_e}\right)^{1/k}}} \log \frac{(1+\sqrt{1-Y_o})(1-\sqrt{1-Y})}{(1-\sqrt{1-Y_o})(1+\sqrt{1-Y})} \quad (13)$$

in which $Y_o = \left(\frac{p_{io}}{p_e}\right)^{(k-1/k)}$ $\ldots\ldots\ldots\ldots\ldots\ldots\ldots\ldots\ldots\ldots$ (14)

The "log" in Eq. 13 represents natural logarithm.

Isentropic Unsteady Solution.—The aforementioned isentropic solution is the quasi-steady solution because the Bernoulli equation used, i.e., Eq. 6, is for steady flow. To get the true unsteady isentropic solution, an unsteady term must be added to Eq. 6 which now becomes (6)

$$\int_1^2 \frac{\partial V}{\partial t}\,dl + \frac{V_2^2}{2} + \frac{k}{k-1}\left(\frac{p_2}{\rho_2}\right) = \frac{k}{k-1}\left(\frac{p_1}{\rho_1}\right) \quad \ldots\ldots\ldots\ldots\ldots\ldots\ldots (15)$$

in which dl = an infinitesimal distance along a streamline. Note that the term $V_1^2/2$ has been dropped from Eq. 15 because $V_2 >> V_1$.

The line integral of Eq. 15 cannot be evaluated exactly. However, approximately

$$\int_1^2 \frac{\partial V}{\partial t}\,dl = \frac{dV_2}{dt}L_e \quad \ldots\ldots\ldots\ldots\ldots\ldots\ldots\ldots\ldots\ldots (16)$$

in which L_e = the effective length of the jet entering the building.

The previous simplification is possible because, as shown in Fig. 1(*b*), the air jet entering the window opening contracts only slightly. It forms a jet column which can be approximated as a cylinder having a length L_e and a cross-sectional area A. The length L_e is usually in the neighborhood of $0.8d$, in which d = the diameter of the opening (if circular), or the length of each side of the opening (if squared).

Substituting Eq. 16 into Eq. 15 and using Eq. 7, it can be shown that

$$\frac{V_o L_e}{A}\left[\frac{1}{\rho_2}\frac{d^2\rho_2}{dt^2} - \frac{1}{\rho_2^2}\left(\frac{d\rho_2}{dt}\right)^2\right] + \frac{V_o^2}{2A^2\rho_2^2}\left(\frac{d\rho_2}{dt}\right)^2$$

$$+ \frac{k}{(k-1)}\left(\frac{p_2}{\rho_2} - \frac{p_1}{\rho_1}\right) = 0 \quad \ldots\ldots\ldots\ldots\ldots\ldots\ldots\ldots \quad (17)$$

Next, using Eq. 8 and the conditions given in Eq. 11, the previous equation becomes

$$X\frac{d^2X}{dT^2} + \left(\frac{V_o}{2AL_e} - 1\right)\left(\frac{dX}{dT}\right)^2 + \left(\frac{V_o}{2AL_e}\right)B^2X(X^{k-1} - 1) = 0 \quad \ldots\ldots \quad (18)$$

Ordinarily, $V_o/2AL_e >> 1$, and the aforementioned equation reduces to

$$CX\frac{d^2X}{dT^2} + \left(\frac{dX}{dT}\right)^2 - B^2X^2(1 - X^{k-1}) = 0 \quad \ldots\ldots\ldots\ldots\ldots \quad (19)$$

in which $C = \dfrac{2AL_e}{V_o}$, $B = \sqrt{\dfrac{k}{(k-1)}\dfrac{p_e}{p_s}\left(\dfrac{p_a}{p_e}\right)^{1/k}}$ $\ldots\ldots\ldots\ldots$ (20)

The initial conditions for solving Eq. 19 are

$$X = X_o = \left(\frac{p_{io}}{p_e}\right)^{1/k} \quad \text{at} \quad T = 0 \quad \text{and} \quad \frac{dX}{dT} = 0 \quad \text{at} \quad T = 0 \quad \ldots\ldots\ldots \quad (21)$$

Comparison of Results

Results of the three foregoing solutions can be compared in an example. The example uses the following values: $\rho_a = 1.1$ kg/m^3; $V = 50$ m/s; $k = 1.4$; $p_s = 1/2\ \rho_a V^2 = 1.375 \times 10^3$ pa; $C_{pe} = 1.0$; $C_{pio} = -0.5$; $p_a = 1.013 \times 10^5$ pa; $p_{io} = p_a - 0.5\ p_s = 1.006 \times 10^5$ pa; $p_e = p_a + p_s = 1.027 \times 10^5$ pa; $X_o = 0.9854$; $Y_o = 0.9941$; $A = 1$ m $\times$ 1 m $= 1$ m^2; $V_o = 500$ m^3; $t_o = V_o/AV = 10$ sec; $L_e = 0.8d = 0.8$ m; $C = 2AL_e/V_o = 0.0032$; and $B = 259$ (from Eq. 20).

From the foregoing values, Eq. 4 becomes

$$\frac{t}{t_o} = 0.0332 - 0.233\sqrt{1 - \frac{p_i}{p_e}} \quad \ldots\ldots\ldots\ldots\ldots\ldots\ldots \quad (22)$$

Eq. 13 becomes

$$\frac{t}{t_o} = 0.155 \log\left(1.165\frac{1 - \sqrt{1 - Y}}{1 + \sqrt{1 + Y}}\right) \quad \ldots\ldots\ldots\ldots\ldots\ldots \quad (23)$$

Eqs. 19 and 21 become, respectively

$$0.0032\,X\frac{d^2X}{dT^2} + \left(\frac{dX}{dT}\right)^2 - 259\,X^2(1 - X^{0.4}) = 0 \quad \ldots\ldots\ldots\ldots \quad (24)$$

and $X = 0.9854$ at $T = 0$; $\dfrac{dX}{dT} = 0$ at $T = 0$ . . . . . (25)

The three different solutions are plotted in Fig. 2. The solution of Eq. 24 was obtained numerically by using the standard Runge-Kutta method with different integration intervals. It was done by using a CSMP (Continuous System Modeling Program) on an Amdahl 470/V7 computer. Note that small but noticeable differences exist among the three solutions.

It can be seen that initially the rise of the internal pressure predicted by Eq. 24 is not as fast as the rise based on the quasi-steady isentropic solution. This is due to the inertia effect of the flow not considered in the quasi-steady approach. It can also be seen that the internal pressure becomes the same as the external pressure in a time t roughly equal to 2% of the time constant t_o. Since the time constant in this example is 10 sec, the internal pressure

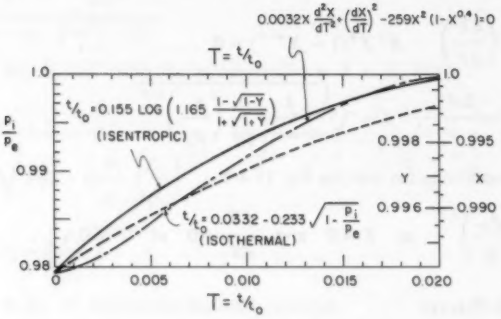

FIG. 2.—Transient Response of Internal Pressure

of the building reaches the external pressure within 0.2 sec of the window breakage—a rather fast response indeed!

Oscillation of Internal Pressure

The preceding study of the change of the internal pressure following window failure was carried out until p_i has reached the value of p_e. It was assumed implicitly that an equilibrium, i.e., a steady state, has been reached as soon as p_i has risen to p_e. In reality, the inertia of air will cause p_i to exceed p_e before the flow is stopped. Then, the higher pressure inside the building causes the flow to reverse direction which in turn causes p_i to decrease as air moves out of the building. The reverse flow does not stop until p_i becomes somewhat less than p_e. After this, air rushes back into the building as in the beginning of the first cycle. The flow will oscillate in this manner until either the fluctuations are damped out after many cycles of oscillation or building failure occurs. The phenomenon is similar to the water hammer waves caused by the sudden closure of a valve in a pipe connected to an upstream reservoir as explained in elementary texts of fluid mechanics.

The aforementioned oscillatory motion has been treated by Holmes (2) in 1979 using the classical Helmholtz resonator model studied in acoustics (8). The Helmholtz model is based on an assumed analogy between the acoustic resonator and a mechanical system consisting of a mass attached to a spring involved in damped oscillations. Based on the Helmholtz model, Holmes derived the following equation to predict internal pressure variation (2):

$$\frac{\rho_a l_e V_o}{n p_a} \ddot{C}_{pi} + \frac{\rho_a V_o^2 p_s}{2c^2 n^2 A_o p_a^2} \dot{C}_{pi} |\dot{C}_{pi}| + A_o C_{pi} = A_o C_{pe} \quad \ldots \ldots \ldots \ldots \quad (26)$$

in which n = the polytropic exponent which is equal to 1.4 and unity, respectively for adiabatic and isothermal flows; c = the orifice coefficient; l_e = the equivalent length of the slug of air in the opening; A_o = the opening area; and dot and double dots above any quality represent respectively the first and second

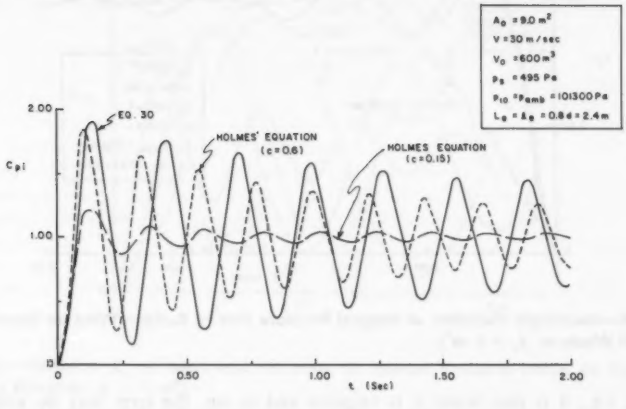

FIG. 3.—Isentropic Variation of Internal Pressure Due to Sudden Window Breakage (Large Window: A_o = 9 m²)

derivatives with respect to time, t. The four terms in Eq. 26 are, in consecutive order, the mass-inertia, viscous-damping, elastic-stiffness, and forcing-function terms.

It will now be shown that an equation similar to Eq. 26 can be derived from the Bernoulli equation using the same approach as presented before in the section on Isentropic Unsteady Solution, except for the fact that a reverse flow is assumed whenever p_i is negative. Using such an approach, the Bernoulli equation yields

$$L_e \dot{V}_j = \left(\frac{k}{k-1}\right)\left(\frac{p_e}{\rho_e} - \frac{p_i}{\rho_i}\right) \pm \frac{V_j^2}{2} \quad \ldots \ldots \ldots \ldots \ldots \ldots \quad (27)$$

in which V_j = the jet velocity which is the same as V_2 for forward flow. The plus and minus signs of the last term of Eq. 27 correspond to $\dot{p}_i < 0$

(reverse flow) and $\dot{p}_i > 0$ (forward flow), respectively.

Using an approach similar to the derivation of Eq. 18, it can be proved that Eq. 27 leads to

$$\ddot{p}_i = Dp_i(p_e^z - p_i^z) + (1 \pm E)\frac{1}{p_i}(\dot{p}_i)^2 \quad \ldots\ldots\ldots\ldots\ldots\ldots \quad (28a)$$

in which $D = \dfrac{k^2 A\, p_2^{1/k}}{(k-1)L_e V_o \rho_a}$, $E = \dfrac{V_o}{2kAL_e}$, and $z = \dfrac{k-1}{k}$ . . . . . (28b)

Knowing that the sign of the last term of Eq. 28*a* is always opposite the sign

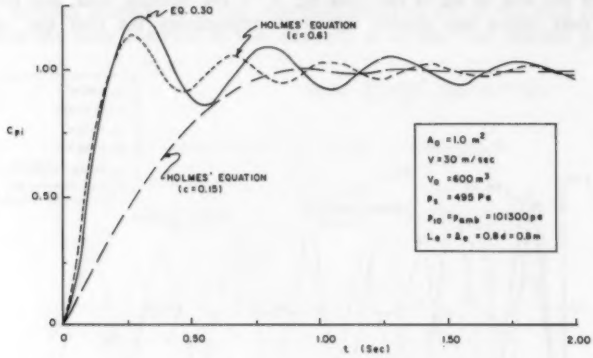

FIG. 4.—Isentropic Variation of Internal Pressure Due to Sudden Window Breakage (Small Window: $A_o = 1$ m²)

of $\dot{p}_i$, i.e., it is plus when $\dot{p}_i$ is negative and so on, the term may be written as

$$\pm\frac{E}{p_i}(\dot{p}_i)^2 = -\frac{E}{p_i}|\dot{p}_i|\dot{p}_i \quad \ldots\ldots\ldots\ldots\ldots\ldots\ldots\ldots\ldots \quad (29)$$

Substituting Eq. 29 into Eq. 28*a* yields

$$\ddot{p}_i = Dp_i(p_e^z - p_i^z) + \frac{1}{p_i}(\dot{p}_i)^2 - \frac{E}{p_i}|\dot{p}_i|\dot{p}_i \quad \ldots\ldots\ldots\ldots\ldots\ldots \quad (30)$$

Equation 30 is the counterpart of Eq. 26 of Holmes. Both equations may be used for the determination of the variation of the internal pressure caused by external pressure change. Note that both equations are second-order nonlinear ordinary differential equations. Since Eq. 30 has a more rigorous foundation, it is believed to be more correct than the Holmes equation. It can be shown that by using the simplifying assumption $\rho_i \simeq \rho_e \simeq \rho_a$, the same derivation which led to Eq. 30 yields Eq. 26. Thus, Eq. 26 is a special case of Eq. 30 when the density change or pressure change is small.

A numerical example will now be considered to compare results computed from Eq. 30 to that from the Holmes equation. Consider the change of internal pressure following sudden window breakage. Assume the external pressure at the window is stagnation pressure ($C_{pe} = 1$), and the initial internal pressure is the same as the ambient pressure which is atmospheric. Furthermore, assume wind speed, building volume, and the window area to be respectively 30 m/s, 600 m^3, and 9 m^2. These numbers are the same used by Holmes (2) in an example. A contraction coefficient of 0.61 is used herein to obtain the effective area A from the window area A_o, i.e., $A = 0.61\ A_o$. Both L_e and l_e are assumed to be $0.8d$ in which d = the width of the square window which is 3 m in this case. Values of C_{pi} versus time were computed using Eq. 30 and the Holmes equation, and the results are plotted in Fig. 3. Although Holmes used a k value of 1.2 (between isothermal and isentropic), a k value of 1.4 was used in this analysis, as the flow was assumed isentropic. The results of Holmes' equation

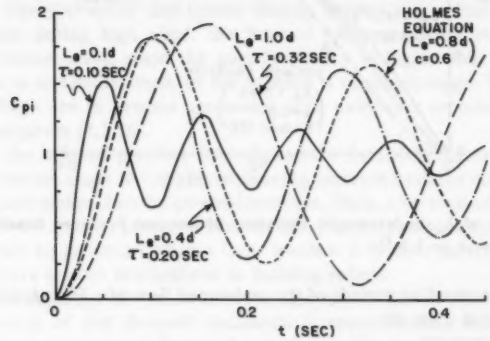

FIG. 5.—Effect of L_e on Isentropic Variation of Internal Pressure Based on Eq. 30 (Large Window: $A_o = 9\ m^2$)

in this analysis do not differ much from those presented in his paper using $k = 1.2$.

As shown in Fig. 3, C_{pi} versus t based on Eq. 30 is similar to that based on Holmes' equation with an orifice coefficient $c = 0.6$. For this case with large window, although the equilibrium internal pressure coefficient is the same as the external pressure coefficient which is 1.0, the maximum C_{pi} during the first cycle of oscillation is about 1.8. This means an overshooting of internal pressure of as much as 80%.

If one uses the same data as in the foregoing example, except a window of an area of 1.0 m^2 which is much smaller than the one used in the example, the same computations lead to the results given in Fig. 4. Note that the maximum overshooting for this case with a smaller window is less than 25%, and the damping is faster than in the previous case with large windows.

In the foregoing examples, it was assumed that $L_e = l_e = 0.8d$. It is of interest to see what value of L_e agrees the best with the Holmes result based on $l_e = 0.8d$. For this purpose, C_{pi} versus t was computed based on values

of L_e ranging from 0.1d–1.0d. The results are plotted in Figs. 5 and 6 respectively for large and small windows. Note that in both cases the computation based on Eq. 30 agrees closely with Holmes' results when L_e is approximately 0.5d. The frequency or period of oscillation of both cases changes with L_e; smaller L_e gives higher frequency or smaller period.

The period of oscillation calculated from Holmes' equation with l_e = 0.8d is 0.23 sec and 0.40 sec, respectively for A_o = 9 m^2 and 1 m^2. These periods are approximately the same as those computed from Eq. 30 by using L_e =

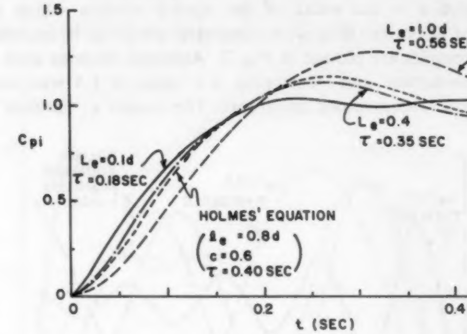

FIG. 6.—Effect of L_e on Isentropic Variation of Internal Pressure Based on Eq. 30 (Small Window: A_o = 1 m^2)

0.5d. The corresponding periods of the undamped flow of a Helmholtz resonator can be calculated from (8)

$$\tau_o = \frac{\pi^{5/4}}{A^{1/4}} \sqrt{\frac{2V_o\rho_a}{kp_a}} = \frac{0.457}{A_o^{1/4}} \quad \text{(31)}$$

in which it was assumed that A = 0.61 A_o. Using Eq. 31, the values of τ_o for A_o = 9 m^2 and 1 m^2 are respectively 0.26 sec and 0.46 sec.

Conclusion and Analysis

This paper demonstrates that the variation of the internal pressure of a building following sudden window breakage can be predicted from the unsteady isentropic Bernoulli equation. The result is a second-order nonlinear differential equation which is a better approximation than the equation derived from the Helmholtz resonator given in classical acoustics. While the result based on the Bernoulli equation is valid for small as well as large pressure variations, the result based on the Helmholtz resonator model is correct only for small pressure changes.

Two matters need clarifications. One is that it may appear that the Bernoulli equation was not valid for this case because of frictional loss. This is not true, however, because the Bernoulli equation was used only between point 1 and point 2 in Fig. 1(b) which are within a region of convergent flow with little energy loss. The bulk of the energy loss is between point 2 and point

3 where the Bernoulli equation was not used. This loss was automatically taken care of by assuming the internal pressure at 3 to be the same as at 2 which means a complete loss of the kinetic energy of the flow. Another matter of concern is the validity of the implicit assumption that the building is rigid. In reality, building walls and roofs deflect somewhat under the action of high pressure. This building flexibility may provide extra damping to the flow. How severe this effect is under ordinary condition is not known. It is an area that deserves attention and future research. Vickery (11) has suggested an empirical approach in which a modified bulk modulus of air is used to embody the building flexibility effect.

The study concludes the following:

1. Following the sudden breakage of a window or door by a strong wind of the order of 50 m/s, the internal pressure adjusts to the external pressure level in a time approximately equal to 0.02 t_o which is usually much less than a second. The previously mentioned finding implies that when a window or door is open during high wind, the internal pressure will fluctuate with the external pressure even when the gust frequency is higher than 1 Hz, unless the window is unusually small, or the building is unusually large. The aforementioned findings are in general agreement with evidences reported recently by other investigators (2,3,10).
2. After the internal pressure has reached the external pressure, the internal pressure does not cease to rise. It continues to increase until the internal pressure becomes much higher than the external pressure. Then, a reversal of flow direction occurs, and the internal pressure starts to fall. Large overshooting of the internal pressure may be produced when a large window is broken during a windstorm. This may have serious implications to building safety.
3. Sudden breakage of window causes a damped oscillation of internal pressure. The frequency of this damped oscillation is approximately the same as that predicted for an undamped Helmholtz oscillator. The frequency increases when the area of the opening increases.
4. Experimental data are needed to determine the value of L_e before Eq. 30 can be expected to yield accurate results. Likewise, experimental data are needed to determine the orifice discharge coefficient before Holmes' equation can be expected to yield accurate results. In the absence of experimental data, it is recommended that a value between 0.5 and 0.8 be used for L_e in computing internal pressure variations.

Appendix I.—References

1. Euteneuer, G. A., "Druckansteig im Inneren von Gebauden bei Windeinfall," *Der Bauingenieur*, Vol. 45, 1970, pp. 214–216.
2. Holmes, J. D., "Mean and Fluctuating Internal Pressures Induced by Wind," presented at the July, 1979, 5th International Conference on Wind Engineering, held at Fort Collins, Colo.
3. Kramer, C., Gerhardt, H. J., and Scherer, S., "Wind Pressure on Block Type Buildings," 3rd Colloquium on Industrial Aerodynamics, Aachen, West Germany, 1978.
4. Liu, H., "Wind Pressure Inside Buildings," *Proceedings of the 2nd United States Wind Engineering Conference*, June, 1975, p. 111-3-1.
5. Liu, H., "Building Code Requirements on Internal Pressure," presented at the Feb.,

1978, 3rd United States National Conference on Wind Engineering Research, held at Gainesville, Fla., p. VI-7-1.
6. Liu, H., "Strengthening Teaching Bernoulli Equation in Fluid Mechanics," *Event No. 2585*, presented at the June, 1978, 86th Annual Conference of the American Society for Engineering Education, held at Vancouver, British Columbia, Canada, 13 pages.
7. Liu, H., and Saathoff, P. J., "Wind-Induced Pressure Fluctuations Inside Building," presented at the Sept., 1979, ASCE 3rd Specialty Conference of the Engineering Mechanics Division, held at Austin, Tex., pp. 812–814.
8. Malecki, I., *Physical Foundations of Technical Acoustics*, Pergamon Press, New York. N.Y., 1969, 743 pp.
9. Newberry, C. W., and Eaton, K. J., *Wind Loading Handbooks*, Building Research Establishment Report, Department of the Environment, London, England, Her Majesty's Stationary Office, 1974.
10. Stathopoulos, T., Surry, D., and Davenport, A. G., "Internal Pressure Characteristics of Low Rise Buildings Due to Wind Action," presented at the July, 1979, 5th International Conference on Wind Engineering, held at Fort Collins, Colo., p. IV-9-1.
11. Vickery, B. J., "Internal Pressure," *The Structural and Environmental Effects of Wind on Buildings and Structures*, Section 10.8, Monash University, Australia, May, 1975.

Appendix II.—Notation

The following symbols are used in this paper:

A = effective area of opening;
A_o = actual area of opening;
B = defined in Eq. 11;
C = $2AL_e/V_o$;
C_{pe} = external pressure coefficient;
C_{pi} = internal pressure coefficient;
C_{pio} = initial value of C_{pi};
c = orifice discharge coefficient;
c_p = specific heat at constant pressure;
c_v = specific heat at constant volume;
D = defined in Eq. 28*b*;
d = dimension of square window;
E = defined in Eq. 28*b*;
k = c_p/c_v;
l = distance along streamline;
L_e = length of air jet entering building;
l_s = length of air slug of acoustic resonator;
M = mass;
n = polytropic exponent;
p = pressure;
p_a = atmospheric pressure;
p_e = external pressure;
p_i = internal pressure;
p_{io} = initial value of p_i;
p_s = stagnation pressure ($\rho_a V^2/2$);
Q = volumetric discharge;
T = t/t_o;

t = time;
t_o = time constant (V_o/AV);
V = wind velocity;
V_j = velocity of air jet entering building;
V_o = internal volume of building;
X = ρ_i/ρ_e;
X_o = initial value of X;
Y = X^{k-1};
Y_o = initial value of Y;
z = $(k-1)/k$;
ρ_a = ambient-air density;
ρ_e = external-air density;
ρ_i = internal-air density;
τ = period of damped oscillation computed from Eq. 30; and
τ_o = period of undamped oscillation calculated from Eq. 31.

JOURNAL OF
THE ENGINEERING
MECHANICS DIVISION

TORSIONAL VIBRATION OF ALONG-WIND EXCITED STRUCTURES

By D. A. Foutch,[1] A. M. ASCE and E. Safak[2]

INTRODUCTION

Although the along-wind vibration of structures subjected to wind loadings has been an active research topic for the past twenty years, very few investigators have considered the rotational vibration of these structures. Torsional motions, if not considered in design, could result in overstressing of the columns at the periphery of the structure and could also damage cladding attachments. The majority of the research to develop methods of analysis has been directed toward predicting the expected maximum along-wind translational response of structures due to buffeting by the wind. The methods that have been developed range from equivalent static load methods (1,14) which utilize design charts to more precise methods requiring computer analysis (12).

Hart (7) derived a general set of equations that could be used to analyze the three-dimensional response of buildings to stochastic wind forces. The required experimental data was not available at the time, however, to apply them to practical problems. Recent work by Patrickson and Friedmann (10) indicated that the dynamic torsional response of buildings may lead to displacements that are of the same order as the along-wind motions. Their work also indicates that velocities and accelerations due to torsional motion may be significant. An experimental and analytical investigation by Hart, et al. (8), demonstrated the importance of torsional vibrations of buildings subjected to wind and earthquake loadings. Both the first and second writers (6) demonstrated analytically that even perfectly symmetric structures may experience serious torsional motion when buffeted by the wind. Several investigators not cited here have provided experimental evidence of relative magnitude of the wind-excited

[1]Asst. Prof. of Civ. Engrg., Univ. of Illinois at Urbana-Champaign, Urbana, Ill. 61801.
[2]Grad. Research Asst., Dept. of Civ. Engrg., Univ. of Illinois at Urbana-Champaign, Urbana, Ill. 61801.

Note.—Discussion open until September 1, 1981. To extend the closing date one month, a written request must be filed with the Manager of Technical and Professional Publications, ASCE. Manuscript was submitted for review for possible publication on March 11, 1980. This paper is part of the Journal of the Engineering Mechanics Division, Proceedings of the American Society of Civil Engineers, ©ASCE, Vol. 107, No. EM2, April, 1981. ISSN 0044-7951/81/0002-0323/$01.00.

torsional response of symmetric as well as nonsymmetric buildings. A more thorough historical review of the subject may be found in Ref. 11.

In this paper, a methodology for analyzing the torsional vibration of wind excited structures is presented. The method is based on random vibration concepts and yields the expected maximum translational and torsional responses. The responses of several single-mass structures are investigated. The goals of this research were twofold. The first objective was to develop a model for analyzing the torsional response of structures that paralleled those used for analyzing along-wind responses. Thus the approach would have the advantage both of being firmly founded on the existing body of knowledge regarding wind structure and its effects, and of being easily adopted by engineers familiar with current methods. The second objective was to investigate the response of several simple structures in order to identify which wind and structural properties significantly influence the torsional response and to determine whether the predicted torsional

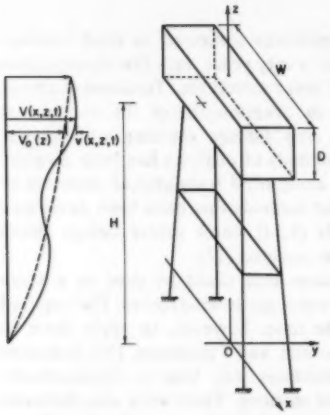

FIG. 1.—Schematic View of Problem

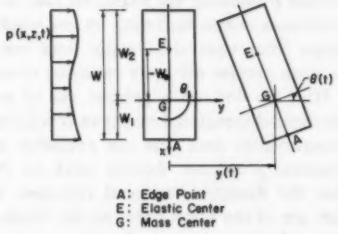

FIG. 2.—Geometry of Problem

responses were large enough to warrant extending the method to building-type structures for use in design. The results clearly indicate that torsional vibration can contribute a significant amount to the total motion of a wind-excited structure.

Governing Equations

Consider the schematic of an idealized single-mass structure with approaching wind shown in Fig. 1. For the coordinate system located at the mass center and for the notation shown in Fig. 2, the equations of motion of the system may be written

$$m\ddot{y} + C_y\dot{y} + k_y y + k_y W_e\theta = F(t) \quad \ldots\ldots\ldots\ldots\ldots\ldots\ldots\ldots (1)$$

$$I_m\ddot{\theta} + C_\theta\dot{\theta} + k_y W_e y + (k_\theta + k_y W_e^2)\theta = T(t) \quad \ldots\ldots\ldots\ldots\ldots\ldots (2)$$

in which $F(t)$ and $T(t)$ = respectively, the random fluctuating force and torque that act on the structure; and k_y and k_θ = respectively, the structure's translational and rotational stiffness with respect to the elastic center. In general, the equations of motion are coupled. In addition, it will be shown that $F(t)$ and $T(t)$ may be correlated. Since $F(t)$ and $T(t)$ are random variables in space and time, the dynamic responses $y(t)$ and $\theta(t)$ will also be random variables.

In the frequency domain the force-response relationships may be written

$$[S_o(n)] = [H(n)]\,[S_i(n)]\,[H^*(n)]^T \quad \ldots\ldots\ldots\ldots\ldots\ldots\ldots\ldots\ldots\ldots (3)$$

in which $[H(n)]$ = the system transfer function; and $[S_i(n)]$ and $[S_o(n)]$ = respectively, the spectral density matrices of the random forces and the system responses.

The derivation of the system transfer function (sometimes called the mechanical admittance or frequency response function) is well known and may be written

$$[H(n)] = \begin{bmatrix} H_{yy}(n) & H_{y\theta}(n) \\ H_{\theta y}(n) & H_{\theta\theta}(n) \end{bmatrix} = \{-\omega^2\,[M] + i\omega\,[C] + [K]\}^{-1} \quad \ldots\ldots (4)$$

in which $[M]$, $[C]$, and $[K]$ = respectively, the system mass, damping, and stiffness matrices; and $\omega = 2\pi n$. Since all of the elements of $[H(n)]$ are readily determined from the properties of the structure, one needs only to derive the elements of the input spectral density matrix to be able to determine the spectral density matrix of the response. Although the relationships for the translational vibrations are well known, they will be included in the following derivations for completeness.

Wind Forces on Structures

The wind velocity, $V(x, z, t)$, may be assumed to be composed of the sum of its mean and fluctuating parts:

$$V(x, z, t) = V_o(z) + v(x, z, t) \quad \ldots\ldots\ldots\ldots\ldots\ldots\ldots\ldots\ldots\ldots (5)$$

in which $v(x, z, t)$ is considered to be a zero mean, normally distributed stationary random process. Neglecting terms that contain derivatives of the wind velocity, it is further assumed that the pressure at a point on the structure's face is given by

$$P(x, z, t) \approx \frac{1}{2}\rho\, C_p\,[V_o(z) + v(x, z, t)]^2 \quad \ldots\ldots\ldots\ldots\ldots\ldots (6)$$

in which ρ = the density of air; and C_p = a pressure coefficient. Since the fluctuating part of the velocity is small compared to its mean, the fluctuating pressure on the face of the structure may be approximated

$$p(x, z, t) \cong \rho C_p\, V_o(z)\, v(x, z, t) \quad \ldots\ldots\ldots\ldots\ldots\ldots\ldots\ldots\ldots (7)$$

These fluctuating pressures produce the randomly varying force and torque

$$F(t) \cong \rho\, C_D \iint_A V_o(z)\, v(x, z, t)\, dx dz \quad \ldots\ldots\ldots\ldots\ldots\ldots\ldots (8)$$

and $$T(t) = \rho C_D \iint_A x\, V_o(z)\, v(x, z, t)\, dxdz \quad \ldots\ldots\ldots\ldots\ldots\ldots (9)$$

in which C_D = the sum of the averaged pressure coefficients of the windward and leeward faces. The use of C_D in this manner implies that the pressure fluctuations on the windward and leeward faces are perfectly correlated. Even though experiments have suggested that this assumption is not usually true (9), it results in conservative estimates of displacements (12), it greatly simplifies the following derivations, and it is probably not unwarranted in light of all the other assumptions that are made. It is also implied in Ref. 9 that pressures on the across-wind faces produce negligible torque. This would normally be true if the along-wind dimension of the structure is small compared to its width and if the structure's stiffness and mass are symmetric about its x axis.

The entries in the 2×2 spectral density matrix of the forces are $S_{FF}(n)$, $S_{TT}(n)$ and the cross spectra, $S_{FT}(n)$, which are respectively the Fourier transforms of the correlation functions of the force and torque and of their cross-correlation function. These may be written in terms of the cross spectra of the fluctuating velocity

$$S_{FF}(n) = (\rho C_D)^2 \iint_A \iint_A V_o(z_1)\, V_o(z_2)\, S_u(x_1, z_1, x_2, z_2, n)\, dx_1\, dz_1\, dx_2\, dz_2 \quad \ldots (10)$$

$$S_{TT}(n) = (\rho C_D)^2 \iint_A \iint_A x_1 x_2\, V_o(z_1)\, V_o(z_2)\, S_u(x_1, z_1, x_2, z_2, n)\, dx_1\, dz_1\, dx_2\, dz_2 \quad (11)$$

$$S_{FT}(n) = (\rho C_D)^2 \iint_A \iint_A x_2\, V_o(z_1)\, V_o(z_2)\, S_u(x_1, z_1, x_2, z_2, n)\, dx_1\, dz_1\, dx_2\, dz_2 \quad (12)$$

Based on experimental evidence, the cross spectra of the wind velocity may be written as the product of the spectrum of the wind velocity and the coherence function (14)

$$S_u(x_1, z_1, x_2, z_2, n) = [S_u(n)] \exp - \left\{ \frac{2n\,[C_x^2(x_1 - x_2)^2 + C_z^2(z_1 - z_2)^2]^{1/2}}{V_o(z_1) + V_o(z_2)} \right\} \quad \ldots\ldots\ldots (13)$$

in which C_x and C_z = the exponential decay coefficients for the x and z directions respectively. Using Davenport's velocity spectrum (2)

$$S_u(n) = \left(\frac{4K V_{33}^2}{n} \right) \frac{X^2}{(1 + X^2)^{4/3}} \quad \ldots\ldots\ldots\ldots\ldots\ldots\ldots\ldots (14)$$

in which $$X = \frac{4000\, n}{V_{33}} \quad \ldots\ldots\ldots\ldots\ldots\ldots\ldots\ldots\ldots\ldots (15)$$

Simiu (12) proposed an equation for the wind spectrum that is believed to be better founded in theory. However, Eqs. 14 and 15 have been more commonly used. It should be pointed out that this paper is concerned primarily with the relative magnitudes of the along-wind and torsional vibrations. Consequently,

the influence of the various assumptions regarding the velocity spectrum and the pressure correlations on the results should be minimal since their effects should be roughly equal for both types of response. A thorough analysis of most of the assumptions and approximations used in analyzing the response of buildings to wind loadings may be found in Ref. 13.

Thus far, the development of the random wind forces on a structure has been general and would apply to any structure that is rectangular in plan. The computations may be greatly simplified for the simple two-degree-of-freedom structure of Fig. 1. Since the mean wind velocity varies slowly with height

$$V_o(z_1) = V_o(z_2) = V_o(H) = V_o \quad \ldots\ldots\ldots\ldots\ldots\ldots\ldots\ldots \quad (16)$$

in which H = the height to the center of the structure. Thus the mean static force on the structure is

$$F_o = \frac{1}{2}\rho\, C_D\, V_o^2\, WD \quad \ldots\ldots\ldots\ldots\ldots\ldots\ldots\ldots \quad (17)$$

in which W = the width; and D = the depth of the structure. Using the relationships presented, Eqs. 10–12 may be written

$$S_{FF}(n) = \frac{4F_o^2}{V_o^2} S_u(n) \mathcal{J}_{yy}(n) \quad \ldots\ldots\ldots\ldots\ldots\ldots\ldots\ldots \quad (18)$$

$$S_{TT}(n) = \frac{4F_o^2 W^2}{V_o^2} S_u(n) \mathcal{J}_{\theta\theta}(n) \quad \ldots\ldots\ldots\ldots\ldots\ldots\ldots\ldots \quad (19)$$

$$S_{FT}(n) = \frac{4F_o^2 W}{V_o^2} S_u(n) \mathcal{J}_{y\theta}(n) \quad \ldots\ldots\ldots\ldots\ldots\ldots\ldots\ldots \quad (20)$$

in which $\mathcal{J}_{yy}(n)$, $\mathcal{J}_{\theta\theta}(n)$, and $\mathcal{J}_{y\theta}(n)$ = the nondimensional aerodynamic admittance functions which are derived as follows. The spectral density matrix of the excitation is now defined and Eq. 3 becomes

$$\begin{bmatrix} S_{yy} & S_{y\theta} \\ S_{\theta y} & S_{\theta\theta} \end{bmatrix} = \begin{bmatrix} H_{yy} & H_{y\theta} \\ H_{\theta y} & H_{\theta\theta} \end{bmatrix} \cdot \frac{4F_o^2 S_u(n)}{V_o^2}$$

$$\cdot \begin{bmatrix} \mathcal{J}_{yy} & W\mathcal{J}_{y\theta} \\ W\mathcal{J}_{\theta y} & W^2\mathcal{J}_{\theta\theta} \end{bmatrix} \cdot \begin{bmatrix} H_{yy}^* & H_{y\theta}^* \\ H_{\theta y}^* & H_{\theta\theta}^* \end{bmatrix}^T \quad \ldots\ldots\ldots\ldots\ldots\ldots \quad (21)$$

in which all of the S, H, and $\mathcal{J}$ terms are functions of frequency, n.

Aerodynamic Admittance Functions

If nondimensional variables $\epsilon = x/W$ and $n = z/D$ are defined, the explicit forms of the aerodynamic admittance functions used in Refs. 18–20 become

$$\mathcal{J}_{yy}(n) = \int_0^1 \int_0^1 \int_{-W_2/W}^{W_1/W} \rho(\epsilon_1, \epsilon_2, \eta_1, \eta_2)\, d\epsilon_1\, d\epsilon_2\, d\eta_1\, d\eta_2 \quad \ldots\ldots\ldots \quad (22)$$

$$\mathcal{J}_{\theta\theta}(n) = \int_0^1 \int_0^1 \int_{-W_2/W}^{W_1/W} \epsilon_1 \epsilon_2 \rho(\epsilon_1, \epsilon_2, \eta_1, \eta_2)\, d\epsilon_1\, d\epsilon_2\, d\eta_1\, d\eta_2 \quad \ldots\ldots\ldots \quad (23)$$

$$\mathscr{J}_{y\theta}(n) = \int_0^1 \int_0^1 \int_{-W_2/W}^{W_1/W} \epsilon_2\, \rho(\epsilon_1, \epsilon_2, \eta_1, \eta_2)\, d\epsilon_1\, d\epsilon_2\, d\eta_1\, d\eta_2 \quad \ldots\ldots (24)$$

in which $\epsilon = \frac{x}{W}$, $\eta = \frac{z}{D}$ . . . . . (25)

and $\rho(\epsilon_1, \epsilon_2, \eta_1, \eta_2)$

$$= \exp\left\{-\frac{n}{V_o}\left[C_x^2 W^2(\epsilon_1 - \epsilon_2)^2 + C_z^2 D^2(\eta_1 - \eta_2)^2\right]\right\}^{1/2} \quad \ldots\ldots (26)$$

In general, the evaluation of the admittance functions requires four-fold numerical integration. However, these may be evaluated analytically if we use the approximation suggested by Davenport (4):

$$\rho(\epsilon_1, \epsilon_2, \eta_1, \eta_2) = \exp\left[-\frac{n\phi}{V_o}(C_x W|\epsilon_1 - \epsilon_2| + C_z D|\eta_1 - \eta_2|)\right] \quad \ldots\ldots (27)$$

in which $\phi = \frac{\sqrt{1 + r^2}}{1 + r}$ . . . . . (28)

and $r = \frac{C_x W}{C_z D}$ . . . . . (29)

Performing the integrations yields the following analytical expressions for the aerodynamic admittance functions:

$$\mathscr{J}_{yy}(n) = \frac{2}{D_x^2}(e^{-D_x} + D_x - 1)\left[\frac{2}{D_z^2}(e^{-D_z} + D_z - 1)\right] \quad \ldots\ldots (30)$$

$$W^2 \mathscr{J}_{\theta\theta}(n) = \left[\frac{2}{3D_x}(W^2 - 3W_1 W_2) - \frac{1}{D_x^2}(W_1^2 + W_2^2) + \frac{2W^2}{D_x^4}\right.$$

$$\left. - \frac{2}{D_x^4}(W^2 + D_x W^2 + D_x^2 W_1 W_2)\, e^{-D_x}\right]\left[\frac{2}{D_z^2}(e^{-D_z} + D_z - 1)\right] \quad \ldots\ldots (31)$$

$$W\mathscr{J}_{y\theta}(n) = \frac{(W1 - W2)}{2}\mathscr{J}_{yy}(n) \quad \ldots\ldots (32)$$

in which $D_x = \frac{n C_x W}{V_o}$ . . . . . (33)

and $D_z = \frac{n C_z D}{V_o}$ . . . . . (34)

The aerodynamic admittance function for translation, Eq. 30, was developed previously by Davenport (1). These functions make possible the direct computation of the complete spectral density matrix of the structure's response. It will be demonstrated that this is required for an accurate estimate of the expected maximum structural deformations. These equations will be considered as follows with regard to a specific example.

Maximum Value of Structural Response

Once the functions of the spectral density matrix of the response have been formulated, the mean-square translational and rotational motions as well as their correlation coefficient may be computed

$$\sigma_y^2 = \int_0^\infty S_{yy}(n)\, dn \quad \ldots\ldots (35)$$

$$\sigma_\theta^2 = \int_0^\infty S_{\theta\theta}(n)\, dn \quad \ldots\ldots (36)$$

$$\text{and} \quad \rho_{y\theta} = \frac{E\,[y(t)\theta(t)]}{\sigma_y\,\sigma_\theta} = \frac{\int_0^\infty s_{y\theta}(n)\, dn}{\sigma_y\,\sigma_\theta} \quad \ldots\ldots (37)$$

Note that since $F(t)$ and $T(t)$ have been defined as zero-mean random forces, the responses y and θ also have zero mean values.

If it is assumed that the total displacement of a point on the structure, $Y(x, z, t)$, is independent of height, z, the translation of any point may be written

$$Y(x, z, t) = Y(x, t) = Y_o(x) + y(t) + x\,\theta(t) \quad \ldots\ldots (38)$$

in which $Y_o(x)$ = the displacement of the point due to the static mean wind force, i.e.:

$$Y_o(x) = Y_o + x\theta_o \quad \ldots\ldots (39)$$

in which Y_o = the mean displacement of the coordinate center; and θ_o = the mean rotation. The rms displacement of any point is

$$\sigma_Y^2(x) = \int S_Y(x, n)\, dn \quad \ldots\ldots (40)$$

in which $S_Y(x, n)$ = the spectral density function of the total response

$$S_Y(x, n) = S_{yy}(n) + x^2\, S_{\theta\theta(n)} + 2x\ \text{Real}\ [S_{y\theta}(n)] \quad \ldots\ldots (41)$$

The expected maximum value of Y in a time interval T (usually assumed to be one hour) can be written

$$Y_{\max}^{(x)} = Y_o(x) + g\sigma_Y(x) \quad \ldots\ldots (42)$$

in which g = a peak factor developed by Davenport (3), and is approximately equal to

$$g = \sqrt{2 \ln \nu T} + \frac{0.577}{\sqrt{2 \ln (\nu T)}} \quad \ldots\ldots (43)$$

$$\text{in which} \quad \nu = \frac{\int_0^\infty n^2 S_Y(x, n)\, dn}{\int_0^\infty S_Y(x, n)\, dn} \quad \ldots\ldots (44)$$

Thus, an estimate of the most probable maximum displacement including torsion of any point on the structure can be made.

Numerical Examples

The equations derived were used to analyze the responses of several variations of the structure in Fig. 1. The basic structure has a width, W, equal to 20 ft (6.1 m) and a depth, D, equal to 20 ft (6.1 m) for an exposure area of 400 sq ft (37.2 m^2). The reference wind velocity of 80 miles/h (129 km/h) and the translational natural frequency, n_y, of 1.0 H_z were held constant for all examples. The effects of magnitude of the torsional natural frequency, the structure's width, and the location of the centers of mass and rigidity on the

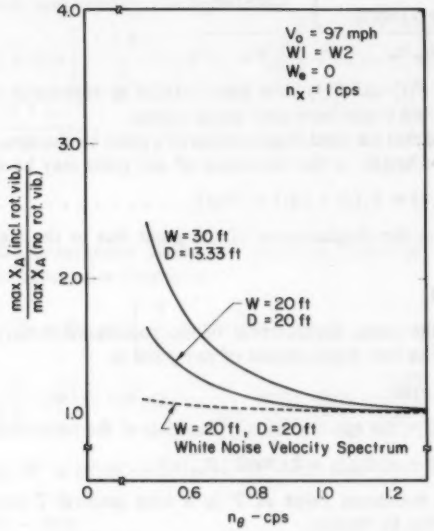

FIG. 3.—Rotational Vibration of Symmetric Structures

maximum probable response values were examined. For each example where the structure is nonsymmetric, the expected maximum edge displacement, max Y_A, computed using Eq. 42 is normalized by the expected maximum displacement that would be computed if the dynamic torsional motion were ignored. The latter quantity is simply the expected maximum along-wind displacement for the center of a symmetric structure plus the displacement due to the static rotation, $x\theta_o$. The normalization was done this way because designers would normally compute the mean rotation in their calculations. Thus, the results reflect the consequence of ignoring only the dynamic torsional response in design.

The examples may be divided into three classes according to the form of Eq. 21. For a perfectly symmetric structure the centers of mass and resistance

both lie on the vertical center line of the structure's face. For this case all of the off-diagonal terms in Eq. 21 are identically equal to zero. Thus, the equations of motion are uncoupled. This means that the translational and rotational motions are statistically independent and thus may be evaluated independently. Note that torsional vibrations will still be excited, however, due to the spatial randomness of the wind.

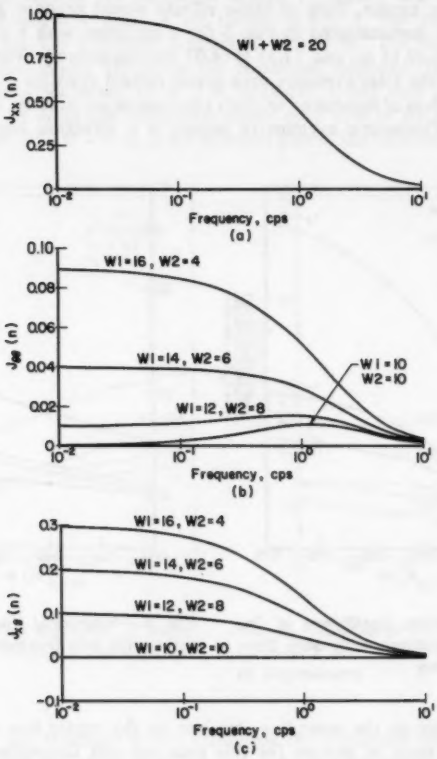

FIG. 4.—Aerodynamic Admittance Functions: (*a*) Translation; (*b*) Torsion; and (*c*) Cross

The effects of varying the structure's torsional natural frequency on the expected maximum displacement of point A are shown in Fig. 3. As n_θ decreases with respect to n_y, the motions at the edge of the structure due to torsional vibrations become large and may actually be substantially larger than those due to translation. Most of the effect associated with lowering the torsional frequency results from the shape of the wind spectrum which increases with

decreasing frequency in this region of the spectrum. This is also demonstrated in Fig. 3 where results are shown for the 20 ft × 20 ft (6.1 m × 6.1 m) structure which was assumed to be excited by an artificial wind with a "white noise" spectrum, but with the same spatial correlation as the natural wind.

It should also be expected that increasing the width of the structure would increase the rotational response. This should result because pressures at the extreme edges of the structure would be less correlated and would lie further from the elastic center. Both of these effects would produce greater dynamic torque. This is demonstrated in Fig. 3 for a structure with a width and depth equal to 30.0 ft (9.15 m) and 13.33 ft (4.07 m) respectively. These values were chosen so that the total exposure area would remain constant.

The second class of structures has only one type of asymmetry, either geometric or structural. Geometric asymmetry occurs if a structure has its centers of

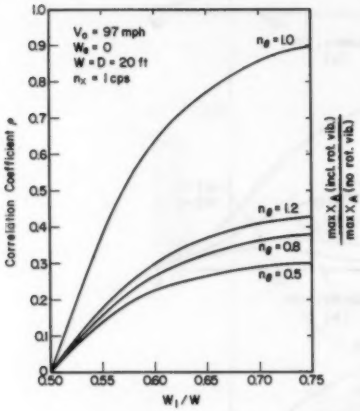

FIG. 5.—Correlation Coefficient of Responses of Structures with only Geometric Asymmetry

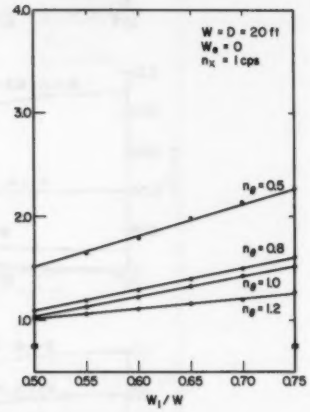

FIG. 6.—Rotational Vibration of Structures with only Geometric Asymmetry

mass and rigidity on the same line, but not on the center line of the exposed face. The equations of motion for this case are still uncoupled, e.g., $H_{y\theta} = H_{\theta y} = 0$. However, the cross aerodynamic admittance functions, $\mathcal{J}_{y\theta}$ and $\mathcal{J}_{\theta y}$, are no longer zero. Therefore, the correlation coefficient for the responses is also nonzero and coupling of the responses results. The aerodynamic admittance functions for 20 ft × 20 ft (6.1 m × 6.1 m) structures with their center of the coordinate system located 10 ft, 12 ft, 14 ft and 16 ft (3.05 m, 3.66 m, 4.27 m, and 4.88 m) from point A are shown in Fig. 4. Note that $\mathcal{J}_{yy}$ is invariant with respect to the coordinate center and that $\mathcal{J}_{\theta\theta}$ and $\mathcal{J}_{y\theta}$ increase as the geometric offset increases. Thus, the correlation coefficient is coordinate-system dependent. Also, as was previously mentioned, $\mathcal{J}_{y\theta}(n)$ is identically equal to zero for W_1 = 10 ft (3.05 m) which corresponds to the coordinate system

located at the geometric center of the structure. The correlation coefficients for these same structures with varying torsional frequency are shown in Fig. 5. The highest correlation in the responses occurs when $n_\theta = n_y$ as should be expected. This value approaches 1.0 as the geometric offset increases. In general, the response correlation increases as n_θ approaches n_y and as W_1/W increases.

The effects of varying the rotational natural frequency and W_1/W on the maximum displacement at point A are shown in Fig. 6. The results show the same trend as for the perfectly symmetric structures. The torsional natural frequency has the largest effect on the rotational response. In addition, the rotational response increases as W_1/W increases. Note that for a structure with its centers of mass and resistance offset only 10% of its width from the geometric center ($W_1/W = 0.6$), if the dynamic part of the torsional displacement

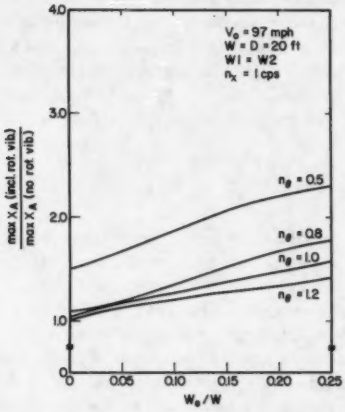

FIG. 7.—Rotational Vibration of Structures with only Structural Asymmetry

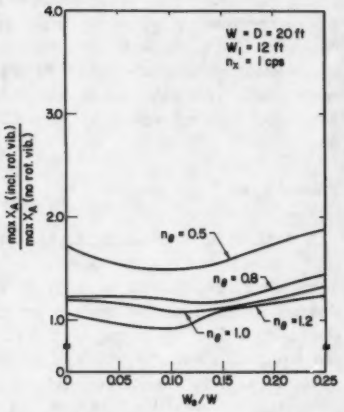

FIG. 8.—Rotational Vibration of Structures with both Structural and Geometric Asymmetry

of the edge of the structure is not computed the maximum displacement will be underestimated by about 25% for $n_\theta = n_y$ and by about 80% for $n_\theta = 0.5\ n_y$. It might be expected that the highest responses would result for $n_\theta = n_y$ since the force and torque are more highly correlated for this case. However, the lower correlation between the force and torque for structures with $n_\theta < n_y$ is overshadowed by the fact that the spectrum of the torque is higher at the lower frequencies.

If the mass center is located at the structure's geometric center but the elastic center is not, structural nonsymmetry results and $H_{y\theta}(n)$ is no longer zero. The cross-aerodynamic admittance functions will again be zero, however, since the reference system is located at the geometric center of the structure. Results for structures with different torsional frequencies and eccentricities are shown

in Fig. 7. These results are very similar to those for structures with only geometric nonsymmetry shown in Fig. 6. Neglecting the dynamic part of the torsional displacement for a structure with an eccentricity of 10% of its width will once more lead to underestimates of the maximum total displacement of 25% for $n_\theta = n_y$ and 80% for $n_\theta = 0.5\, n_y$.

The most general case occurs when the centers of mass, resistance, and geometry lie on different lines. This results in all of the matrices of Eq. 21 being full. Shown in Fig. 8 are the results for structures with their mass center offset 10% of the structure's width [W_1 = 12 ft (3.66 m)] from its geometric center. As expected, these motions increase with decreasing torsional natural frequency. Fig. 8 is somewhat misleading since it shows decreasing torsional response with increasing eccentricity for W_e/W less than 0.1. In this region, the elastic center moves from the mass center for $W_e/W = 0$ to the geometric center for $W_e/W = 0.1$. The fact that the torsional motion decreases in this region indicates the distance between the elastic center and the geometric center where the average pressure center lies is more influential than the distance between the elastic and mass centers. For a structure with W_e = 2 ft (0.61 m) the elastic center is at the geometric center. By ignoring the dynamic torsional response for this case, the maximum displacement of the edge of the structure would be underestimated by about 25% for $n_\theta = n_y$ and 50% for $n_\theta = 0.5\, n_y$.

Summary and Conclusions

A method for estimating the expected maximum dynamic torsional response of a wind-excited two degree-of-freedom structure was presented. Aerodynamic admittance functions were derived which were used to estimate the spectral density function of the random torque and cross-spectral density function of the force and torque acting on the structure. These are required for estimating the structure's translational and torsional mean square responses. Results for several examples indicated that, in general, the dynamic torsional response increases as the width of the structure's exposed face increases, as the structural or geometric eccentricity increases, and as the torsional natural frequency decreases. It was shown that for an eccentricity of only 10% of the structure's width, the total response of a structure can be significantly underestimated if the dynamic torsional response is not included in the analysis. The results in Figs. 6–8 suggest that an approximately linear relationship exists between the torsional dynamic response and the eccentricity. If this is true for the full three-dimensional problems, simple design rules could result.

General design rules were not derived from these results since the structures studied were simple and limited in number. The results do indicate, however, that torsional vibrations may be a problem in real structures. Consequently, the writers are extending the procedures developed in this paper to three-dimensional building-type structures and will include across-wind forces in the analysis. In addition to the effects of higher modes of vibration and of pressure correlations along the full height of the structure, the influence of assumptions regarding the shape of the design wind spectrum and the form of the along-wind and cross-wind pressure correlation functions on the torsional response of buildings will be investigated.

Acknowledgment

This research was partially funded by the National Science Foundation under grant NSF ENV 77-07190 and by the University of Illinois at Urbana-Champaign. This support is gratefully acknowledged. The reading of the manuscript by D. A. Pecknold and Y. K. Wen is also appreciated. The results of this study were summarized in Ref. 5.

Appendix I.—References

1. Davenport, A. G., "Gust Loading Factors," *Journal of the Structural Division*, ASCE, Vol. 93, No. ST3, Proc. Paper 5255, June, 1967, pp. 11–34.
2. Davenport, A. G., "The Spectrum of Horizontal Gustiness Near the Ground in High Winds," *Quarterly Journal of the Royal Meteorological Society*, Vol. 87, London, England, 1961.
3. Davenport, A. G., "The Distribution of Largest Values of a Random Function with Application to Gust Loading," *Proceedings of the Institute of Civil Engineering*, Vol. 28, 1964, pp. 187–196.
4. Davenport, A. G., "The Prediction of the Response of Structures to Gusty Wind," International Seminar of the Safety of Structures under Dynamic Loading," Vol. 1, Norwegian Institute of Technology, June, 1977, pp. 257–284.
5. Foutch, D. A., and Safak, E., "Torsional Vibration of Wind-Excited Structures," *Proceedings*, 3rd ASCE/EMD Specialty Conference, Sept., 1979, pp. 255–258.
6. Foutch, D. A., and Safak, E., "Torsional Vibration of Wind-Excited Symmetric Structures," *Journal of Wind Engineering and Industrial Aerodynamics*, Vol. 7, No. 2, Mar., 1981, pp. 191–201.
7. Hart, G. C., "Building Dynamics Due to Stochastic Wind Forces," *Journal of the Structural Division*, ASCE, Vol. 96, No. ST3, Proc. Paper 7154, Mar., 1970, pp. 535–550.
8. Hart, G. C., DiJulio, R. M., Jr., and Lew, M., "Torsional Response of High-Rise Buildings," *Journal of the Structural Division*, ASCE, Vol. 101, No. ST2, Proc. Paper 11126, Feb., 1975, pp. 397–416.
9. Lam Put, R., "Dynamic Response of a Tall Building to Random Wind Loads," *Proceedings*, International Conference on Wind Effects on Buildings and Structures, 1971, pp. III, 4.1.11.
10. Patrickson, C. P., and Friedmann, R., "A Study of the Coupled Lateral and Torsional Response of Tall Buildings to Wind Loadings," *UCLA-ENG-76126*, University of California at Los Angeles, School of Engineering and Applied Science, Dec., 1976.
11. Safak, E., and Foutch, D., "Vibration of Buildings under Random Wind Loads," *Structural Research Series No. 480*, Civil Engineering Studies, University of Illinois, Urbana, Ill., May, 1980.
12. Simiu, E., "Wind Spectra and Dynamic Alongwind Response," *Journal of the Structural Division*, ASCE, Vol. 100, No. ST9, Proc. Paper 10815, Sept., 1974, pp. 1897–1910.
13. Simiu, E., and Marshall, R. D., "Wind Loadings and Modern Building Codes," presented at the April 22–26, 1974, ASCE National Structural Engineering Meeting, held at Cincinnati, Ohio (Preprint 2268).
14. Vickery, B. J., "On the Reliability of Gust Loading Factors," *Civil Engineering Transactions*, Apr., 1971, pp. 1–9.

Appendix II.—Notation

The following symbols are used in this paper:

A = wind exposure area, $W \times D$;
C_D = drag coefficient;
C_p = pressure coefficient;

C_x, C_z = exponential decay coefficients;
c_y, c_θ = viscous damping values;
D = depth of structure;
D_x, D_z = defined in Eqs. 33 and 34;
$E[\ ]$ = ensemble average;
F_o = mean wind force;
$F(t)$ = fluctuating total wind force;
g = peak factor defined in Eq. 43;
H = height to center of structure's exposure area;
$[H(n)]$ = system transfer function;
I_m = mass moment of inertia;
$\mathcal{J}_{yy}(n), \mathcal{J}_{\theta\theta}(n), \mathcal{J}_{y\theta}(n)$ = translational, rotational, and cross-aerodynamic admittance functions;
K = surface drag coefficient;
k_y, k_θ = translational and rotational stiffness;
m = mass;
n = frequency, in cycles per second;
$P(x, z, t)$ = total wind pressure;
$p(x, z, t)$ = fluctuating wind pressure;
r = defined in Eq. 29;
$S_{FF}(n), S_{TT}(n), S_{FT}(n)$ = spectrum of fluctuating force, torque, and cross spectrum;
$[S_i(n)], [S_o(n)]$ = spectral density matrices of force and response;
$S_u(x), S_u(x_1, z_1, x_2, z_2, n)$ = spectrum and cross spectrum of fluctuating wind velocity;
$S_Y(x, n)$ = spectrum of total response;
$S_{yy}(n), S_{\theta\theta}(n), S_{y\theta}(n)$ = spectrum of dynamic translation, rotation, and cross spectrum;
T = averaging time interval;
$T(t)$ = fluctuating torque;
V_{33} = reference mean wind velocity at height of 33 ft;
V_o = mean wind velocity at center of structure;
$V(x, z, t)$ = total wind velocity at point x, z, t;
$v(x, z, t)$ = fluctuating wind velocity at point x, z, t;
W = width of structure;
$W1, W2$ = distances from mass center to edges;
W_e = distance between mass center and elastic center;
X = defined in Eq. 15;
x = cross-wind direction coordinate axis;
$Y(x, z, t)$ = total displacement at height z;
$Y(x, t)$ = total displacement at center height;
$Y_o(x)$ = mean displacement;
Y_o = mean displacement at center;
$Y_{\max}(x)$ = maximum probable displacement;
y = along-wind coordinate axis;
$y(t)$ = along-wind dynamic displacement;
z = vertical coordinate axis;
ϵ = x/W;
η = z/D;

θ_o = mean rotation;
$\theta(t)$ = dynamic rotation;
ω = frequency, in radians per second;
ρ = density of air;
$\rho(\epsilon_1, \epsilon_2, \eta_1, \eta_2)$ = coherence function, defined in Eq. 26;
$\rho_{y\theta}$ = correlation coefficient;
σ_y, σ_θ = root-mean-square response for translation and rotation;
$\sigma_Y(x)$ = root-mean-square of total displacement;
ϕ = coefficient given in Eq. 28; and
ν = coefficient given in Eq. 44.

JOURNAL OF
THE ENGINEERING
MECHANICS DIVISION

NATURAL FREQUENCIES OF CURVED GIRDERS

By Chai Hong Yoo,[1] M. ASCE and Jon P. Fehrenbach,[2] A. M. ASCE

INTRODUCTION

Curved girders are used frequently in highway bridge structures. With the application of digital computers and the development of numerical methods, the mathematical difficulties associated with curved beam elements have been largely overcome.

Extensive work has been published concerning the behavior of horizontally curved members, as summarized by McManus, et al. (14). These investigations are primarily concerned with the analysis of curved beams subjected to static loadings. However, comparatively little work has been done regarding the dynamic response of curved beams. The free vibration of a circular ring has been studied by Love (13) and Timoshenko (24), among others (15). Culver (6) and Chaudhuri and Shore (5) studied the free vibration of horizontally curved beams. Practically all of these previous papers lack generality; some are limited to in-plane vibration, while others are restricted to doubly-symmetric sections or out-of-plane vibration only.

The purpose of this paper is to derive a general matrix formulation to determine the natural frequencies of spatial curved beams as shown in Fig. 1, including the warping contribution. Also included are the rotary inertia effects with respect to flexure and torsion, and the effects of antisymmetry of cross sections, which were found to be important.

GOVERNING DIFFERENTIAL EQUATIONS

The equations of equilibrium in terms of linearized componental deformations for the free vibration of spatially curved beams projected on coordinate axes

[1]Assoc. Prof. of Civ. Engrg., Marquette Univ., 1515 West Wisconsin Ave., Milwaukee, Wisc. 53233.

[2]Structural Engr., Boeing Commercial Airplane Co., Seattle, Wash.

Note.—Discussion open until September 1, 1981. To extend the closing date one month, a written request must be filed with the Manager of Technical and Professional Publications, ASCE. Manuscript was submitted for review for possible publication on March 18, 1980. This paper is part of the Journal of the Engineering Mechanics Division, Proceedings of the American Society of Civil Engineers, ©ASCE, Vol. 107, No. EM2, April, 1981. ISSN 0044-7951/81/0002-0339/$01.00.

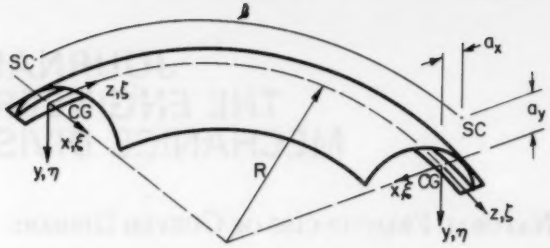

FIG. 1.—Thin-Walled Curved Beam Coordinates

as shown in Fig. 1 can be written (25)

$$-\frac{EI_y}{R}\left(\xi''' + \frac{\xi'}{R^2}\right) - EA\left(\zeta'' - \frac{\xi'}{R}\right) = -\rho A\ddot{\zeta} \quad \ldots\ldots\ldots\ldots\ldots\ldots (1a)$$

$$EI_y\left(\xi^{iv} + \frac{\xi''}{R^2}\right) - \frac{EA}{R}\left(\zeta' - \frac{\xi}{R}\right) = -\rho A(\ddot{\xi} + a_y\ddot{\phi})$$

$$+ \rho I_y\left(\ddot{\xi}'' + \frac{\ddot{\xi}}{R^2}\right) \quad \ldots\ldots\ldots\ldots\ldots\ldots\ldots\ldots\ldots\ldots (1b)$$

$$E\left(\frac{I_w}{R^2} + I_x\right)\eta^{iv} - \frac{GK_T}{R^2}\eta'' + \frac{EI_w}{R}\phi^{iv} - (EI_x + GK_T)\frac{\phi''}{R}$$

$$= -\rho A(\ddot{\eta} - a_x\ddot{\phi}) + \rho I_x\left(\ddot{\eta}'' - \frac{\ddot{\phi}}{R}\right) \quad \ldots\ldots\ldots\ldots\ldots\ldots (1c)$$

$$\frac{EI_w}{R}\eta^{iv} - (EI_x + GK_T)\frac{\eta''}{R} + EI_w\phi^{iv} - GK_T\phi'' + \frac{EI_x}{R^2}\phi$$

$$= -\rho A(r_p^2\ddot{\phi} + a_y\ddot{\xi} - a_x\ddot{\eta}) + \rho I_w\left(\ddot{\phi}'' + \frac{\ddot{\eta}''}{R}\right) \quad \ldots\ldots\ldots\ldots\ldots (1d)$$

in which ζ = axial deformation in the direction of the circular axis, z; ξ and η = displacements in the direction of the principal x and y axes, respectively; ϕ = rotation about the shear center (primes denote derivatives with respect to the z axis, and dots represent derivatives with respect to time); E and G = elastic and shear moduli, respectively; ρ = mass density; r_p = polar radius of gyration with respect to the shear center; A = cross-sectional area; a_x and a_y = coordinates of the shear center taken from the centroid of the section; I_x and I_y = principal moments of inertia of the section; K_T = torsional constant; I_w = warping constant; R = radius of curvature of the circular axis; x and y = coordinates of the cross section; w = normalized sectorial coordinate; and x, y, and z make pointwise right-hand Cartesian coordinates.

The right-hand side terms in Eqs. 1*a* through 1*d* represent equivalent static loading according to D'Alembert's principle. Eqs. 1*a* and 1*b* are coupled in

terms of ζ and ξ and govern the behavior of the beam in axial deformation and bending about the y axis, usually the minor axis. Hence, the minor axis flexural behavior is affected by the extensibility of the member. Similarly, Eqs. 1*c* and 1*d* are coupled in terms of η and ϕ and describe the problem of flexure and torsion.

Minimum Potential Energy

The variation of the minimum potential energy functional for the curved beam can be obtained by modifying the expression obtained for a straight beam (9,11). The internal forces acting on the curved beam elements are

$$N_z = EA\left(\zeta' - \frac{\xi}{R}\right) \quad \ldots\ldots\ldots\ldots\ldots\ldots\ldots\ldots\ldots\ldots\ldots\ldots\ldots\ldots\ldots\ldots (2a)$$

$$M_y = EI_y\left(\xi'' + \frac{\xi}{R^2}\right) \quad \ldots\ldots\ldots\ldots\ldots\ldots\ldots\ldots\ldots\ldots\ldots\ldots\ldots\ldots\ldots\ldots (2b)$$

$$M_x = -EI_x\left(\eta'' - \frac{\phi}{R}\right) \quad \ldots\ldots\ldots\ldots\ldots\ldots\ldots\ldots\ldots\ldots\ldots\ldots\ldots\ldots\ldots\ldots (2c)$$

$$T_z = GK_T\left(\phi' + \frac{\eta'}{R}\right) \quad \ldots\ldots\ldots\ldots\ldots\ldots\ldots\ldots\ldots\ldots\ldots\ldots\ldots\ldots\ldots\ldots (2d)$$

$$T_w = -EI_w\left(\phi''' + \frac{\eta'''}{R}\right) \quad \ldots\ldots\ldots\ldots\ldots\ldots\ldots\ldots\ldots\ldots\ldots\ldots\ldots\ldots\ldots\ldots (2e)$$

$$BM = -EI_w\left(\phi'' + \frac{\eta''}{R}\right) \quad \ldots\ldots\ldots\ldots\ldots\ldots\ldots\ldots\ldots\ldots\ldots\ldots\ldots\ldots\ldots\ldots (2f)$$

in which N_z = axial force; M_x and M_y = internal bending moments about the x and y axes, respectively; T_z = St. Venant's torque; T_w = warping torque; and BM = bimoment.

Examining Eqs. 2 and the expression for the corresponding internal forces of the straight beam (25) reveals that deformations projected on coordinate axes of the curved beam are coupled, due only to the initial curvature. Thus, replacing the straight beam terms in the variation of the minimum potential energy functional for the straight beam with the corresponding curved beam terms (Eqs. 2) results in an expression of energy variation for the free vibration of a curved beam which is

$$\delta\Pi = \int_0^l \left\{ EA\left(\zeta' - \frac{\xi}{R}\right)\left[\delta(\zeta') - \frac{\delta\xi}{R}\right] + EI_y\left(\xi'' + \frac{\xi}{R^2}\right)\left[\delta(\xi'') + \frac{\delta\xi}{R^2}\right] + EI_x\left(\eta'' - \frac{\phi}{R}\right)\left[\delta(\eta'') - \frac{\delta\phi}{R}\right] + EI_w\left(\phi'' + \frac{\eta''}{R}\right)\left[\delta(\phi'') + \frac{\delta(\eta'')}{R}\right] + GK_T\left(\phi' + \frac{\eta'}{R}\right)\left[\delta(\phi') + \frac{\delta(\eta')}{R}\right] \right\} dz$$

$$+ \int_0^l \left\{ \rho A \left(\ddot{\zeta}\delta\zeta + \ddot{\xi}\delta\xi + \ddot{\eta}\delta\eta + r_\rho^2 \ddot{\phi}\delta\phi + a_y \ddot{\xi}\delta\phi - a_x \ddot{\eta}\delta\phi \right.\right.$$

$$\left. + a_y \ddot{\phi}\delta\xi - a_x \ddot{\phi}\delta\eta \right) - \rho \left[I_y \left(\ddot{\xi}'' + \frac{\ddot{\xi}}{R^2} \right) \delta\xi + I_x \left(\ddot{\eta}'' - \frac{\ddot{\phi}}{R} \right) \delta\eta \right.$$

$$\left.\left. + I_w \left(\ddot{\phi}'' + \frac{\ddot{\eta}''}{R} \right) \delta\phi \right] \right\} dz = J_0(0, l) \quad \ldots\ldots\ldots\ldots\ldots\ldots\ldots\ldots (3)$$

in which $J_0(0,1)$ is called the conjunct or concomitant, which is the sum of all integrated terms. For natural boundary conditions, the conjunct is equal to zero and the system is said to be self-adjoint.

Displacement Field

A general displacement field for the static behavior of a curved beam is assumed as (27)

$$\Delta = [\Delta_1 \Delta_2]^* \quad \ldots\ldots\ldots\ldots\ldots\ldots\ldots\ldots\ldots\ldots\ldots\ldots\ldots\ldots (4)$$

in which the asterisk denotes transposition. Each node rotates about three axes,

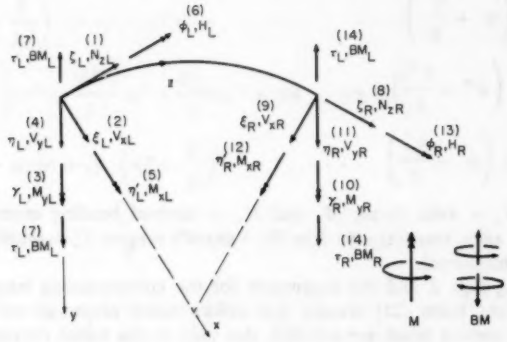

FIG. 2.—Generalized Forces and Displacements

undergoes displacements along these axes, and warps, for a total of seven degrees of freedom at each node, as shown in Fig. 2. In order to avoid unnecessary complication, the general displacement field is divided into Δ_1 and Δ_2 pertinent to the displacements associated with the two sets of coupled equations, Eqs. 1*a* and 1*b* and Eqs. 1*c* and 1*d*. Since these equations are coupled, there must be a coupled boundary condition in each set of equations. Introducing two kinematic boundary conditions (5), γ and τ, which are defined as

$$\gamma = \left(\xi' + \frac{\zeta}{R} \right) \quad \ldots\ldots\ldots\ldots\ldots\ldots\ldots\ldots\ldots\ldots\ldots\ldots\ldots\ldots (5)$$

and $$\tau = \left(\phi' + \frac{\eta'}{R}\right) \quad \ldots\ldots (6)$$

the subdisplacement fields can be written

$$\Delta_1 = [N_1]\{\Delta_1\} \quad \ldots\ldots (7)$$

$$\Delta_2 = [N_2]\{\Delta_2\} \quad \ldots\ldots (8)$$

in which $[N_1]$ and $[N_2]$ = matrices of shape functions as given by Yoo (27). The generalized displacements are chosen as nodal displacements, as shown in Fig. 2. Thus

$$\{\Delta_1\} = [\zeta_L \xi_L \gamma_L \zeta_R \xi_R \gamma_R]^* \quad \ldots\ldots (9)$$

and $$\{\Delta_2\} = [\eta_L - \eta'_L \phi_L - \tau_L \eta_R - \eta'_R \phi_R - \tau_R]^* \quad \ldots\ldots (10)$$

in which the subscripts L and R denote the left end and right end, respectively, of an element. The negative signs in Eq. 10 are due to the assumed positive directions of the corresponding degrees of freedom as shown in Fig. 2.

For the dynamic problem under consideration, a generalized displacement field is assumed as

$$\bar{\Delta}(t,z) = \sum_i q_i(t)\Delta_i(z) \quad \ldots\ldots (11)$$

in which $\Delta_i(z)$ = assumed displacement modes, i.e., the exact solutions of the coupled homogeneous differential equations governing the static behavior of the curved beam problem, Eq. 1. The unknown amplitudes of vibration may be defined as

$$q_i(t) = q_i \exp(i\omega t) \quad \ldots\ldots (12)$$

in which ω = angular velocity in radians per sec, and q_i is a Kroneckar delta, i.e., $q_i = 1$ and all other $q_j = 0$ (for $i \neq j$). Hence, the general displacement field for the dynamic problem can be

$$\bar{\Delta} = [q][N]\{\Delta\} \quad \ldots\ldots (13)$$

in which $\{\Delta\} = 14 \times 1$ column matrix representing the nodal degrees of freedom at both ends of an element, and $[N]$ = matrix of shape functions defining the elastic behavior of the structure. The shape functions are used for both the static and dynamic problems. Therefore, the static solutions are exact regardless of the grid refinement of the structural model; the dynamic solutions were found to be extremely fast converging upper bounds, as can be expected due to the use of the variational procedure.

Finite Element Discretization

Introducing the displacement field of Eq. 13, and noting that $\ddot{\bar{\Delta}} = -\omega^2\Delta$, Eq. 3 may be rewritten

$$[\delta\Delta][K_{ij}]\{\Delta\} - \omega^2[\delta\Delta][m_{ij}]\{\Delta\} = 0 \quad \ldots\ldots (14)$$

in which $[K_{ij}]$ and $[m_{ij}]$ = element stiffness and mass matrices, respectively,

of the element. The elements of the stiffness matrix, K_{ij}, are obtained from the first bracketed term of Eq. 3 and can be expressed as

$$K_{ij} = \int_0^l \left[EA \left(N'_{\xi i} - \frac{N_{\xi i}}{R} \right) \left(N'_{\zeta j} - \frac{N_{\xi j}}{R} \right) \right.$$

$$\left. + EI_y \left(N''_{\xi i} + \frac{N_{\xi i}}{R^2} \right) \left(N''_{\xi j} + \frac{N_{\xi j}}{R^2} \right) \right] dz \quad \text{(in which} \quad i, j = 1, 2, 3, 8, 9, 10)$$

$$+ \int_0^l \left[EI_x \left(N''_{\eta i} - \frac{N_{\phi i}}{R} \right) \left(N''_{\eta j} - \frac{N_{\phi j}}{R} \right) + EI_w \left(N''_{\phi i} + \frac{N''_{\eta i}}{R} \right) \left(N''_{\phi j} + \frac{N''_{\eta j}}{R} \right) \right.$$

$$\left. + GK_T \left(N'_{\phi i} + \frac{N'_{\eta i}}{R} \right) \left(N'_{\phi j} + \frac{N'_{\eta j}}{R} \right) \right] dz$$

(in which $i, j = 4, 5, 6, 7, 11, 12, 13, 14$) . . . . . (15)

The elements of the mass matrix, m_{ij}, can be derived from the second bracketed term of Eq. 3, and are expressed as (9)

$$m_{ij} = \rho \int_0^l \left\{ A \left[N_{\zeta i} N_{\zeta j} + (N_{\xi i} + a_y N_{\phi i}) N_{\xi j} + (N_{\eta i} - a_x N_{\phi i}) N_{\eta j} \right. \right.$$

$$\left. + (r_p^2 N_{\phi i} + a_y N_{\xi i} - a_x N_{\eta i}) N_{\phi j} \right] - I_x \left(N''_{\eta i} - \frac{N_{\phi i}}{R} \right) N_{\eta j}$$

$$\left. - I_y \left(N''_{\xi i} + \frac{N_{\xi i}}{R^2} \right) N_{\xi j} - I_w \left(N''_{\phi i} + \frac{N''_{\eta i}}{R} \right) N_{\phi j} \right\} dz \quad . . . . . (16)$$

in which $i, j = 1, 2, \ldots, 14$.

Applying Castigliano's Theorem, Part I, Eq. 14 becomes

$$[K_{ij}]\{\Delta\} - \omega^2 [m_{ij}]\{\Delta\} = \{Q\} \quad . . . . . (17)$$

in which $\{Q\}$ = generalized forcing vector. For eigenvalue problems defining the natural frequencies, the Q vector becomes the null vector. Assembling the element matrix equation of motion, Eq. 17, for the entire structure results in the final eigenvalue equation for the dynamic problem

$$[K]\{\Delta\} = \omega^2 [m]\{\Delta\} \quad . . . . . (18)$$

Examination of Eq. 16 reveals that the element of the mass matrix $[m_{ij}]$ contains terms which reflect the effects of the shear center location when it does not coincide with the centroid of the section. These effects are not reflected in ordinary consistent mass matrix formulation. Therefore, the assembled structural mass matrix $[m]$, when obtained by setting $a_x = a_y = 0$ (i.e., shear center coincident with the centroid), will be identical to that obtained by consistent formulation. Eq. 18 is a general eigenvalue problem.

A combined Sturm sequence and inverse iteration technique, as described by Gupta (10), is used for the solution of the eigenvalue problem. The method is an efficient and numerically stable algorithm for the accurate computation of specified roots and associated vectors of the general eigenproblem.

Examples

In order to demonstrate the versatility and reliability of the proposed method and the computer program developed, several example problems will be presented. Some of the results will be compared with results obtained from previously published sources.

Convergence.—The shape functions which describe the static behavior of the curved beam were also used to describe the dynamic behavior of the curved beam. Therefore, the dynamic solutions will necessarily be approximate. Due

TABLE 1.—Convergence of Single Span Curved Beam Solution

Number of elements (1)	Neglecting Effect of Rotational Inertia		Including Effect of Rotational Inertia	
	ω_1 (2)	Difference, as a percentage (3)	ω_1 (4)	Difference, as a percentage (5)
2	4.2106	+0.542	4.2078	+0.475
4	4.1895	+0.038	4.1897	+0.043
8	4.1881	+0.005	4.1883	+0.010
16	4.1879	—		

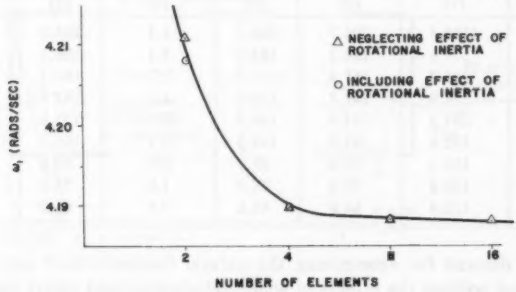

FIG. 3.—Convergence of Single Span Curved Beam Solution

to the utilization of the variational procedure, the dynamic solutions were expected to be upper bounds. The results of the computer analysis confirmed this.

Consider the example of a single span horizontally curved wide flange beam of length 1600 in. (4064 cm). The cross-sectional properties of the beam are: $A = 14.7$ in.^{2} (94.8 cm^2), $I_x = 395$ in.^{4} (16440 cm^4), $I_y = 56.4$ in.^{4} (2347.4 cm^4), $I_w = 1880$ in.^{6} (504855.2 cm^6), and $K_T = 1.79$ in.^{4} (74.5 cm^4).

Values used for the elastic modulus and shear modulus are $E = 29000$ ksi (200.1 GN/m^2) and $G = 11200$ ksi (77.3 GN/m^2). The beam is considered to have all end conditions fixed. The radius of beam curvature is 1528 in.

(3881.1 cm), and the beam spans an angle of 60°. The results of the analysis are shown in Table 1 and Fig. 3.

The percentages of variation are calculated using the result of the 16-element configuration as the exact value for comparative purposes. The convergence is evident; even the result of the relatively crude two-element configuration varies only minimally from the exact value. In addition, it can be seen that the effects of rotary inertia are quite insignificant, and can be disregarded for practical purposes.

Comparative Studies.—Culver (6) determined the natural frequencies of a horizontally curved beam utilizing the assumptions that the beam is prismatic and doubly symmetric, and considering only vibrations normal to the plane of curvature.

Shore and Chaudhuri (20) studied the free vibration of horizontally curved beams, considering vertical displacement and rotation about the z-axis. Expressions were derived for determining the natural frequencies of curved beams both with and without the effects of shear deformation and rotary inertia being considered. The previous problem presented here determined that the effects of rotary inertia are negligible; therefore the expression for natural frequency of curved beams without consideration of the effects of shear deformation and rotary inertia will be used as a basis for comparison with the results of this study.

TABLE 2.—Correlation of Results for Curved Beam Frequencies

Spanning Angle, in degrees (1)	Radius of Curvature, in inches (2)	Yoo and Fehrenbach	Culver (6)		Shore and Chaudhuri (20)	
		ω_1, in radians per second (3)	ω_1, in radians per second (4)	Difference, as a percentage (5)	ω_1, radians per second (6)	Difference, as a percentage (7)
10	1155.5	204.7	202.5	1.1	203.3	0.7
20	577.8	190.2	184.3	3.1	186.3	2.1
30	385.2	165.8	162.2	2.2	164.7	0.7
40	288.9	141.7	140.0	1.2	142.8	0.8
50	231.1	121.3	120.9	0.3	122.8	1.2
60	192.6	103.9	103.8	0.1	105.2	1.3
70	165.1	89.6	88.9	0.8	90.0	0.4
80	144.4	76.8	76.0	1.0	76.8	0.0
90	128.4	64.0	64.6	0.9	65.2	1.9

The example to be considered here is a single span curved beam of length 201.68 in. (512.27 cm). The beam curvature is varied so that the beam spans a variety of angles ranging from 10° to 90°. Cross-sectional properties of the beam are: $A = 14.4$ in.^{2} (92.9 cm^2), $I_x = 273$ in.^{4} (11362 cm^4), $I_y = 93$ in.^{4} (3871 cm^4), $I_w = 2070$ in.^{6} (555878 cm^6), $K_T = 35.34$ in.^{4} (1470.85 cm^4), and $r_p = 5.042$ in. (12.81 cm). The beam is considered to have pinned conditions at both ends. In Table 2, the natural frequencies determined by this study

are compared with those calculated according to Culver and Shore and Chaudhuri. Excellent correlation is observed.

Shear Center Effects.—Several examples were analyzed to determine the effect of the shear center location on the dynamic response of the curved beam. The first example considered was the singly symmetric section shown in Fig. 4. The curved beam has length 240 in. (609.6 cm) and has fixed conditions at its ends. The radius of curvature is 275.02 in. (698.55 cm) and the beam spans an angle of 50°. Cross-sectional properties are: $A = 15.4$ in.^{2} (99.4 cm^2),

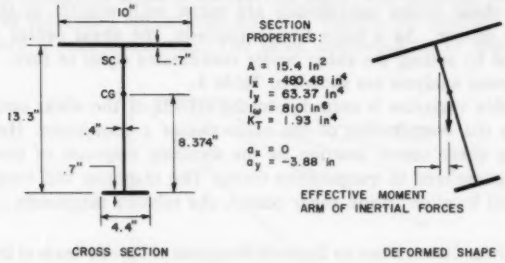

FIG. 4.—Singly Symmetric Curved Beam Cross Section (1 in. = 2.54 cm)

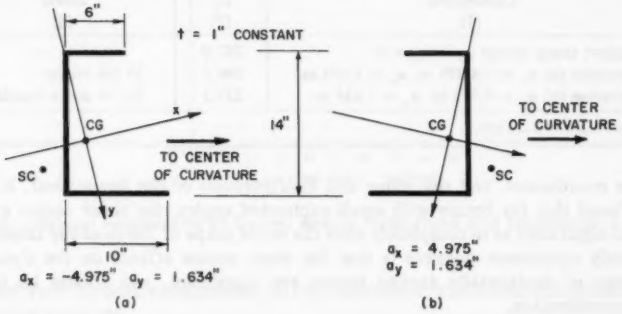

FIG. 5.—Unsymmetric Curved Beam Cross Section (1 in. = 2.54 cm)

$I_x = 480.48$ in.^{4} (19998 cm^4), $I_y = 63.37$ in.^{4} (2637 cm^4), $I_w = 810$ in.^{6} (217517 cm^6), and $K_T = 1.93$ in.^{4} (80.3 cm^4).

When the shear center effects are included, the resultant natural frequency of the beam is found to be 261.41 rads/sec. If the shear center effects are eliminated (by setting $a_x = a_y = 0$), the natural frequency of the beam is 262.97 rads/sec, only slightly stiffer than the beam with shear center effects included.

It can be seen in the deformed shape of the beam shown in Fig. 4 that the x-coordinate of the shear center will contribute most significantly to the inertial forces of beam vibration. Therefore, for the singly symmetric section

symmetric about its vertical axis, the effect of shear center location on the dynamic response of the beam will be relatively small. However, in beams not symmetric about the vertical axis, shear center effect will be found to be significant.

Two variations of an unsymmetric channel section are shown in Fig. 5. The cross-sectional properties of the section are: A = 28 in.^{2} (180.6 cm^2), I_x = 824.25 in.^{4} (34305 cm^4), I_y = 180.05 in.^{4} (7493.7 cm^4), I_w = 3661.6 in.^{6} (983286 cm^6), K_T = 9.33 in.^{4} (388.3 cm^4), and r_p = 5.426 in. (13.78 cm). The beam has a length of 240 in. (609.6 cm) and spans an angle of 50°. Moments of inertia and shear center coordinates are taken with respect to the principal axes of the section. As a basis for comparison, the shear center effects can be eliminated by setting the shear center coordinates equal to zero. The results of the computer analysis are shown in Table 3.

Considerable variation is seen due to the effects of the shear center, caused primarily by the contribution of the shear center x-coordinate. However, the effect of the shear center location on the dynamic response of curved beams cannot be generalized in quantitative terms. The response will vary according to the general location of the shear center, the relative magnitude of the shear

TABLE 3.—Shear Center Effect on Dynamic Response of Curved Beam of Unsymmetric Cross Section

Conditions (1)	ω_1 (2)	Effect (3)
Neglect shear center $a_x = a_y = 0$	297.0	—
Variation (a) a_x = −4.975 in. a_y = 1.634 in.	396.5	33.5% stiffer
Variation (b) a_x = 4.975 in. a_y = 1.634 in.	237.3	20.1% more flexible

Note: 1 in. = 2.54 cm.

center coordinates, and the shape and configuration of the beam itself. It was also found that for beams with small subtended angles, the shear center effect was so significant as to completely alter the mode shape of the dynamic response. The only conclusion possible is that the shear center effects on the dynamic response of horizontally curved beams are significant, and should be taken into consideration.

Parametric Studies.—One of the primary concerns of this study was to develop a chart or series of charts which would be readily applicable to the determination of the fundamental natural frequencies of horizontally curved beams. In order to develop a chart that would be universal in application, it was necessary to determine a set of parameters which would control the dynamic response of the beam and define a unique, correct solution to the problem.

As a result of this study, the problem was defined according to the following set of parameters. The first parameter is the ratio of the torsional rigidity of the beam to the flexural rigidity of the beam. This parameter was called the rigidity ratio α_k and defined as

$$\alpha_k = \frac{GK_T}{EI_x} \qquad (19)$$

in which α_k was defined over a range from 0.002 to 0.400. A rigidity ratio of 0.002 is roughly equivalent to that of an isolated wide-flanged beam, while a ratio of 0.400 may be considered (28) to simulate the behavior of a curved beam in a built-up deck section, i.e., a beam that is supported and stiffened by various means at the web and flanges. It should be noted that the warping rigidity, EI_w, has little effect on the natural frequencies except for curved beams of extremely short spans.

A second parameter is a slenderness ratio, defined as L/r_p, in which L = length of the curved beam, and r_p = polar radius of gyration. The third parameter used was the subtended angle of the curved beam. The problem was analyzed for a range of subtended angles from 0 to 90°. Finally, the problem was solved with a variety of end conditions. The three combinations of end conditions

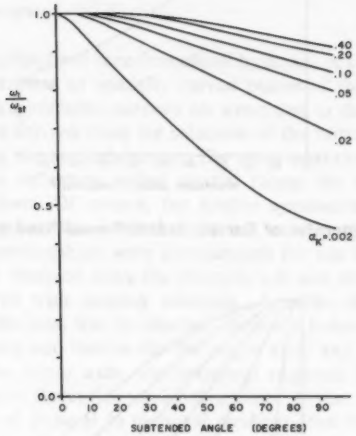

FIG. 6.—Natural Frequencies of Curved Beams Fixed-Fixed End Conditions, L/r_p = 160

studied were: (1) Both ends pinned; (2) both ends fixed; and (3) one end pinned-one end fixed supports.

Having defined the foregoing as controlling parameters in the dynamic response of the curved beam, numerous problems using different combinations of the parameters were defined and solved by the computer program developed for this study (9). The resulting solutions (eigenvalues) are generalized on the charts as the eigenvalue ratio ω_1/ω_{st}, in which ω_1 = fundamental frequency of the curved beam under consideration, and ω_{st} = fundamental frequency of a straight beam having the same length, cross section, material properties, and end conditions as the curved beam.

A selection of the charts which resulted from this analysis is shown in Figs. 6 through 8. A more complete range of charts has been developed and presented by Fehrenbach (9).

Several general patterns of dynamic behavior can be readily observed in the

charts. For very small subtended angles, the eigenvalue ratio approaches unity; that is, the curved beam behaves as a straight beam. As the subtended angle

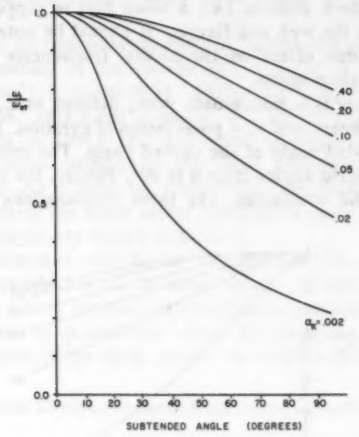

FIG. 7.—Natural Frequencies of Curved Beams Pinned-Fixed End Conditions, L/r_p = 160

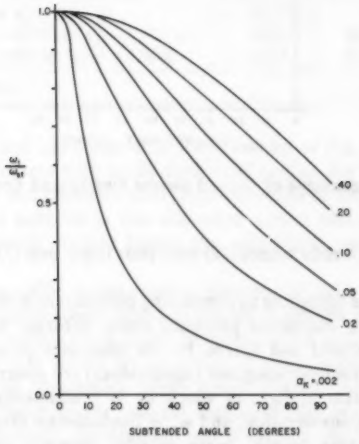

FIG. 8.—Natural Frequencies of Curved Beams Pinned-Pinned End Conditions, L/r_p = 160

increases, the curved beam becomes increasingly more flexible, and the eigenvalue ratio decreases accordingly.

Higher ranges of α_k denote stiffer torsional rigidities. As torsional rigidities increase, the effect of the beam curvature is effectively diminished, and the curved beam behavior more closely approaches the equivalent straight beam behavior; accordingly, the eigenvalue ratio increases. Except for the low ranges of torsional rigidity ($\alpha_k \leq 0.002$) and slenderness ratio ($L/r_p \leq 40$), the effect of the slenderness ratio on the natural frequencies of curved beams is minimal (less than 10%).

Finally, the end conditions have a noticeable effect on the curved beam behavior. Fixed-fixed end conditions contribute greatly to the overall stiffness of the beam, resulting in higher eigenvalue ratios. As can then be expected, pinned-fixed end conditions are somewhat more flexible, with pinned-pinned ends being the most flexible combination of end conditions.

Summary and Conclusions

Stiffness relationships have been formulated by means of variational procedures for the vibration problem of spatially curved beams of thin-walled open cross section. The resulting stiffness matrices are exact due to the utilization of shape functions which are derived from the solutions of the homogeneous differential equations governing the static behavior. The mass matrices are general, in that they include terms reflecting added inertial forces for singly symmetric or nonsymmetric sections. Of course, for doubly symmetric sections, the mass matrices are identical to the so-called consistent mass matrices.

These element relationships were programmed for use in digital computers, and solutions were obtained using the program that was developed. The results were then compared with existing solutions. A series of charts reflecting a wide range of applications was developed. Since the behavior of curved beams is coupled in bending and torsion for the major axis, and in bending and axial deformation for the minor axis, the structural response is quite significantly affected by the ratio of flexural to torsional rigidities. In the charts, the parameters used are the ratio of flexural to torsional rigidities, the slenderness ratio with respect to the polar radius of gyration, the subtended angle of the beam, and the type of end conditions. The rigidity ratio ranges from 0.002, which represents most isolated wide-flange sections, to 0.400, which reflects the equivalent rigidity ratio for curved girders in a deck system. It has been noted that the actual torsional rigidity of a girder in a deck system is much higher (tens and hundreds of times) than that of individual members (28). The slenderness ratio varies from 40 to 240, and the subtended angle from 0 to 90°. End conditions which were considered are pinned-pinned, pinned-fixed, and fixed-fixed.

The charts can be utilized effectively in determining natural frequencies of curved beams, as demonstrated in several examples. Good correlation was observed with existing solutions obtained by Culver (6) and Shore and Chaudhuri (20).

Examination of the computed eigenvectors reveals that for doubly symmetric members with both ends pinned, the vibration mode shapes for translation and rotation are half sine waves, as used in most of the classical solution techniques. However, for members with other than pinned-pinned end conditions, and shear center not coincident with the centroid, the mode shapes sometimes cannot be defined by a simple trigonometric term.

In addition, the element relationships as developed herein have been utilized exclusively in examples of horizontally curved beams. However, the relationships developed herein can be used to describe the behavior of curved beams in any spatial configuration; for in-plane or longitudinal vibrations.

Appendix I.—References

1. Bathe, K., and Wilson, E., *Numerical Methods in Finite Element Analysis*, Prentice-Hall, Englewood Cliffs, N.J., 1976.
2. Biggs, J. M., *Introduction to Structural Dynamics*, McGraw-Hill Book Co., New York, N.Y., 1964.
3. Bleich, F., *Buckling Strength of Metal Structures*, McGraw-Hill Book Co., New York, N.Y., 1952.
4. Chaudhuri, S. K., "Dynamic Response of Horizontally Curved I-Girder Bridges Due to a Moving Vehicle," dissertation presented to the University of Pennsylvania, at Philadelphia, Pa., in 1975, in partial fulfillment of the requirements for the degree of Doctor of Philosophy.
5. Chaudhuri, S. K., and Shore, S., "Dynamic Analysis of Horizontally Curved I-Girder Bridges," *Journal of the Structural Division*, ASCE, Vol. 103, No. ST8, Proc. Paper 13121, Aug., 1977, pp. 1589–1604.
6. Culver, C. G., "Natural Frequencies of Horizontally Curved Beams," *Journal of the Structural Division*, ASCE, Vol. 93, No. ST2, Proc. Paper 5187, Apr., 1967, pp. 189–203.
7. Dabrowski, R., "Equations of Bending and Torsion of Curved Thin-Walled Bars With Asymmetric Cross Section," *Archiwum Mechaniki Stosowanej*, Vol. 12, No. 5–6, 1960, pp. 789–799.
8. Engel, S., "Structural Analysis of Circular Curved Beams," *Journal of the Structural Division*, ASCE, Vol. 93, No. ST1, Proc. Paper 5099, Feb., 1967, pp. 221–234.
9. Fehrenbach, J. P., "Natural Frequencies of Horizontally Curved Beams," thesis presented to Marquette University, at Milwaukee, Wis., in 1979, in partial fulfillment of the requirements for the degree of Master of Science.
10. Gupta, K. K., "Eigenproblem Solution by a Combined Sturm Sequence and Inverse Iteration Technique," *International Journal for Numerical Methods in Engineering*, Vol. 7, 1973, pp. 17–42.
11. Krajcinovic, D., "A Consistent Discrete Elements Technique for Thin-Walled Assemblages," *International Journal of Solids and Structures*, Vol. 5, 1969, pp. 639–662.
12. Lavelle, F. H., "Analysis of Curved Steel Girder Bridges," *Engineering Journal*, AISC, Vol. 3, No. 3, July 1966.
13. Love, A. E. H., *A Treatise on the Mathematical Theory of Elasticity*, 4th ed., Dover Publications, New York, N.Y., 1944.
14. McManus, P. F., Nasir, G. A., and Culver, C. G., "Horizontally Curved Girders—State of the Art," *Journal of the Structural Division*, ASCE, Vol. 95, No. ST5, Proc. Paper 6546, May, 1969, pp. 853–870.
15. Ojalvo, I. U., "Coupled Twist-Bending Vibrations of Incomplete Elastic Rings," *International Journal of Mechanical Sciences*, Pergamon Press Ltd., Vol. 4, 1962, pp. 53–72.
16. Reddy, M. N., and Tuma, J. J., "Analysis of Laterally Loaded Continuous Curved Beams," *Journal of the Structural Division*, ASCE, Vol. 93, No. ST1, Proc. Paper 5118, Feb., 1967, pp. 495–513.
17. Saint-Venant, B., "Memoire sur le calcul de la résistance et de la flexion des pièces solides à simple ou à double courbure, en prenant simultanément en considération les divers efforts auxquels elles peuvent etre soumises dans tous les sens," *Comptes-Rendus*, l'Academie des Sciences de Paris, Vol. XVII, 1843, pp. 942 and 1020–1031. See A. E. H. Love (12).
18. Schmitt, W., "Interchange Utilizes Arc Welded Horizontally Curved Girder Spans," paper submitted to Lincoln Arc Welding Foundation, 1966.
19. Schulz, M., and Chedraui, M., "Tables for Circularly Curved Horizontal Beams with Symmetric Uniform Load," *ACI Journal*, American Concrete Institute, Vol. 53, Title No. 53–58, May 1957, pp. 1033–1040.

20. Shore, S., and Chaudhuri, S. K., "Free Vibration of Horizontally Curved Beams," *Journal of the Structural Division*, ASCE, Vol. 98, No. ST3, Proc. Paper 8755, March, 1972, pp. 793–796.
21. Simitses, G. L., *An Introduction to the Elastic Stability of Structures*, Prentice-Hall, Englewood Cliffs, N.J., 1976.
22. Tan, C. P., and Shore, S., "Dynamic Response of a Horizontally Curved Bridge," *Journal of the Structural Division*, ASCE, Vol. 94, No. ST3, Proc. Paper 5862, March, 1968, pp. 761–781.
23. Tan, C. P., and Shore, S., "Response of Horizontally Curved Bridge to Moving Load," *Journal of the Structural Division*, ASCE, Vol. 94, No. ST9, Proc. Paper 6125, Sept., 1968, pp. 2135–2151.
24. Timoshenko, S., *Strength of Materials*, Part 2, 3rd ed., D. Van Nostrand Co., Inc., Princeton, N.J., 1955.
25. Vlasov, V. Z., *Thin Walled Elastic Beams*, 2nd ed., National Science Foundation, Washington, D.C., 1961.
26. Yonezawa, H., "Moments and Free Vibrations in Curved Girder Bridges," *Journal of the Engineering Mechanics Division*, ASCE, Vol. 88, No. EM1, Proc. Paper 3052, February, 1962, pp. 1–21.
27. Yoo, C. H., "Matrix Formulation of Curved Girders," *Journal of the Engineering Mechanics Division*, ASCE, Vol. 105, No. EM6, Proc. Paper 10578, Dec., 1979, pp. 971–988.
28. Yoo, C. H., and Heins, C. P., "Plastic Collapse of Horizontally Curved Bridge Girders," *Journal of the Structural Division*, ASCE, Vol. 98, No. ST4, Proc. Paper 8848, Apr., 1972, pp. 899–914.

Appendix II.—Notation

The following symbols are used in this paper:

A = cross-sectional area;
a_x, a_y = coordinates of shear center measured from the centroid;
BM = bimoment;
E = Young's modulus;
G = shear modulus;
I_x, I_y = principal moments of inertia;
I_w = warping constant;
J = conjunct or concomitant;
$[K]$ = stiffness matrix;
K_T = St. Venant's torsional constant;
L = beam length;
l = element length;
M_x, M_y = bending moments about the x and y axes, respectively;
$[m]$ = mass matrix;
$[N]$ = matrix of shape functions;
N_z = axial force;
$\{Q\}$ = generalized forcing function;
$q_i(t)$ = amplitude of beam vibration;
R = radius of curvature;
r_p = polar radius of gyration;
T_s, T_w = St. Venant's and warping torsion;
w = normalized sectorial coordinate;
x, y, z = pointwise orthogonal coordinates;
α_k = rigidity ratio;

γ = kinematic degree of freedom;
Δ = displacement field;
Δ_i = assumed displacement modes for dynamic behavior;
$\{\Delta\}$ = vector of nodal point displacements;
δ = variational operator;
ξ, η, ζ = displacements in the x, y and z directions, respectively;
Π = energy functional;
ρ = mass density;
τ = kinematic degree of freedom;
ϕ = angle of rotation about the z axis;
ω = angular frequency;
ω_1 = curved beam natural frequency; and
ω_{st} = straight beam natural frequency.

JOURNAL OF
THE ENGINEERING
MECHANICS DIVISION

LOGICAL ANALYSIS OF STRUCTURAL FAILURE[a]

By David I. Blockley[1]

INTRODUCTION

There are many occasions when an engineer has to make a judgment based on his interpretation of a large amount of rather imprecise information. One example is the determination of the cause or causes of a structural failure and the synthesis of general lessons we can learn for the future. The final trigger incident which precipitates a particular collapse may not be the most interesting aspect of it; very often there are complex underlying human interactions. Human error, of one form or another, has been shown to be a dominant reason for many of our failures (4,6,10). Indeed this conclusion should not surprise us because in the final analysis all error is human error. It is people who have to decide what to do; it is people who have to decide how it should be done; and it is people who have to do it. Engineers in the past, flushed with the successes of their applications of the physical sciences to engineering problems, have rather neglected their reliance on human infallibility. In engineering only the product, the hardware, is a physical system; the system which designs it, produces it, and uses it, is human and therefore complex and vulnerable.

There are many ways in which the possibility of human error in the future, may be reduced. For example, more attention might be given to the topic in the education and training of engineers; Melchers has pointed to the need for better control of the work (7). In this paper, however, it is proposed to concentrate on one aspect of the problem. How can conclusions be distilled from past failures (and successes) when much of the information available is rather imprecise? The work described is a beginning; it stems from the belief that there is a need for a logical way of examining information about failures, storing

[a]Presented at the April 14–18, 1980, ASCE Convention and Exposition, held at Portland, Oreg. (Preprint 80-003).

[1]Lect., Dept. of Civ. Engrg., Univ. of Bristol, Queens Building, Univ. Walk, BS8 1TR England.

Note.—Discussion open until September 1, 1981. To extend the closing date one month, a written request must be filed with the Manager of Technical and Professional Publications, ASCE. Manuscript was submitted for review for possible publication on February 26, 1980. This paper is part of the Journal of the Engineering Mechanics Division, Proceedings of the American Society of Civil Engineers, ©ASCE, Vol. 107, No. EM2, April, 1981. ISSN 0044-7951/81/0002-0355/$01.00.

them as computer data structures and using these data as a basis for comparison with future proposals. The data structures are to be set up using fuzzy logic. In this paper attention will be confined to some of the basic ideas of fuzzy logic, with little mathematical, treatment, and an illustration of its application.

Information

Information can be defined as a set of propositions. The propositions may be logically related and of varying *content* and quality or *dependability*. There is not sufficient space here for a full consideration of these concepts (see Ref. 5) but it is necessary to outline briefly the difference between the dependability of a proposition and its truth or even the probability of its truth. If a proposition is true then obviously it is dependable but the reverse is not necessarily so. For example, modern relativistic physics has shown that Newton's Laws are false, but nevertheless the predictions of Newtonian mechanics as embodied in structural analytical techniques are highly dependable. A modern philosophical view is that all theories are models of our understanding of the world which we are constantly attempting to refute. No matter how many times observations are made which agree with a theory, it is not proved to be true; all that can be said is that it is a highly tested, confirmed and *dependable* theory. On the other hand, only one observation which disagrees with a theory proves that theory to be false. This logical asymmetry between verification and falsification has been pointed out by Popper (8). The argument stems from Hume who in 1739 first raised questions about the empirical explanation of science as a process of induction. He showed that induction has to assume that nature is regular. Just because past futures have been like past pasts, it does not logically follow that future futures will be like future pasts.

If a proposition is precise, it has high content and is unlikely to be true, or in other words the probability that it is true is low. On the other hand, if a proposition is vague, it has low content and is likely to be true, or the probability that it is true is high. For example, if a line AB is measured and it is stated "the length AB is 1.26359736 m" than it is highly likely that the last few decimal places are wrong. If it is stated "the length AB is between 0 m and 10 m" then the proposition is almost certainly true. This idea that there is an *inverse relationship* between the *content* of a proposition and its *truth* also comes from Popper (8). Engineers and scientists are not interested primarily in theories and propositions which have a high probability of being true, but in theories and propositions which have high content (and therefore low probability) but which are highly dependable. It is clear therefore that any measure of the dependability of a proposition is not the probability that it is true.

Fuzzy Logic

Zadeh, who first published the idea of fuzzy sets in 1965, maintained that the way humans are able to summarize masses of information and then extract important items relevant to a problem, is because we think approximately. We think in terms of classes or sets of objects where the transition from membership to nonmembership is not abrupt but gradual. As an example the fuzzy term

safe could be defined as a fuzzy set on the possible values of probability of failure, Fig. 1(*a*), and a term **expensive** could be defined on a utility space, Fig. 1(*b*). Zadeh later suggested a generalization of ordinary two valued logic where the binary concepts of true and false underlying the whole of logic and mathematics, are generalized to fuzzy sets on the interval [0, 1].

The work described here is based upon Baldwin's considerable development of this idea using the idea of a fuzzy truth restriction (2,3,5). Very little of the underlying mathematics of fuzzy logic will be presented, instead an attempt will be made to give some appreciation of the ideas.

Using the definitions made earlier we may wish to make the following simple proposition—Proposition: if (a structure is **safe**) then (it is **expensive**) is **very true**. This is an observation about the world. Suppose now a particular observation

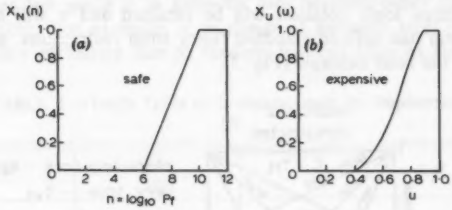

FIG. 1.—Fuzzy Sets

is made "Structure *A* is **quite safe** is **true**," what can we deduce? The argument is, in fact, a logical *modus ponens* deduction of the form:

Proposition: a structure is **safe** implies a structure is **expensive** is **very true**.
Observation: Structure *A* is **quite safe** is **true**
Conclusion: The structure is **expensive** is τ or recast the **structure** is **B′** is **true**.

Expressed symbolically:

$$\mathbf{A} \supset \mathbf{B} \text{ is } \tau_1$$
$$\mathbf{A} \text{ is } \tau_2$$
$$\therefore \mathbf{B} \text{ is } \tau_3$$
$$\therefore \mathbf{B}' \text{ is true}$$

in which **A**, **B**, **B′** = propositions; τ = truth restrictions; and Baldwin's mathematics (5) allows the calculation of τ_3 and **B′** if τ_1 and τ_2 are known. Baldwin has shown in this case that $\tau_3 = \tau_{A'} \circ \mathbf{I}(\tau_1)$ in which **A′** is **A** truth functionally modified by τ_2 or $\chi_{A'}(n) = \chi_{\tau_2}[\chi_A(n)]$; **A**, **A′** $\subset N$, $n \in N$ and $\mathbf{I}(\tau_1)$ is an implication relation, such as that of Lukasiewicz, truth functionally modified by τ_1. The term $\chi_A(n)$ is the fuzzy membership function. The operation $\mathbf{A} = \mathbf{B} \circ \mathbf{C}$ is a fuzzy composition. Finally $\chi_{B'}(u) = \chi_{\tau_3}[\chi_B(u)]$; **B**, **B′** $\subset U$, $u \in U$.

Another form of logical deduction, which will be used later, is that of *modus tollens* or

A $\supset$ **B** is τ_1

B is τ_2

$\therefore$ **A** is τ_3

$\therefore$ **A′** is **true**

in which $\tau_3 = \mathbf{I}(\tau_1) \circ \tau_{B'}$. Compound propositions may also be handled.

Although fuzzy logic was developed as a generalization of ordinary two valued logic, Baldwin recognizes that the interpretation of the philosophical meaning of the fuzzy truth restriction τ will depend on the particular application. It is possible to interpret τ as a measure of plausibility, possibility, importance, or dependability. In this paper τ will be regarded as a restriction upon dependability although the fuzzy logic notation will be retained and τ will be referred to as truth. Baldwin has defined standard fuzzy truth restrictions, some of which will be used in the later example (Fig. 2).

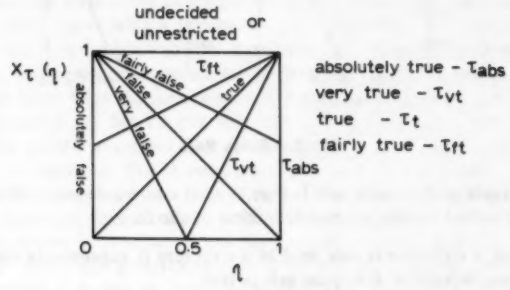

FIG. 2.—Some Truth Restrictions, τ

Before applying these ideas to structural safety there is one important characteristic of the modus tollens deduction which must be described and which relates to Popper's argument about the asymmetry between verification and falsification. It may be best understood by simplifying the argument down to that of ordinary logic where each of the propositions is either true or false. Consider the deduction

Newton's Laws (A) $\supset$ deflection of beam is 20 mm (B)
the beam deflects 20 mm (B)

$\therefore$ Newton's Laws are?

The truth table of ordinary logic is Table 1.

As we have observed, B is true and $A \supset B$ is true, then lines 1, and 3 of Table 1 are of interest. However, this means that A is true or false, so that the observation B does not verify A nor falsify it, it leaves us undecided. Consequently in fuzzy logic, the best (in the sense of verification) that can

be done in the modus tollens deduction when **A** and **B** are fuzzy statements **A**, **B** with fuzzy truth restrictions τ, is to leave **A** as unrestricted. The best that can be done to falsify **A** is show that it is **absolutely false**. It follows therefore that to use modus tollens, the propositions should be set up so that they may be falsified.

Fuzzy Logic in Structural Safety

If (a design is **perfectly safe**) (**S**) then (it has a **low** probability of failures in any of the defined limit states) (**NP**) is **absolutely true** i.e., **S** $\supset$ **NP** is τ_{abs}. This means that **NP** is a necessary condition on **S** and **S** is a sufficient condition on **NP**. In other words if a design is **safe** then it must have a **low** probability of failure *but* just because it has a **low** probability of failure in some defined limit state does not mean it is **perfectly safe** because other factors are also relevant to safety. For example, if (a design is **perfectly safe**) (**S**) then (it has a **low** probability of failure due to random hazards such as fire, floods etc.) (**RH**) and (it has a **low** probability of failure due to human error) (**HE**) is **absolutely true**. These may be written:

TABLE 1.—Truth Table of Ordinary Logic for Implication

Line number (1)	A (2)	B (3)	$A \supset B$ (4)
1	true	true	true
2	true	false	false
3	false	true	true
4	false	false	true

S $\supset$ **NP** is τ_{abs}

S $\supset$ **RH** is τ_{abs}

S $\supset$ **HE** is τ_{abs}

Note that **S** includes the term **perfectly safe** which is impossible to satisfy. By obtaining truth restrictions upon **NP**, **RH**, **HE** it is possible to calculate the extent to which **S** is false. In other words **S** will be falsified by truth restrictions upon **NP**, **RH**, and **HE** which represent the extent to which it is believed that they falsify **S**.

Now clearly **NP**, **RH**, **HE** are too general to allow truth restrictions to be set to them. It is clearly possible to write down further necessary conditions for them as follows:

HE $\supset$ (No design error) **DE** is τ_{vt}

HE $\supset$ (No construction error) **CE** is τ_{vt}

HE $\supset$ (The "climate" is **perfect**) **CL** is τ_{vt}

HE $\supset$ [(The structure is **sensitive** to the way it is used) **SU** $\cap$ (**adequate** instruction and warning given to user) **WI**] $\cup$ [(The structure is **not sensitive** to use) **SN**] is τ_{ft}

Carrying this subdivision on

DE ⊃ (**No** well-known mode of failure missed) **DEM** is τ_{abs}

DE ⊃ (**No** calculation errors) **DEE** is τ_{vt}

DE ⊃ (Design consultants have **adequate** experience) **DEC** is τ_t

DE ⊃ (Personnel available for design work are **suitably** experienced) **DED** is τ_t

DE ⊃ (Personnel available for site supervision are **suitably** experienced) **DES** is τ_t

DE ⊃ (Specifications are **perfectly adequate**) **DEP** is τ_{vt}

DE ⊃ [Quantity and quality of research and development information is **sufficient**] **DER** is τ_{vt}

DE ⊃ (There is **no** mode of structural behavior **inadequately** understood by existing technology) **DET** is τ_{abs}

DEE ⊃ (Checking procedures are adequate) **DEEC** is τ_{vt}

DEE ⊃ (Conditions of work and employment are **good**) **DEEW** is τ_{ft}

CE ⊃ (Construction methods to be used are **well**-tried and tested) **CEM** is τ_{ft}

CE ⊃ (Likelihood of construction mistakes is **low**) **CEE** is τ_t

CE ⊃ (Construction company has **adequate** experience) **CEC** is τ_t

CE ⊃ (Personnel available for falsework design are **adequately** experienced) **CED** is τ_t

CE ⊃ [(Personnel available for site work are **adequately** experienced) **CES**] ∩ [(they are **able** to appreciate technical problems associated with the design) **CEP**] is τ_t

CEE ⊃ [(Record of company is good; mistakes infrequent in past) **CEEC**] ∩ [(personnel working in good conditions) **CEEG**] ∩ [(good happy relationship between personnel in company) **CEEH**] ∩ (structure is not sensitive to erection method) **CEEM** is τ_{abs}

CL ⊃ (**Perfectly** normal contract procedure) **CLC** is τ_{vt}

CL ⊃ (**No** undue political pressures) **CLP** is τ_t

CL ⊃ (**No** undue industrial pressures) **CLI** is τ_t

CL ⊃ (**No** undue financial pressures) **CLF** is τ_t

RH ⊃ (All random hazards have been identified) **RHI** is τ_t

RH ⊃ [(The experience for this site suggests risk of random hazards is **low**) **RHE** ∩ (there is **no** change in environment to suggest this assessment is wrong) **RHC**] ∪ [(**perfectly** adequate established data have been collected) **RHD** ∩ (the probability of failure based on these data is **low**) **RHP**] is τ_{abs}

NP ⊃ {The notional probability of failure [assuming a perfect calculation model (**LSM**)] is **low**) (**NPF**) is τ_{vt}

NP ⊃ (The probability of a new presently unknown effect in the material causing failure is **low**) (**MMM**) is τ_{vt}

NP ⊃ (The probability of a new presently unknown effect in the structural form causing failure is **low**) (**SSS**) is τ_{vt}

NP ⊃ (The probability of a new presently unknown loading effect causing failure is **low**) (**LLL**) is τ_{vt}

(The possibility that the calculation model is perfect is **high**) (**LSMP**) ⊃ (the calculated notional probability of failure is **perfectly dependable**) (**NPFR**) is τ_{vt}

(The calculation model for the limit state is **perfect**) **LSM** ⊃ (the model used for the loads is perfect) **(LSML)** is τ_{vt}

LSM ⊃ (The model used for the resistance is **perfect**) **(LSMR)** is τ_{vt}

LSML ⊃ (The system used for the loads is **perfect**) **(LSMLS)** is τ_{abs}

LSML ⊃ (The parameter statistics for the loads are **perfect**) **(LSMLP)** is τ_{vt}

LSMLS ⊃ (The model has been used before with **no** problems) **(F1)** is τ_{abs}

LSMLS ⊃ (There is **no** change between this useage and previous ones) **(F2)** is τ_{abs}

or

LSMLS ⊃ (The test data available are **perfectly satisfactory**) **(F3)** is τ_{abs}

LSMLP ⊃ (The statistics have been used before with **no** problems) **(F4)** is τ_{abs}

LSMLP ⊃ (There is **no** underlying change in the useage) **(F5)** is τ_{abs}

or

LSMLP ⊃ (The data available is **perfect**) **(F6)** is τ_{abs}

LSMR ⊃ (The system used for the resistance calculation is **perfect**) **(LSMRS)** is τ_{abs}

LSMR ⊃ (The parameter statistics for the resistance calculation are **perfect**) **(LSMRP)** is τ_{vt}

LSMRS ⊃ (The system model has been used before with **no** problems) **(F7)** is τ_{abs}

LSMRS ⊃ (There is **no** underlying change in usage) **(F8)** is τ_{abs}

or

LSMRS ⊃ (**Perfect** prototype test data is available) **(F9)** is τ_{abs}

LSMRP ⊃ (The parameter statistics for the resistance calculation have been used before with **no** problems) **(F10)** is τ_{abs}

LSMRP ⊃ (There is **no** underlying change in usage) **(F11)** is τ_{abs}

or

LSMRP ⊃ (**Perfectly** relevant measurements from sample surveys are available) **(F12)** is τ_{abs}

These logical relations are summarized in Fig. 3. In the figure the square boxes represent propositions and the circles are logical operators. Each proposition has a number (i) which is its truth value τ_i. Each logical operator may be truth functionally modified by a truth value such as τ_{abs}, τ_{vt} or τ_t. A particular proposition may appear more than once in the hierarchy, because its truth value at a stage in the argument derives from the restriction on the truth of the proposition by only one or a few of the necessary conditions upon it. As one proceeds up the hierarchy from the input truth restrictions at the bottom, following the arrows then more and more of these restrictions are taken into account.

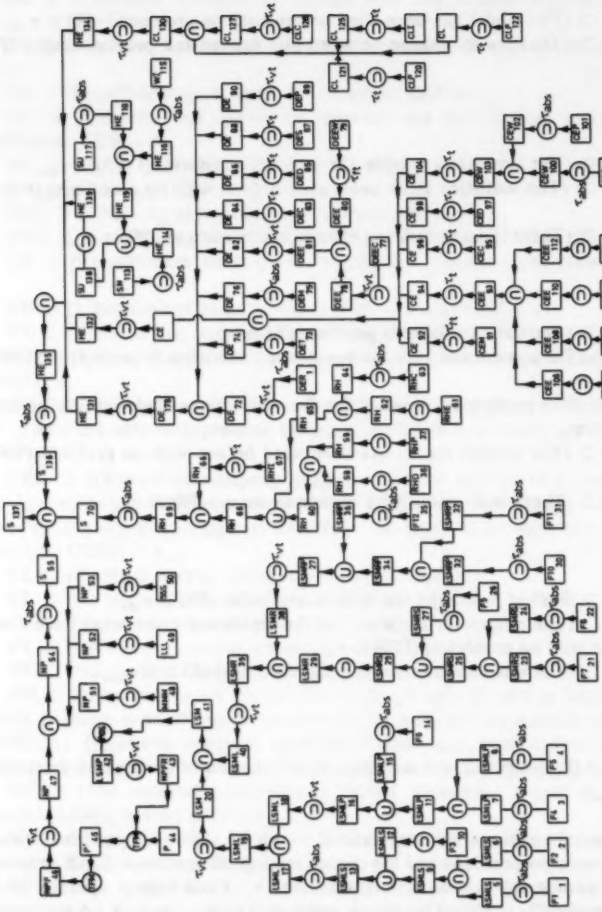

FIG. 3.—Logical Hierarchy for Structural Safety

Finally, e.g., the restriction on S from the whole subhierarchy of **HE** is τ_{136}; the restriction on S from the subhierarchy of **RH** is τ_{70} and on S from **NP** is τ_{55}. The intersection of these three restrictions gives the final restriction on S. The operations involving propositions with truth restrictions 41–46 are not described in this paper (5).

Examples

This hierarchy of logical relations has been used to obtain fuzzy safety measures for two famous failures, the Tay Bridge (9) and the Tacoma Narrows Bridge

TABLE 2.—Assessments for Examples

Proposition (1)	Truth Restriction		Proposition (4)	Truth Restriction	
	Tacoma (2)	Tay (3)		Tacoma (5)	Tay (6)
F1	fairly false	absolutely false	DER	very false	false
F2	false	very false	DET	absolutely false	fairly false
F3	absolutely false	absolutely false	DEM	unrestricted	very false
F4	absolutely false	absolutely false	DEEC	unrestricted	fairly false
F5	very false	absolutely false	DEEW	unrestricted	fairly false
F6	absolutely false	absolutely false	DEC	unrestricted	fairly false
F7	false	fairly false	DED	unrestricted	unrestricted
F8	absolutely false	fairly false	DES	unrestricted	very false
F9	absolutely false	absolutely false	DEP	unrestricted	false
F10	very false	unrestricted			
F11	absolutely false	fairly false			
F12	absolutely false	absolutely false	CEM	unrestricted	fairly false
			CEEC	unrestricted	unrestricted
MMM	unrestricted	very false	CEEG	unrestricted	very false
SSS	absolutely false	fairly false	CEEH	unrestricted	false
LLL	very false	absolutely false	CEEM	fairly false	false
			CEC	unrestricted	unrestricted
RHD	unrestricted	absolutely false	CED	unrestricted	unrestricted
RHP	unrestricted	unrestricted	CES	unrestricted	fairly false
RHE	unrestricted	fairly false	CEP	unrestricted	very false
RCH	unrestricted	unrestricted			
RHI	false	false	SN	unrestricted	fairly false
			SU	unrestricted	absolutely false
CLC	unrestricted	fairly false	WI	unrestricted	absolutely false
CLP	unrestricted	false			
CLI	unrestricted	fairly false			
CLF	unrestricted	absolutely false			

(1). The safety measure is a fuzzy truth restriction which falsifies S. Subjective assessments for the 45 input propositions at the bottom of the hierarchy are shown in Table 2. A computer program is available to process these inputs and to produce fuzzy truth restrictions on every proposition at every stage in the hierarchy.

The resulting truth restrictions for the Tay Bridge assessments are shown

in Fig. 4. The numbers of the truth restrictions in that figure must be related to the propositions in the boxes in Fig. 3. The critical truth restriction which yields the most false restriction upon S is τ_{55} which derives from **NP** which in turn derives from the restriction **absolutely false** given to the proposition **LLL** (that the probability of a new presently unknown loading effect causing failure is **low**). The truth restrictions deriving from **HE** and **RH** are τ_{136} and τ_{70} respectively and have similar values. The truth restrictions from which τ_{136} derive are shown in Fig. 4(*b*). These show that the design errors (τ_{131}), the severity of the "climate" (τ_{131}) the construction errors (τ_{132}) and the misuse of the structure (τ_{133}) are rather similar. The restriction upon **RH** of τ_{70} derives

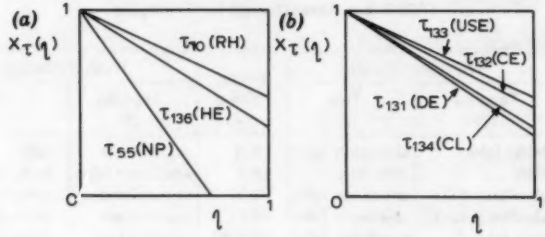

FIG. 4.—Results for Tay Bridge

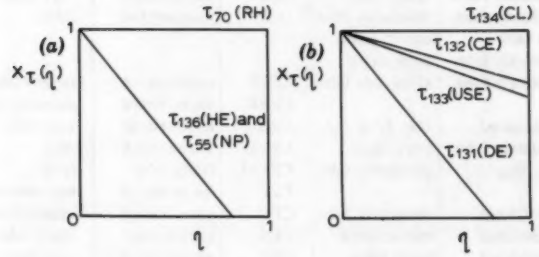

FIG. 5.—Results for Tacoma Narrows Bridge

directly from the restriction **absolutely false** on **RHD** which refers to the lack of data about the severity of wind storms in the Tay Estuary.

The truth restrictions for the Tacoma Narrows Bridge assessments are shown in Fig. 5. This time τ_{136} and τ_{55} for **HE** and **NP** are identical and τ_{70} for **RH** is **undecided**. Here τ_{55} derives directly from the assessment **absolutely false** on **SSS** which refers to the new mode of oscillation of the bridge due to its unusual structural form. The restriction upon **HE** comes from τ_{131} on **DE** with little reason to falsify **HE** from construction error, use or climate (**CE, SU, CL**). The restriction τ_{131} on **DE** derives directly from the input **absolutely false** on **DET** the proposition that there was **no** mode of structural behavior inadequately understood by the existing technology of the time.

The inputs of Table 2 seem therefore to produce truth restrictions on **S**, **NP**, **HE**, and **RH** which agree with what might be expected intuitively from the mass of data about the two accidents.

Future Use

There are two major problems which must be dealt with in this analysis. Firstly it could be argued that the truth restriction upon S for a structure which we know to have failed should be **absolutely false**. Secondly, the answer derives from assessments made with the benefit of hindsight and is therefore of little use for comparison with data regarding the future. In order to correct both of these difficulties it is necessary for research such as that by Walker and Sibly (10), which attempts to understand the thoughts of, and the pressures on, the designers of these bridges. Just what assessments might they have made? The reason that the fuzzy truth restrictions on S are not **absolutely false** is that it is not possible to have a totally clear idea of the cause of failure and so every truth restriction on the critical path through the logical hierarchy is not **absolutely true** or **false**. With increasing clarity or certainty regarding the reasons for the actual failure so can the uncertainty in τ_{137} on S be reduced. The restrictions of Figs. 4 and 5 *contain* **absolutely false**. The truth modifiers contained within the hierarchy of Fig. 3 have to be empirically adjusted to reflect the available information and the result stored as a computer data file. It is anticipated that this process could be performed on all failures from the published information where incomplete information is available then the truth restrictions are simply left as unrestricted. Work is to proceed on methods of combining these files in a sort of learning procedure which would provide an accumulated experience within the computer against which all new assessments may be compared.

Appendix.—References

1. Amman, A. H., et al., "The failure of the Tacoma Narrows Bridge," Federal Works Agency, Washington, D.C., Mar., 1941.
2. Baldwin, J. F., "A New Approach to Approximate Reasoning using a Fuzzy Logic," *Research Report EM/FS3*, University of Bristol, Feb., 1978.
3. Baldwin, J. F., "A Model of Fuzzy Reasoning and Fuzzy Logic," *Research Report EM/FS10*, University of Bristol, July, 1978.
4. Blockley, D. I., "Analysis of Structural Failures," *Proceedings*, Institution of Civil Engineers, Part 1, Vol. 62, Feb., 1977, pp. 51–74.
5. Blockley, D. I., *The Nature of Structural Design and Safety*, Ellis Harwood, Chichester, England, 1980.
6. Matousek, M., "Outcomings of a Survey on 800 Construction Failures," *Colloquium on Inspection and Quality Control*, International Association of Bridge and Structural Engineering, Cambridge, England, July, 1977.
7. Melcher, R. E., "The Influence of Control Processes in Structural Engineering," *Proceedings*, Institution of Civil Engineers, Part 2, Vol. 64, Dec., 1978, pp. 791–807.
8. Popper, K. R., *Conjectures and Refutations*, Routledge and Keegan Paul, London, England, 1976.
9. *Report of the Court of Enquiry upon the circumstances attending the fall of a portion of the Tay Bridge on 28th Dec.*, 1879, Her Majesty's Stationary Office, London, England, 1880.
10. Sibly, P. G., and Walker, A. C., "Structural Accidents and their Causes," *Proceedings*, Institution of Civil Engineers, Vol. 62, Part 1, May, 1977, pp. 191–208.

JOURNAL OF
THE ENGINEERING
MECHANICS DIVISION

ULTIMATE LOAD BEHAVIOR OF CURVED I-BEAMS

By Yuhshi Fukumoto,[1] M. ASCE and Susumu Nishida[2]

INTRODUCTION

The purpose of this study is to derive fundamental equations of a single curved I-beam subjected to the action of bending and torsional moments and also to investigate the behavior of curved flexural members under large torsional deflection. The derived equilibrium equations are solved by the transfer matrix method for both elastic and inelastic ranges.

Recently, the Task Committee on Curved Girders (3) presented a design guide for curved steel I-girder bridge and the Task Committee on Curved Box Girder (4) summarized the researches conducted to investigate the static and dynamic behavior of curved steel box girder bridges.

The two committees have identified one problem among others—relatively little data are available for use in developing ultimate load design criteria for curved girders and the committees suggested that further research on ultimate load behavior is needed for analytical procedures. Keeping the foregoing points in mind, the writers have proceeded with the present study.

Experimental studies are also made to determine the effect of curvature on the ultimate load behavior. Six simply supported single curved I-beams are tested under a concentrated load. Curvatures of the I-beams vary from the straight beam with a specified initial crookedness, $f_0/L \doteqdot L/8R = 1/1000$, to the curved beam of $L/8R = 1/100$, in which L = the curved length of the beam; and R = the radius of horizontal curvature.

THEORETICAL ANALYSIS

Assumptions.—The following assumptions are made in the analysis of a single horizontally curved I-beam shown in Fig. 1: (1) Length and radius of curvature

[1]Prof. of Civ. Engrg., Nagoya Univ., Chikusa-Ku Nagoya, Japan.
[2]Asst. Prof., Kanazawa Inst. of Tech., Kanazawa, Japan.

Note.—Discussion open until September 1, 1981. To extend the closing date one month, a written request must be filed with the Manager of Technical and Professional Publications, ASCE. Manuscript was submitted for review for possible publication on April 18, 1980. This paper is part of the Journal of the Engineering Mechanics Division, Proceedings of the American Society of Civil Engineers, ©ASCE, Vol. 107, No. EM2, April, 1981. ISSN 0044-7951/81/0002-0367/$01.00.

are very large as compared with the cross-sectional dimensions; (2) no cross-sectional distortions occur during deflection; (3) shear strain along the middle surface of the thin walls due to shear in equilibrium with the change of normal stress is small and may be neglected; (4) shear strain in the plane normal to the middle surface of the thin walls is small and may be neglected; and (5) transverse displacements are much larger than the longitudinal displacements.

Strain-Displacement Relations.—As shown in Fig. 1, the x-axis and y-axis coincide with the respective principal centroidal axes of the cross-section and the z-axis is tangent to the curved axis of the member. The origin of the cylindrical coordinates (ρ, θ, and η) is taken at the center of curvature.

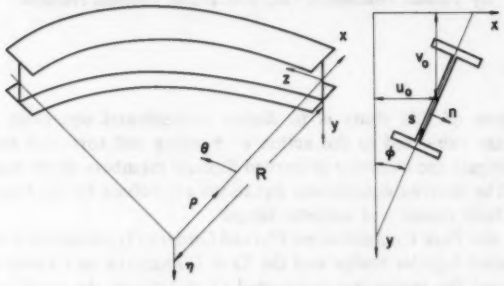

FIG. 1.—Analytical Model of Curved Member

From the finite displacement theory (11) the following strain-displacement relations may be obtained considering the fifth assumption

$$\epsilon_x = \frac{\partial u}{\partial x} + \frac{1}{2}\left[\left(\frac{\partial u}{\partial x}\right)^2 + \left(\frac{\partial v}{\partial x}\right)^2\right] \quad \ldots\ldots\ldots\ldots\ldots\ldots\ldots\ldots (1a)$$

$$\epsilon_y = \frac{\partial v}{\partial y} + \frac{1}{2}\left[\left(\frac{\partial u}{\partial y}\right)^2 + \left(\frac{\partial v}{\partial y}\right)^2\right] \quad \ldots\ldots\ldots\ldots\ldots\ldots\ldots\ldots (1b)$$

$$\epsilon_\theta = \left(\frac{\partial w}{\rho\partial\theta} + \frac{u}{\rho}\right) + \frac{1}{2}\left[\left(\frac{\partial w}{\rho\partial\theta} + \frac{u}{\rho}\right)^2 + \left(\frac{\partial v}{\rho\partial\theta}\right)^2\right] \quad \ldots\ldots\ldots\ldots (1c)$$

$$\gamma_{xy} = \frac{\partial u}{\partial y} + \frac{\partial v}{\partial x} + \frac{\partial u}{\partial x}\frac{\partial u}{\partial y} + \frac{\partial v}{\partial x}\frac{\partial v}{\partial y} \quad \ldots\ldots\ldots\ldots\ldots\ldots\ldots\ldots (1d)$$

$$\gamma_{x\theta} = \left(\frac{\partial u}{\rho\partial\theta} - \frac{w}{\rho}\right) + \frac{\partial w}{\partial x} + \frac{\partial u}{\partial x}\left(\frac{\partial u}{\rho\partial\theta} - \frac{w}{\rho}\right) + \frac{\partial v}{\partial x}\frac{\partial v}{\rho\partial\theta} \quad \ldots\ldots\ldots\ldots (1e)$$

$$\gamma_{y\theta} = \frac{\partial v}{\rho\partial\theta} + \frac{\partial w}{\partial y} + \frac{\partial u}{\partial y}\left(\frac{\partial u}{\rho\partial\theta} - \frac{w}{\rho}\right) + \frac{\partial v}{\partial y}\frac{\partial v}{\rho\partial\theta} \quad \ldots\ldots\ldots\ldots\ldots\ldots (1f)$$

in which u, v, and w denote the displacements in the x, y, and θ directions, respectively. The second assumption leads to the following equations:

$$\epsilon_x = \epsilon_y = \gamma_{xy} = 0 \qquad (2)$$

in which $u = u_0 - y \sin \phi - x(1 - \cos \phi)$;

$$v = v_0 + x \sin \phi - y(1 - \cos \phi) \qquad (3)$$

where u_0 and v_0 = the displacements of the centroid from the original position; and ϕ = the angle of rotation about the θ-axis.

Using Eq. 3 and the third and fourth assumptions which imply $\gamma_{x\theta} = \gamma_{y\theta} = 0$ on the middle surface, the longitudinal displacement, w, may be derived as shown:

$$\begin{aligned} w = w_0 &- \left[\left(u_0' - \frac{w_0}{R}\right)\cos\phi + v_0' \sin\phi\right] x \\ &- \left[v_0' \cos\phi - \left(u_0' - \frac{w_0}{R}\right)\sin\phi\right] y + \left[\int \frac{R}{\rho} y dx - \int \frac{R}{\rho} x dy\right]\phi' \\ &+ \int \frac{\rho - R}{\rho} dx \left[\left(u_0' - \frac{w_0}{R}\right)\cos\phi + v_0' \sin\phi\right] \\ &+ \int \frac{\rho - R}{\rho} dy \left[v_0' \cos\phi - \left(u_0' - \frac{w_0}{R}\right)\sin\phi\right] \qquad (4) \end{aligned}$$

in which the terms with prime denote the partial derivatives with respect to θ and constant R (i.e., with respect to $\partial/R\partial\theta$); and w_0 = the longitudinal displacement of the centroid. The integral terms of Eq. 4 may be transformed using the curvilinear coordinate axes (s, n), in which s is taken along the middle surface of the thin walls; and n is normal to the s-axis. Then, Eq. 4 may be rewritten in the following convenient form:

$$\begin{aligned} w = w_0 &- \left[\left(u_0' - \frac{w_0}{R}\right)\cos\phi + v_0' \sin\phi\right] x \\ &- \left[v_0' \cos\phi - \left(u_0' - \frac{w_0}{R}\right)\sin\phi\right] y - \left(\phi' - \frac{v_0'}{R}\right)\omega \qquad (5a) \end{aligned}$$

in which ω denotes unit warping with respect to the centroid and may simply be defined by the following equation for the approximation $R/\rho^* \doteqdot 1$:

$$\omega = \int_0^s \frac{R}{\rho^*} \rho_s \, ds - \frac{R}{\rho^*} \rho_n n = \omega^* - \rho_n n \qquad (5b)$$

$$\text{where} \quad \rho_s = x^* \frac{dy^*}{ds} - y^* \frac{dx^*}{ds}; \quad \rho_n = x^* \frac{dx^*}{ds} + y^* \frac{dy^*}{ds} \qquad (5c)$$

The terms with asterisk, ρ^*, x^*, and y^*, show the values of ρ, x, and y, respectively, on the middle surface of the thin walls.

The general equation of shear strains on any surface parallel to the middle surface of the thin wall may be given by

$$\gamma_{s\theta} = \gamma_{x\theta} \frac{\partial x}{\partial s} + \gamma_{y\theta} \frac{\partial y}{\partial s} \qquad (6a)$$

With the aid of Eqs. 3 and 5, Eq. 6*a* may be formulated as shown:

$$\gamma_{s\theta} = \frac{\partial x}{\partial s}\left(\frac{\partial u}{\rho \partial \theta} - \frac{w_0}{\rho}\right) + \frac{\partial y}{\partial s}\frac{\partial v}{\rho \partial \theta} + \frac{\partial w}{\partial s}$$

$$+ \frac{\partial u}{\partial s}\left(\frac{\partial u}{\rho \partial \theta} - \frac{w_0}{\rho}\right) + \frac{\partial u}{\partial s}\frac{\partial v}{\rho \partial \theta} \quad \ldots\ldots\ldots\ldots\ldots\ldots\ldots\ldots\ldots\ldots (6b)$$

$$\gamma_{ss} = \gamma_{s\theta} = 2n\left(\phi' - \frac{v_0'}{R}\right) \quad \ldots\ldots\ldots\ldots\ldots\ldots\ldots\ldots\ldots\ldots (6c)$$

in which the higher-order terms are small and are neglected.

Substituting Eqs. 3 and 5 into Eq. 1*c* and considering the first assumption, $R/\rho \doteq 1$, the following equation may be deduced

$$\epsilon_z = \epsilon_\theta = \left(w_0' + \frac{u_0}{R}\right) - \left[\left(u_0'' - \frac{w_0'}{R}\right)\cos\phi + v_0'' \sin\phi + \frac{1 - \cos\phi}{R}\right] x$$

$$- \left[v_0'' \cos\phi - \left(u_0'' - \frac{w_0'}{R}\right)\sin\phi + \frac{\sin\phi}{R}\right] y - \left(\phi'' - \frac{v_0''}{R}\right)\omega$$

$$+ \frac{1}{2}\left[\left(u_0' - \frac{w_0}{R}\right)^2 + v_0'^2 + (x^2 + y^2)\phi'^2\right] \quad \ldots\ldots\ldots\ldots\ldots\ldots\ldots\ldots (7)$$

Equilibrium Equations and Boundary Conditions.—The curved member in this analysis is in equilibrium under the action of distributed loads along the length and external forces at both ends. Using the variational method (8–10), internal and external works may be formulated as

$$\int_0^L \int_A (\sigma_z \delta \epsilon_z + \tau_{sz} \delta \gamma_{sz})\, dA dz = \int_0^L (q_x \delta u_0 + q_y \delta v_0$$

$$+ q_z \delta w_0 + m_z \delta \phi)\, dz + \bar{N} \delta w_0|_0^L + \bar{V}_x \delta u_0|_0^L + \bar{V}_y \delta v_0|_0^L$$

$$+ \bar{M}_z \delta\phi|_0^L - \bar{M}_y \delta\left(u_0' - \frac{w_0}{R}\right)\Bigg|_0^L - \bar{M}_x \delta v_0'|_0^L - \bar{M}_\omega \delta\left(\phi' - \frac{v_0'}{R}\right)\Bigg|_0^L \quad \ldots\ldots (8)$$

in which σ_z = normal stress; τ_{sz} = shearing stress; and $\bar{N}$, $\bar{V}_x$, $\bar{V}_y$, $\bar{M}_z$, $\bar{M}_x$, $\bar{M}_y$, $\bar{M}_\omega$ = end forces at both ends. Substituting Eqs. 6 and 7 into Eq. 8 and requiring that the equation be satisfied for arbitrary virtual displacements leads to the equilibrium equations and the boundary conditions, as follows:

$$N' + \frac{1}{R}(M_y \cos\phi - M_x \sin\phi)' + \frac{N}{R}\left(u_0' - \frac{w_0}{R}\right) + q_z = 0 \quad \ldots\ldots\ldots (9a)$$

$$(M_y \cos\phi - M_x \sin\phi)'' - \frac{N}{R} + \left[N\left(u_0' - \frac{w_0}{R}\right)\right]' + q_x = 0 \quad \ldots\ldots\ldots (9b)$$

$$(M_y \cos\phi + M_y \sin\phi)'' - \frac{M_\omega'' + T_{st}'}{R} + (N v_0')' + q_y = 0 \quad \ldots\ldots\ldots (9c)$$

$$M''_\omega + T'_{st} + (K\phi')' - M_y\left[\left(u''_0 - \frac{w'_0}{R}\right)\sin\phi - v''_0\cos\phi - \frac{\sin\phi}{R}\right]$$

$$- M_x\left[v''_0\sin\phi - \left(u''_0 - \frac{w'_0}{R}\right)\cos\phi - \frac{\cos\phi}{R}\right] + m_z = 0 \quad \ldots\ldots\ldots (9d)$$

$$(N - \bar{N})\,\delta w_0|_0^L = 0 \quad \ldots\ldots\ldots (9e)$$

$$\left[(M_y\cos y - M_x\sin\phi)' - N\left(u'_0 - \frac{w_0}{R}\right) - \bar{V}_x\right]\delta u_0|_0^L = 0;$$

$$[(M_y\cos\phi - M_x\sin\phi) - \bar{M}_y]\,\delta\left(u'_0 - \frac{w_0}{R}\right)\Bigg|_0^L = 0 \quad \ldots\ldots\ldots (9f)$$

$$\left[(M_x\cos\phi + M_y\sin\phi)' - \frac{M'_\omega + T_{st}}{R} + Nv'_0 - \bar{V}_y\right]\delta v_0|_0^L = 0;$$

$$[(M_x\cos\phi + M_y\sin\phi) - \bar{M}_x]\,\delta v'_0|_0^L = 0 \quad \ldots\ldots\ldots (9g)$$

$$[(M'_\omega + T_{st} + K\phi') - \bar{M}_z]\,\delta\phi|_0^L = 0; \quad (M_\omega - \bar{M}_\omega)\delta\left(\phi' - \frac{v'_0}{R}\right)\Bigg|_0^L = 0 \quad (9h)$$

in which $N = \int_A \sigma_z\,dA$; $M_x = \int_A \sigma_z y\,dA$; $M_y = \int_A \sigma_z x\,dA$;

$$M_\omega = \int_A \sigma_z\omega\,dA; \quad T_{st} = \int_A 2\tau_{st}\,n\,dA; \quad K = \int_A \sigma_z(x^2 + y^2)\,dA \quad \ldots (10)$$

The force-displacement relations for doubly symmetric cross sections may be obtained by substituting Eq. 7 into Eq. 10 as shown

$$N = \int_A E\epsilon_z\,dA = EA\left[\left(w'_0 + \frac{u_0}{R}\right) + \frac{1}{2}\left(u'_0 - \frac{w_0}{R}\right)^2\right.$$

$$\left. + \frac{1}{2}v'^2_0\right] + \frac{1}{2}EI_p\phi'^2 \quad \ldots\ldots\ldots (11a)$$

$$M_x = \int_A E\epsilon_z y\,dA = -EI_x\left[v''_0\cos\phi - \left(u''_0 - \frac{w'_0}{R}\right)\sin\phi + \frac{\sin\phi}{R}\right] \quad (11b)$$

$$M_y = \int_A E\epsilon_z x\,dA = -EI_y\left[\left(u''_0 - \frac{w'_0}{R}\right)\cos\phi + v''_0\sin\phi + \frac{1 - \cos\phi}{R}\right] \quad (11c)$$

$$M_\omega = \int_A E\epsilon_z\omega_n\,dA = -EI_\omega\left(\phi'' - \frac{v''_0}{R}\right) \quad \ldots\ldots\ldots (11d)$$

$$T_{st} = \int G\gamma_{zs}(2n)\,dA = \mathrm{G}\,K_T\left(\phi' - \frac{v'_0}{R}\right) \quad \ldots\ldots\ldots (11e)$$

$$K = \int_A E\epsilon_z(x^2 + y^2)\,dA = EI_p\left[\left(w_0' + \frac{u_0}{R}\right) + \frac{1}{2}\left(u_0' - \frac{w_0}{R}\right) + \frac{1}{2}v_0'\right] + \frac{1}{2}EI_{pp}\phi'^2 \quad \ldots\ldots\ldots\ldots\ldots\ldots\ldots\ldots\ldots\ldots (11f)$$

in which $A = \int_A dA$; $I_x = \int_A y^2\,dA$; $I_y = \int_A x^2\,dA$; $I_p = \int_A (x^2 + y^2)\,dA$; $I_\omega = \int_A \omega_n^2\,dA$; $K_T = \int_A (2n)^2\,dA$; $I_{pp} = \int_A (x^2 + y^2)^2\,dA$; and ω = equal to the normalized unit warping ω_n for doubly symmetric cross sections. Eq. 11*e* represents St. Venant's torsion which naturally appears because of the variation of shear strain through the thickness of the plate.

The procedure followed in the derivation of Eqs. 9–11 is similar to that for the straight members as described in Refs. 8 and 9 except the necessary changes required for the curved members.

Transfer Matrix Method.—From the boundary conditions (Eqs. 9*e*–9*h*) the displacements and the forces in the state vectors may be derived as shown:

$$\theta_y = u_0' - \frac{w_0}{R}; \quad \theta_x = v_0'; \quad \Theta = \phi' - \frac{v_0'}{R}; \quad M_z = M_\omega' + T_{st} + K\phi';$$

$$\bar{M}_x = M_x\cos\phi + M_y\sin\phi; \quad V_y = (M_x\cos\phi + M_y\sin\phi)' - \frac{M_\omega' + T_{st}}{R} + Nv_0'; \quad \bar{M}_y = M_y\cos\phi - M_x\sin\phi;$$

$$V_x = (M_y\cos\phi - M_x\sin\phi)' + N\left(u_0' - \frac{w_0}{R}\right) \quad \ldots\ldots\ldots\ldots\ldots\ldots (12)$$

in which the terms with the $\bar{M}$ denote the bending moments with respect to global coordinate system.

The equilibrium equations from Eqs. 9–12 may be represented by a matrix form as

$$\frac{d}{dz}\mathbf{V} = \mathbf{GV} \quad \ldots\ldots\ldots\ldots\ldots\ldots\ldots\ldots\ldots\ldots\ldots\ldots\ldots\ldots (13)$$

in which $\mathbf{V}$ = the state vector defined by $\mathbf{V}^T = (w_0\ N\ u_0\ \theta_y\ \bar{M}_y\ V_x\ v_0\ \theta_x\ \bar{M}_x\ V_y\ \phi\ \rho\ M_z\ M_\omega\ 1)$; and $\mathbf{G} = 15 \times 15$ matrix.

The field transfer matrix relating the state vectors at the left side to the right side of the divided elements may be derived by integrating Eq. 13 using the Runge-Kutta Method. The linear analysis of curved beams by the transfer matrix has been presented in Ref. 1. A computer program was developed here to provide the numerical results utilizing the successive approximation method for the solution of the nonlinear matrix equation (Eq. 13).

Stiffness of Partially Yielded Cross Section.—Using the force-displacement relations for the doubly symmetric cross section, Eq. 7 may be transformed into:

$$\epsilon_z = \frac{N}{EA} + \frac{M_y}{EI_y}x + \frac{M_x}{EI_x}y + \frac{M_\omega}{EI_\omega}\omega_n + \frac{1}{2}\left(\frac{x^2 + y^2}{A} - r_0^2\right)\phi'^2 \quad \ldots\ldots (14)$$

in which r_0 denotes the polar radius of gyration of area. In the foregoing equation, the last term is small and may be neglected. In that case, it may be noted that ϵ_z changes linearly with respect to x, y, and ω_n. However, ϵ_z does not vary linearly with respect to displacement quantities, as may be seen from Eqs. 11 and 14.

In the inelastic range, penetration of yielding reduces the stiffnesses of the member. Eq. 14 is applicable to the partially yielded cross section where the stiffnesses change from elastic to inelastic ones. For the ideal elastic-plastic stress-strain relationship, the inelastic stiffnesses of the cross section may be derived using the secant modulus of elasticity as shown

$$E_z = \frac{\sigma}{\epsilon}; \quad EA = \int_A E_z\, dA; \quad EI_x = \int_A E_z y^2\, dA;$$

$$EI_y = \int_A E_z x^2\, dA; \quad EI_\omega = \int_A E_z \omega_n^2\, dA \quad \ldots\ldots\ldots\ldots\ldots\ldots \quad (15)$$

The inelastic stiffnesses are, thus, determined by trial and error procedure using Eqs. 14 and 15. Using the total strain theory, St. Venant's torsional stiffness of the partially yielded cross section may be derived as follows

$$GK_T = \frac{E}{2(1+\nu)} \int_{A_e} \frac{1}{3} t^3\, ds + \int_{A_p} \frac{E}{2 + 2\nu + 3\left(\dfrac{E}{E_z} - 1\right)} \frac{1}{3} t^3\, ds \qquad (16)$$

in which A_e and A_p correspond to the elastic and plastic parts, respectively.

Experimental Studies

Six welded curved I-beams are tested to investigate the load-deflection relations and the ultimate load behavior under a concentrated load at the span center.

Curved I-Beams and Test Rig.—The cross-sectional dimensions and the radius of curvature of test beams are summarized in Table 1. Beams AR-3 and BR-3 are designated as the laterally unsupported straight beams with the initial crookedness of $L/1{,}000$. The curved flange plates are cut out from 8-mm thick

TABLE 1.—Dimensions and Curvatures of Curved I-Beam

Beam No.	d	b	w	t	$(L/8R)_N$	$(L/8R)_M$	L	Remarks
AR-1	251.6	101.6	5.6	8.4	1/100	1/109	1700	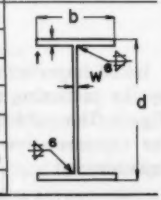
AR-2	251.9	101.0	5.7	8.3	1/200	1/238	1700	
AR-3	251.9	100.9	5.8	8.3	1/1000	1/798	1700	
BR-1	250.1	100.6	5.5	8.4	1/100	1/97	2800	
BR-2	251.8	100.6	5.7	8.3	1/200	1/206	2800	
BR-3	250.4	100.9	5.6	8.3	1/1000	1/1379	2800	
Nominal	250.0	100.0	6.0	8.0				

L = Length of Span along the Curved Web Center Line
N,M = Nominal Value and Measured Value

plate, and the flat web plate is bent elastically and welded into the position to give a specified curvature.

In these experiments, beams are restrained at their supports as described in Ref. 5, providing restraint against twist but not against warping. Load is applied at the center of the compression flange through the sole plate of t = 25 mm by a tension jack through the loading frame as shown in Fig. 2. The jack which is attached to the load cell is then connected to the gravity-load-simulator to hold the applied load vertical during test.

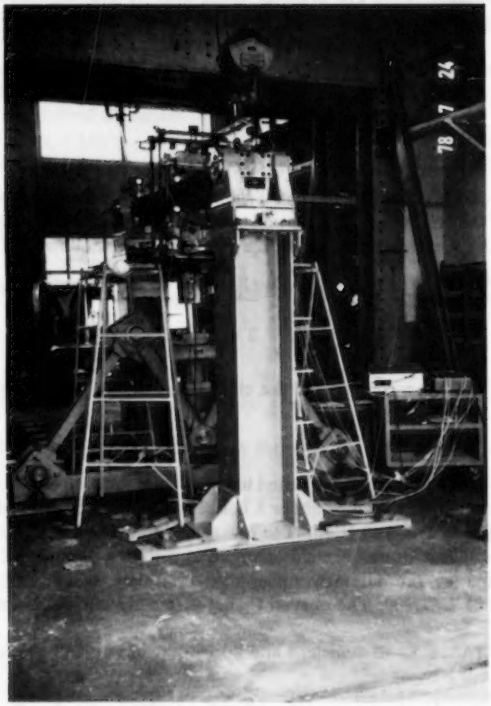

FIG. 2.—Test Setup

Initial Imperfections.—The longitudinal residual stress distributions obtained by the sectioning method for AR-1, AR-2, and AR-3 beams are presented in Fig. 3. The solid line curve through the experimental results is considered as the representative distribution curve and may be defined by the following equations:

$$\sigma_r = 873\left(\frac{2y}{d}\right)^4 - 226\left(\frac{2y}{d}\right)^2 - 88 \quad \text{in web,}$$

in meganewtons per square meter;

$$\sigma_r = 853\left(\frac{2x}{b}\right)^3 - 1{,}059\left(\frac{2x}{b}\right) + 314 \quad \text{in flange,}$$

in meganewtons per square meter . . . . . (17)

The foregoing equations satisfy the self equilibrium conditions of resultant axial force and bending moments about both axes as shown:

$$\int_A \sigma_r\, dA = \int_A \sigma_r y\, dA = \int_A \sigma_r x\, dA = 0 \quad \ldots\ldots\ldots\ldots\ldots\ldots \quad (18)$$

Measurement of out-of-straightness were made at seven equally spaced points for each fabricated curved specimen. Fig. 4 shows u_0, v_0, and ϕ_0 curves for

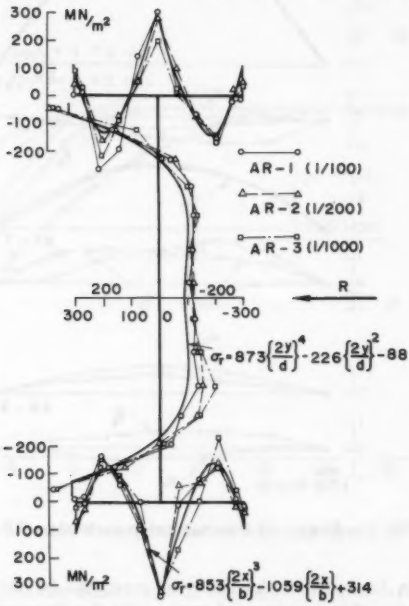

FIG. 3.—Measured Residual Stress Distributions

the BR-series. The curved solid thin lines indicate the prescribed u_0 curves for the test beams. It is found that there is less than 0.7 mm difference between the prescribed and the obtained curves.

Ultimate Load Behavior.—Fig. 5 shows the relations between the load and the midspan displacements u, v, and ϕ for BR-1. The test results are represented by the thick lines joining the test points and the thin curved lines represent the numerical results as described in the next section. As load is increased,

the beam is stressed elastically until parts of the beam are strained into the inelastic state. The ultimate capacity is reached when the progressive yielding reduces the stiffness of the beam to zero. Good agreement may be seen between the test and numerical results for the BR-1 beam.

Figs. 6 and 7 show the relationship between midspan load and angle of rotation at midspan for the AR-series and BR-series, respectively. The test results are represented by the solid lines joining the points marked with small circles,

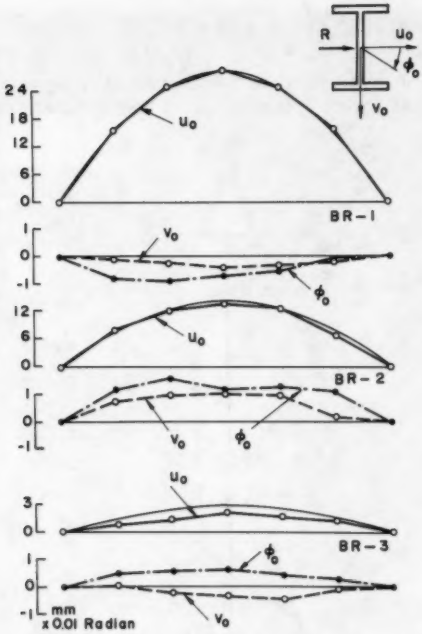

FIG. 4.—Shapes of Geometrical Imperfection (BR-Series)

and the broken lines depict the behavior predicted by the present study. In most of the cases, the experimental curves and the theoretical curves are very close. In the aforementioned figures, it is seen that the load-deformation relations for AR-3 and BR-3 correspond to the lateral buckling behavior of beams with initial crookedness of $L/1{,}000$. The inset to Figs. 6 and 7 lists the experimental and theoretical ultimate loads of the test beams.

Numerical Results

Elastic Analysis.—An example of the numerical results obtained under the loading of equal end moments is shown in Fig. 8. A simply supported beam

with nominal dimensions of I-250 mm × 100 mm × 5.5 mm × 8 mm and material properties $\sigma_y = 235\ \text{MN/m}^2$ (2,400 kgf/cm^2), $E = 2.06 \times 10^5\ \text{MN/m}^2$ (2.1×10^6 kgf/cm^2) and $\nu = 0.3$ is used for numerical computation. Parameter $L/8R$ which is similar to rise/span ratio of circular arches is introduced here for the horizontally curved configuration.

The curved length L of the beam in Fig. 8 corresponds to $\bar{\lambda} = 1.0$ in which $\bar{\lambda} = \sqrt{M_p/M_E}$ and is the modified beam slenderness (7); and M_E = the elastic critical moment of laterally unsupported straight beam with the span length L.

In Fig. 8, the curved thick lines show the elastic large-deformation behavior predicted by the present study, and the thin lines show the simplified results obtained by considering only the first term in Taylor's expansion of ϕ whereby Eqs. 9–11 are linearized.

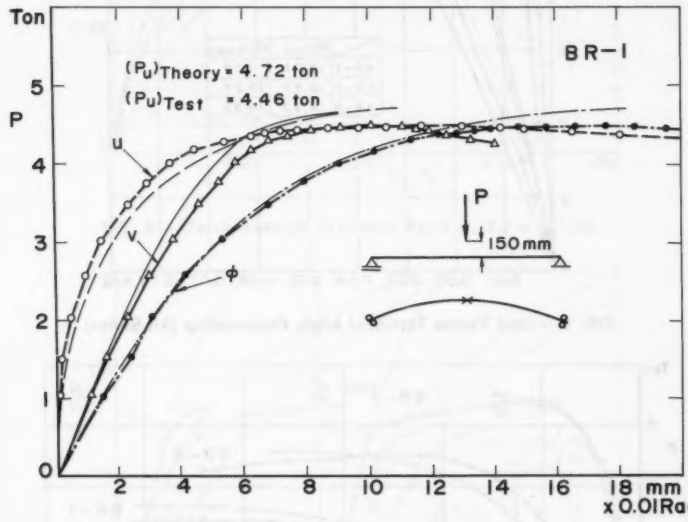

FIG. 5.—Load Versus Deflection Relationship (BR-1)

In Fig. 8, $(M_{cr})_{App}$ is the critical elastic moment (10) of a curved beam and is defined as,

$$(M_{cr})_{App} = \sqrt{\left(1 - \frac{L^2}{\pi^2 R^2}\right)\frac{\pi^2 EI_y}{L^2}\left(GK_T + \frac{\pi^2 EI_\omega}{L^2}\right)} \quad \ldots\ldots\ldots \quad (19)$$

Eq. 19 is determined as the moment when the displacement u or ϕ (the curved thin lines in Fig. 8) approaches infinity. It is interesting to note that the u/b-value increases gradually with M_0/M_p until the u/b versus M_0/M_p curve reverses the direction at $u \doteqdot 0.8b$ in the elastic large deflection analysis while the v/d-value and ϕ-value increase with the value of M_0/M_p.

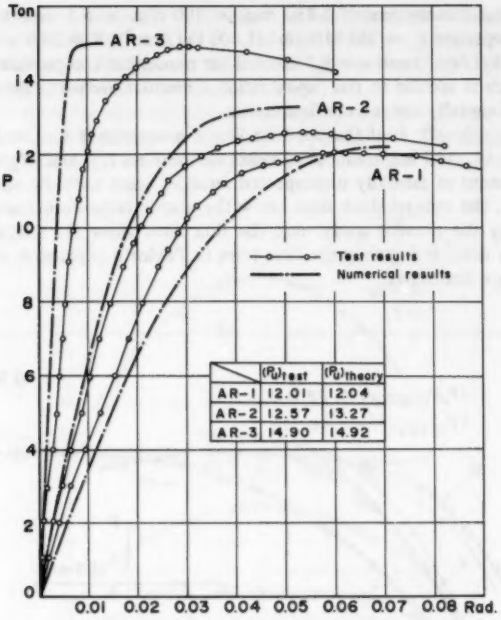

FIG. 6.—Load Versus Torsional Angle Relationship (AR-Series)

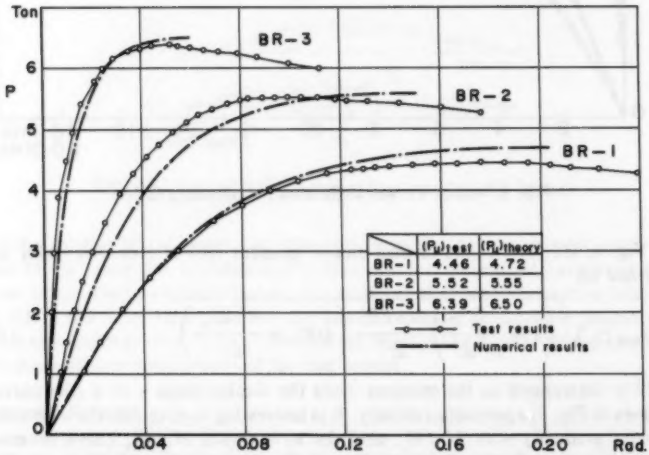

FIG. 7.—Load Versus Torsional Angle Relationship (BR-Series)

Inelastic Analysis.—Fig. 9 shows the results of the inelastic analysis of the same beam as in Fig. 8. The curved thick lines are for the inelastic analysis, while the thin lines are for the elastic analysis. The figures on the left show

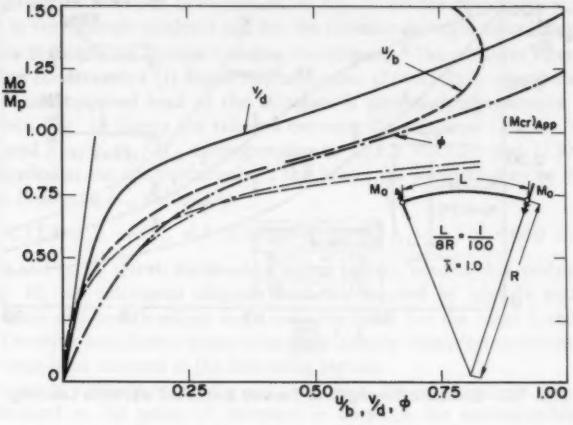

FIG. 8.—Elastic Analysis of Curved Beam ($L/8R = 1/100$)

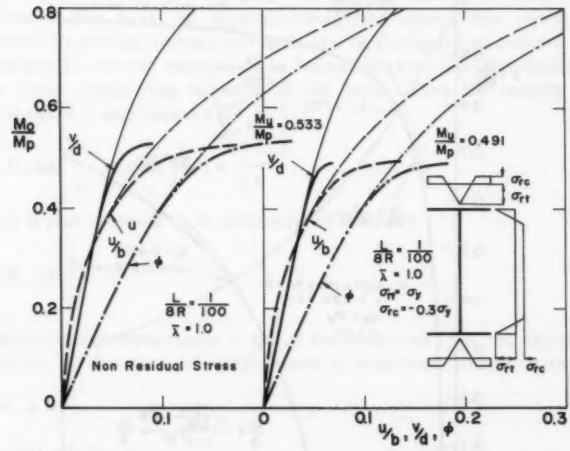

FIG. 9.—Inelastic Analysis of Curved Beam ($L/8R = 1/100$)

the inelastic behavior and the resulting ultimate moment without residual stresses and the figures on the right show the same with a specified welded-type residual stress distribution as shown in the inset to Fig. 9. It is seen from Fig. 9 that

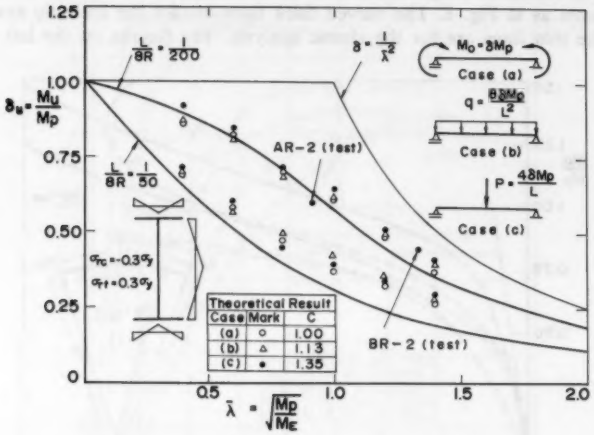

FIG. 10.—Ultimate Strength of Curved Beam for Variable Loading

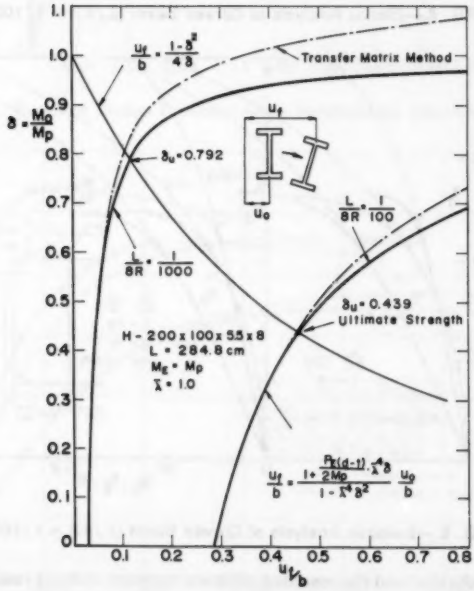

FIG. 11.—Approximate Ultimate Strength

the early yielding due to the residual stresses reduces the ultimate moment from $0.53\,M_p$–$0.49\,M_p$.

The numerical results obtained for the AR-series and BR-series are shown together with the test results in the inset tables to Figs. 5–7. The modified residual stress distributions as expressed by Eq. 17 and the prescribed u_0 curves are used in the inelastic analysis and for the ultimate strength calculation.

Ultimate Strength for Certain Loading Conditions.—The ultimate strength for the loading conditions of (1) Equal end moments; (2) uniformly distributed load; and (3) a concentrated load at the midspan is determined separately for the three cases. Fig. 10 shows the relation between the obtained ultimate strength M_u/M_p and $\bar{\lambda} = \sqrt{M_p/M_E}$ corresponding to $L/8R = 1/200$ and $1/50$. When load is applied at the centroidal axis of the beam, the $\bar{\lambda}$-values may be obtained using the following M_E values (2):

$$M_{E(b)} = 1.13\,M_{E(a)}; \quad M_{E(c)} = 1.35\,M_{E(a)} \qquad (20)$$

The inset to Fig. 10 shows the residual stress pattern used in this analysis.

In Fig. 10, the calculated ultimate moments marked by triangle and circles for the three different loadings are nearly the same for the same $\bar{\lambda}$ and $L/8R$ values. The thick solid lines represent the approximate ultimate moment calculated by the formula as covered in the following section.

Approximate Ultimate Strength.—Approximate ultimate strength may simply be determined at the point of intersection between the second-order elastic curve and the second-order rigid plastic curve as shown in Fig. 11. The dimensions of the test specimen are given in Fig. 11. The chain curves marked "Transfer Matrix Method" represent second-order elastic results obtained from the numerical solution of Eqs. 9–11. An approximate second-order elastic curve, leading to a relationship for the ultimate strength, can be developed as follows.

The horizontally curved beam could be defined in a cartesian coordinate system with the z-axis connecting the ends of the beam. Then the initially circular horizontal curve is approximate by

$$u_0(z) = U_0 \sin\frac{\pi z}{L}, \quad \text{with} \quad U_0 = \frac{L^2}{8R} \qquad (21a)$$

and $\phi_0(z)$ is also assumed to be sinusoidal of the form

$$\phi_0(z) = \Phi_0 \sin\frac{\pi z}{L} \qquad (21b)$$

The displacement components u and ϕ are measured from the initial curved configuration, so that the total displacement u, measured from the z-axis is

$$u_{\text{total}} = u_0 + u \qquad (22a)$$

and the total rotation is

$$\phi_{\text{total}} = \phi_0 + \phi \qquad (22b)$$

The differential equations with initial deflection u_0 and ϕ_0 under equal end moment are given by (12):

$$EI_y \frac{d^4 u}{dz^4} + M_0 \frac{d^2 \phi}{dz^2} = M_0 \Phi_0 \left(\frac{\pi}{L}\right)^2 \sin \frac{\pi z}{L};$$

$$EI_\omega \frac{d^4 \phi}{dz^4} - \mathbf{G} K_T \frac{d^2 \phi}{dz^2} + M_0 \frac{d^2 u}{dz^2} = M_0 U_0 \left(\frac{\pi}{L}\right)^2 \sin \frac{\pi z}{L} \quad \ldots\ldots\ldots (23)$$

With simply supported boundary conditions, a possible solution is given by

$$u = U \sin \frac{\pi z}{L} \quad \text{and} \quad \phi = \Phi \sin \frac{\pi z}{L} \quad \ldots\ldots\ldots\ldots\ldots\ldots (24a)$$

with the following solutions for U and Φ:

$$U = \frac{U_0 + \dfrac{r_0^2 P_{zE}}{M_0} \Phi_0}{\left(\dfrac{M_E}{M_0}\right)^2 - 1}; \quad \Phi = \frac{\Phi_0 + \dfrac{P_E}{M_0} U_0}{\left(\dfrac{M_E}{M_0}\right)^2 - 1} \quad \ldots\ldots\ldots\ldots\ldots (24b)$$

in which $P_E = \pi^2 EI_y / L^2$; $r_0^2 P_{zE} = \mathbf{G} K_T + \pi^2 EI_\omega / L^2$; and $M_E = \sqrt{r_0^2 P_{zE} P_E}$.

Now, u_f is defined as the total lateral displacement of the compression flange at midspan. Therefore, due to the horizontal curvature, it follows that $u_f = U_0 + U + (d - t)/2x\,(\Phi_0 + \Phi)$. If $\Phi_0 = 0$, it can be shown that

$$u_f = \frac{\left(\dfrac{M_E}{M_0}\right)^2 + \dfrac{d - t}{2} \dfrac{P_E}{M_0}}{\left(\dfrac{M_E}{M_0}\right)^2 - 1} \quad \ldots\ldots\ldots\ldots\ldots\ldots\ldots (25a)$$

But, $(M_0/M_E)^2 = (M_0/M_p)^2 (M_p/M_E)^2 = \delta^2 \bar{\lambda}^2$ in which $\delta = M_0/M_p$. Finally

$$\frac{u_f}{b} = \frac{1 + \dfrac{P_E (d - t)}{2M_p} \bar{\lambda}^4 \delta}{1 - \bar{\lambda}^4 \delta^2} \frac{U_0}{b} \quad \ldots\ldots\ldots\ldots\ldots\ldots (25b)$$

As seen from the figure, the curves resulting from Eq. 25*b* closely coincide with the second-order elastic curves obtained for the curved beam for $L/8R = 1/100$ as well as for 1/1,000.

The dropping curve represents the second-order rigid plastic curve (6) which is governed by the lateral direction plastic strength of the compression flange of a bending beam. This relation can be developed as follows.

Under the axial compressive force N in the flange, plastic moment M_{pf} due to the lateral bending of the compression flange may be expressed by

$$M_{pf} = \frac{M_p b}{4(d - t)} \left(1 - \frac{M_0}{M_p}\right)\left(1 + \frac{M_0}{M_p}\right) \quad \ldots\ldots\ldots\ldots\ldots\ldots (26)$$

in which $M_0 \doteq N(d - t)$; and $M_p \doteq \sigma_y bt(d - t)$.

Considering $M_{pf} = N u_f$, Eq. 26 may be reduced to the following Eq. 27 which is the equation of the dropping curve in Fig. 11

$$\frac{u_f}{b} = \frac{1 - \delta^2}{4\delta} \quad \ldots \ldots \ldots \ldots \ldots \ldots \ldots \ldots \ldots \ldots \ldots \ldots \ldots (27)$$

Approximate ultimate strength δ_u ($= M_u/M_p$) at the point of intersection between the second-order elastic curve and the second-order rigid plastic curve may be determined from the following resulting equation obtained by equating Eqs. 25*b* and 27.

$$\bar{\lambda}^4 \delta^4 - \left\{ \left[1 + \frac{P_E(d-t)}{2M_p} \left(\frac{L^2}{2Rb} \right) \right] \bar{\lambda}^4 + 1 \right\} \delta^2 - \left(\frac{L^2}{2Rb} \right) \delta + 1 = 0 \quad \ldots (28)$$

The approximate ultimate strength $\delta_u = 0.439$ and 0.792 shown in Fig. 11 are then obtained from Eq. 28 for $L/8R = 1/100$ and $1/1{,}000$, respectively. The approximate ultimate strengths for $L/8R = 1/200$ and $1/50$ are shown by the thick lines in Fig. 10. From Fig. 10, it is seen that there is a good agreement between the theoretical ultimate strength results (marked ●, ○, △) and the approximate strength curves and it may be noted that the approximate strength curves are on the conservative side compared to the theoretical results. Two test results for AR-2 (test) and BR-2 (test) and marked as such are also shown for comparison with the calculated results.

Conclusions

A method of analyzing the elastic and inelastic large-deflection behavior of the horizontally curved I-beam is presented for certain loading conditions using the transfer matrix method. Load versus *u*, *v*, and ϕ relations are investigated into the elastic finite displacement range as shown in Fig. 8, and the results of the inelastic analysis considering the residual stress distributions are shown in Fig. 9. From Fig. 10, it is seen that the ultimate strength for the three different loading conditions are almost the same.

The equilibrium equations are then reduced to the linear simultaneous differential equations and the critical elastic moment is thus obtained. Approximate ultimate strength is determined at the point of intersection between the second-order elastic curve which is asymptotic to the bifurcation solution and the second-order rigid plastic curve. Good agreement is found between the theoretical and the approximate results.

The experimental studies for six beams also show good agreement with the theoretical ones in respect of the *u*, *v*, and ϕ curves and the ultimate strength.

Appendix I.—References

1. Becker, G., "Ein Beitrag zur statischen Berechnung beliebig gelagerter ebener gekrümmter Stäbe mit einfach symmetrichen dünnwandigen offenen Profilen von in Stabachse veränderlichem Querschnitt unter Berücksichtigung der Wölbkrafttorsion," *Der Stahlbau,* Heft 11, 1965, pp. 334–346, Heft 12, 1965, pp. 368–377.
2. Clark, J. W., and Hill, H. N., "Lateral Buckling of Beam," *Transactions,* ASCE, Vol. 127, Part II, Paper No. 3366, 1962, pp. 180–201.
3. "Curved I-Girder Bridge Design Recommendations," by the Task Committee on Curved Girders of ASCE-AASHTO, William L. Armstrong, Chmn., *Journal of the Structural Division,* ASCE, Vol. 103, No. ST5, Proc. Paper 12955, May, 1977, pp. 1137–1168.
4. "Curved Steel Box-Girder Bridges; State-of-The-Art," by the Task Committee on

Curved Box Girders of ASCE-AASHTO, Dann H. Hall, Chmn., *Journal of the Structural Division*, ASCE, Vol. 104, No. ST11, Proc. Paper 14156, Nov., 1978, pp. 1719–1739.
5. Fukumoto, Y., Itoh, Y., and Kubo, M., "Strength Variation of Laterally Unsupported Beams," *Journal of the Structural Division*, ASCE, Vol. 106, No. ST1, Proc. Paper 15142, Jan., 1980, pp. 165–181.
6. Horne, M. M., and Merchant, W., *The Stability of Frames*, Pergamon Press, New York, N.Y., 1965.
7. "Laterally Supported and Unsupported Beams," by the Working Group 4 "lateral torsional buckling," *Introductory Report on Stability of Steel Structures*, Second International Colloquium, Liege, Belgium, Apr., 1977, pp. 127–143.
8. Murray, D. W., and Rajasekaran, S., "Technique for Formulating Beam Equations," *Journal of the Engineering Mechanics Division*, ASCE, Vol. 101, No. EM5, Proc. Paper 11613, Oct., 1975, pp. 561–573.
9. Nishino, F., Kasemset, C., and Lee, S. L., "Variational Formulation of Stability Problems for Thin-Walled Members," *Ingenieur Archiv*, Band 43, Heft 1, 1973, pp. 58–68.
10. Nishida, S., Yoshida, H., and Fukumoto, Y., "Large Deflection Analysis of Curved Members with Thin-Walled Open Cross-Section," *Proceedings of 24th Symposium of Structural Engineering*, Feb., 1978, pp. 77–84 (in Japanese).
11. Saada, A. S., *Elasticity Theory and Application*, Pergamon Press, New York, N.Y., 1974.
12. Sakai, F., "Unified Formulation of Basic Equations of Elastic Stability for Thin-Walled Members with Open Cross-Section," *Proceedings of the Japan Society of Civil Engineers*, No. 221, Jan., 1974, pp. 1–15 (in Japanese).
13. "Survey of Curved Girder Bridges," by the Joint AASHO-ASCE Committee on Flexural Members, Roger L. Brockenbrough, Chmn., *Civil Engineering*, ASCE, Vol. 43, No. 2, Feb., 1973, pp. 54–56.

Appendix II.—Notation

The following symbols are used in this paper:

A = area of cross section;
E, E_s = modulus of elasticity and secant modulus;
G = shear modulus;
I_x, I_y = moment of inertia about x-axis and y-axis;
I_ω = warping moment of inertia;
K_T = St. Venant's torsional constant;
K = cross-sectional value;
L = length of curved I-beam;
$(M_{cr})_{App}$ = approximate critical moment of curved beam;
M_E = elastic lateral buckling moment;
M_p = full plastic moment;
M_x, M_y = moment about x-axis and y-axis defined by local coordinate system;
$\bar{M}_x, \bar{M}_y$ = moment about x-axis and y-axis defined by global coordinate system;
M_ω = warping torsional moment;
N = axial force;
R = radius of curved beam;
T_{st} = St. Venant torsional moment;
u, v, w = displacement in x, y, and z directions, respectively;
(x, y, z) = curvilinear coordinate axes;

z = coordinate axis connecting ends of beam;
γ = shear strain;
$\delta = M_0/M_p$ = nondimensional moment;
ϵ = strain;
$\bar{\lambda} = \sqrt{M_p/M_E}$ = modified beam slenderness;
ρ_n, ρ_s = tangential and normal components to distance between point in cross section and centroid;
(ρ, θ, η) = cylinderical coordinate axes;
σ = normal stress;
ϕ = angle of torsion;
ω = unit warping with respect to centroid; and
ω_n = normalized unit warping.

JOURNAL OF
THE ENGINEERING
MECHANICS DIVISION

ELASTIC STRESSES IN FRETTING FATIGUE

By Jung S. Chung,[1] Cenap Oran,[2] M. ASCE, and David W. Hoeppner[3]

INTRODUCTION

Fretting fatigue is the combined action of fretting and fatigue. Fretting corrosion, which is the result of minute relative movements between two bodies that are held in contact by a normal force, was first examined in detail by Eden, Rose, and Cunningham in 1911 (2). Extensive experiments have been reported since, and various theories have been advanced to explain the fretting mechanism. For a brief survey of the literature on the subject, the reader may wish to refer to Refs. 5, 7, and 10.

In some of the recent fretting fatigue experiments conducted by the third writer (who recorded his observations in an unpublished report), cleavage cracking was observed immediately below the contact area. As a possible explanation of this observation it has been suggested that high triaxial strain is developed below the contact surface which, in the presence of some localized discontinuities (such as micropores or included particles), could result in a localized cleavage fracture.

In light of the foregoing observations, it appears desirable to take a close analytical look at the distribution of stresses in the vicinity of the contact area in a typical fretting-fatigue problem. The specific physical problem considered herein for this purpose (see Fig. 1) consists of a large rectangular plate of unit thickness, and two smaller fretting pads, also of unit thickness, which exert a pair of equal and opposite transverse forces, P, as shown in the figure.

[1]Former Grad. Student, Dept. of Mech. Engrg., Univ. of Missouri, Columbia, Mo. 65211.

[2]Prof. of Civ. Engrg., Univ. of Missouri, 1047 Engrg. Building, Columbia, Mo. 65211.

[3]Cockburn Prof. of Engrg. Design, Faculty of Applied Sci. and Engrg., Univ. of Toronto, Toronto, Canada; formerly Prof. of Mech. Engrg., Univ. of Missouri, Columbia, Mo. 65211.

Note.—Discussion open until September 1, 1981. To extend the closing date one month, a written request must be filed with the Manager of Technical and Professional Publications, ASCE. Manuscript was submitted for review for possible publication on September 12, 1980. This paper is part of the Journal of the Engineering Mechanics Division, Proceedings of the American Society of Civil Engineers, ©ASCE, Vol. 107, No. EM2, April, 1981. ISSN 0044-7951/81/0002-0387/$01.00.

The plate is fixed along one end and subjected to a cyclic axial force, Q, acting at the other end. Under the action of the cyclic load, the plate elongates and shortens as a function of time, and frictional forces develop between the plate and the fretting pads. The specific purpose of the present study is to analyze the stresses produced in the plate by the combined action of the cyclic axial load, and the normal and frictional forces that occur between the plate and the fretting pads.

Assumptions

The analysis presented herein is based on the following assumptions:

1. The material is homogeneous, isotropic, and linearly elastic.
2. The frequency of the cyclic load is much lower than the lowest natural frequency of the plate, thus implying that the problem does not involve any substantial dynamic effects.
3. The plate is thin, so that the problem can be approximated as a "plane stress" problem.
4. The length of the contact area is much smaller than the dimensions of the plate, i.e., $2b << L_o$ and $2b << H_o$, as indicated in Fig. 1. This implies,

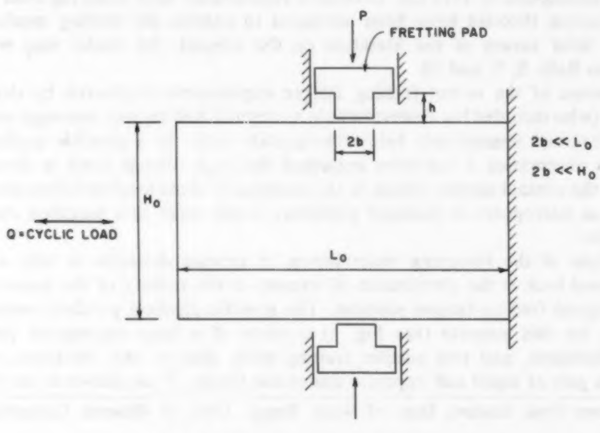

FIG. 1.—Physical System Analyzed

in particular, that in analyzing the stresses in the vicinity of the contact area, the finite plate can be approximated as a semi-infinite one, thus making it possible to take advantage of some basic analytical results that are already available in the literature (8).

5. Letting P, V, and M denote the stress resultants exerted by the fretting pad (see Fig. 2) one can write

$$V = \mu P \qquad (1)$$

$$M = \frac{Vh}{2} \qquad (2)$$

in which μ = friction coefficient; and h = outstanding height of the fretting pad. Note that Eq. 2 is based on the assumption that the fretting pad behaves essentially as a column fixed against rotation at both ends.

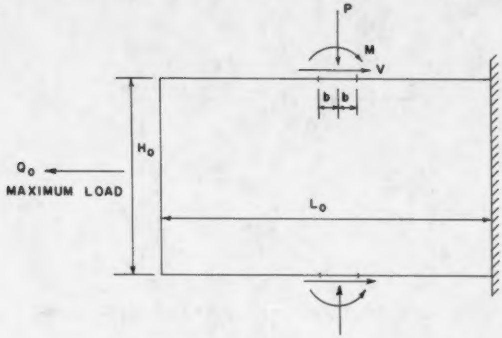

FIG. 2.—Loads Used in Analysis

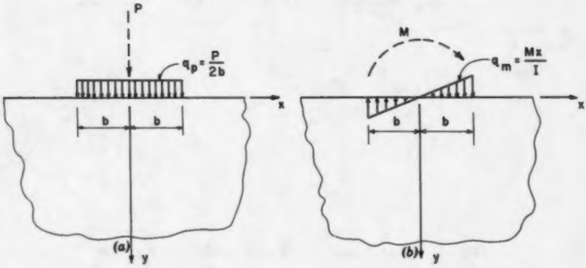

FIG. 3.—Distribution of Contact Loads: (a) Effect of P; (b) Effect of M

6. The actual distribution of the contact forces is not known. For analytical convenience it is assumed that the distributed normal loads, q_P and q_M, associated with P and M vary in accordance with the ordinary theory of beams, i.e.

$$q_P(x) = \frac{P}{2b} \qquad (3)$$

$$q_M(x) = \frac{Mx}{I} = \frac{3\mu Ph}{4b^3}x \qquad (4)$$

in which I = moment of inertia; the coordinate system (x,y) is as shown in Fig. 3; and q_P and q_M are considered positive when compressive. It is further assumed that no separation occurs between the plate and the fretting pads, i.e.

$$q_P + q_M \geq 0 \quad \ldots\ldots\ldots\ldots\ldots\ldots\ldots\ldots\ldots\ldots\ldots\ldots\ldots\ldots\ldots\ldots\ldots\ldots\ldots\ldots\ldots\ldots (5)$$

at all contact points. Since slippage is considered to have taken place in a few cycles of loading, it appears reasonable to express the friction force

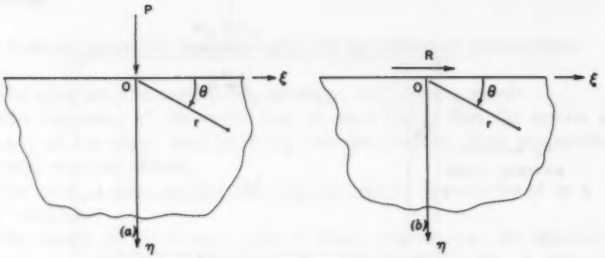

FIG. 4.—Classical Solutions: (*a*) Normal Force; (*b*) Tangential Force

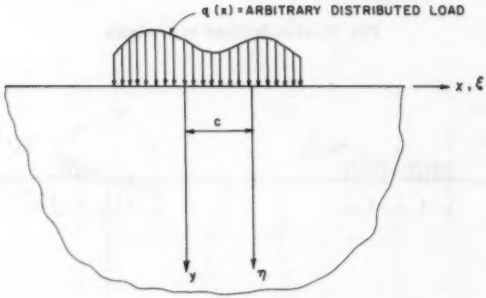

FIG. 5.—Fixed and Moving Coordinate Systems

distribution as in the following. [Analytical results based on an alternate assumption (namely, the assumption of a parabolic distribution as that of shear stresses in the ordinary theory of beams) can be found in Ref. 1.]

$$s = \mu(q_P + q_M) \quad \ldots\ldots\ldots\ldots\ldots\ldots\ldots\ldots\ldots\ldots\ldots\ldots\ldots\ldots\ldots\ldots\ldots\ldots\ldots\ldots\ldots\ldots (6)$$

except near the corners of the fretting pads where $s = 0$ from theoretical considerations.

Two Classical Solutions

In the special case of a semi-infinite plate subjected to a concentrated normal load, Q, as shown in Fig. 4(*a*), the stress distribution is given by (8)

$$\sigma'_r = -\frac{2Q}{\pi}\frac{\sin\theta}{r} \quad \ldots\ldots (7a)$$

$$\sigma'_\theta = 0 \quad \ldots\ldots (7b)$$

$$\tau'_{r\theta} = 0 \quad \ldots\ldots (7c)$$

or, in cartesian coordinates (ξ, η), by

$$\sigma'_\xi = -\frac{2Q}{\pi}\frac{\xi^2\eta}{(\xi^2+\eta^2)^2} \quad \ldots\ldots (8a)$$

$$\sigma'_\eta = -\frac{2Q}{\pi}\frac{\eta^3}{(\xi^2+\eta^2)^2} \quad \ldots\ldots (8b)$$

$$\tau'_{\xi\eta} = -\frac{2Q}{\pi}\frac{\xi\eta^2}{(\xi^2+\eta^2)} \quad \ldots\ldots (8c)$$

In the case of a tangential force, R, as shown in Fig. 4(b), the corresponding expressions are:

$$\sigma''_r = -\frac{2R}{\pi}\frac{\cos\theta}{r} \quad \ldots\ldots (9a)$$

$$\sigma''_\theta = 0 \quad \ldots\ldots (9b)$$

$$\tau''_{r\theta} = 0 \quad \ldots\ldots (9c)$$

and $$\sigma''_\xi = -\frac{2R}{\pi}\frac{\xi^3}{(\xi^2+\eta^2)^2} \quad \ldots\ldots (10a)$$

$$\sigma''_\eta = -\frac{2R}{\pi}\frac{\xi\eta^2}{(\xi^2+\eta^2)^2} \quad \ldots\ldots (10b)$$

$$\tau''_{\xi\eta} = -\frac{2R}{\pi}\frac{\xi^2\eta}{(\xi^2+\eta^2)^2} \quad \ldots\ldots (10c)$$

respectively. These two classical solutions, used in conjunction with the principle of superposition, form the basis of all the analytical results presented in this study.

Stresses Produced by Distributed Loads

Of the two cartesian coordinate systems shown in Fig. 5, (x, y) is fixed, and (ξ, η) is moving, subject to the conditions

$$\xi = x - c \quad \ldots\ldots (11a)$$

$$\eta = y \quad \ldots\ldots (11b)$$

in which c = relative distance between the origins of the two systems.

Consider now a distributed normal load, $q(x)$, acting on the edge of the semi-infinite plate, as shown in Fig. 5. The stresses produced by $q(x)$ can be obtained from Eqs. 8 and 11 by substituting $q(c)dc$ for Q and integrating. Thus

$$\sigma_x = -\frac{2}{\pi}\int \frac{(x-c)^2 y}{[(x-c)^2+y^2]^2}\, q(c)\, dc \quad \ldots\ldots\ldots\ldots\ldots\ldots \quad (12a)$$

$$\sigma_y = -\frac{2}{\pi}\int \frac{y^3}{[(x-c)^2+y^2]^2}\, q(c)\, dc \quad \ldots\ldots\ldots\ldots\ldots\ldots \quad (12b)$$

$$\tau_{xy} = -\frac{2}{\pi}\int \frac{(x-c)y^2}{[(x-c)^2+y^2]^2}\, q(c)\, dc \quad \ldots\ldots\ldots\ldots\ldots\ldots \quad (12c)$$

Stresses Produced by P.—The distributed contact load, $q_P(x)$, associated with P is given in Eq. 3. Substituting Eq. 3 into Eqs. 12 and integrating from $-b$ to b

$$(\sigma_x)_P = \frac{Py}{2\pi b}\left\{\frac{2b\,(b^2-x^2+y^2)}{[(x+b)^2+y^2]\,[(x-b)^2+y^2]}\right.$$
$$\left. -\frac{1}{y}\left[\tan^{-1}\left(\frac{x+b}{y}\right)-\tan^{-1}\left(\frac{x-b}{y}\right)\right]\right\} \quad \ldots\ldots\ldots\ldots\ldots\ldots \quad (13a)$$

$$(\sigma_y)_P = -\frac{Py}{2\pi b}\left\{\frac{2b\,(b^2-x^2+y^2)}{[(x+b)^2+y^2]\,[(x-b)^2+y^2]}\right.$$
$$\left. +\frac{1}{y}\left[\tan^{-1}\left(\frac{x+b}{y}\right)-\tan^{-1}\left(\frac{x-b}{y}\right)\right]\right\} \quad \ldots\ldots\ldots\ldots\ldots\ldots \quad (13b)$$

$$(\tau_{xy})_P = -\frac{2P}{\pi}\frac{xy^2}{[(x+b)^2+y^2]\,[(x-b)^2+y^2]} \quad \ldots\ldots\ldots\ldots\ldots\ldots \quad (13c)$$

Stresses Produced by M.—Similarly, the stresses produced by M can be obtained by simply substituting Eq. 4 into Eq. 12 and integrating. Thus

$$(\sigma_x)_M = -\frac{3\mu Phy}{2\pi b^3}\left\{\frac{bx\,(x^2+y^2-b^2)}{[(x+b)^2+y^2]\,[(x-b)^2+y^2]}\right.$$
$$\left. +\frac{1}{2}\log\left[\frac{(x-b)^2+y^2}{(x+b)^2+y^2}\right]+\frac{x}{2y}\left[\tan^{-1}\left(\frac{x+b}{y}\right)-\tan^{-1}\left(\frac{x-b}{y}\right)\right]\right\} \quad (14a)$$

$$(\sigma_y)_M = \frac{3\mu Phy}{2\pi b^3}\left\{\frac{bx\,(x^2+y^2-b^2)}{[(x+b)^2+y^2]\,[(x-b)^2+y^2]}\right.$$
$$\left. -\frac{x}{2y}\left[\tan^{-1}\left(\frac{x+b}{y}\right)-\tan^{-1}\left(\frac{x-b}{y}\right)\right]\right\} \quad \ldots\ldots\ldots\ldots\ldots\ldots \quad (14b)$$

$$(\tau_{xy})_M = -\frac{3\mu Phy}{2\pi b^3}\left\{\frac{b\,(x^2+y^2+b^2)}{[(x+b)^2+y^2]\,[(x-b)^2+y^2]}\right.$$
$$\left. -\frac{1}{2y}\left[\tan^{-1}\left(\frac{x+b}{y}\right)-\tan^{-1}\left(\frac{x-b}{y}\right)\right]\right\} \quad \ldots\ldots\ldots\ldots\ldots\ldots \quad (14c)$$

in which log denotes natural logarithm.

Stresses Produced by V.—By analogy to Eqs. 12, the stresses produced by a distributed tangential load, $s(x)$, can be obtained from Eqs. 10 and 11 by substituting $s(c)dc$ for R and integrating. Inasmuch as $s(x)$ is associated with V in the present problem, one can write:

$$(\sigma_x)_V = -\frac{2}{\pi}\int \frac{(x-c)^3}{[(x-c)^2+y^2]^2}\, s(c)\,dc \quad \ldots\ldots\ldots\ldots\ldots\ldots \quad (15a)$$

$$(\sigma_y)_V = -\frac{2}{\pi}\int \frac{(x-c)\,y^2}{[(x-c)^2+y^2]^2}\, s(c)\,dc \quad \ldots\ldots\ldots\ldots\ldots\ldots \quad (15b)$$

$$(\tau_{xy})_V = -\frac{2}{\pi}\int \frac{(x-c)^2\,y}{[(x-c)^2+y^2]^2}\, s(c)\,dc \quad \ldots\ldots\ldots\ldots\ldots\ldots \quad (15c)$$

Rewriting Eq. 6 as

$$s(x) = \mu\, q_P + \mu\, q_M \quad \ldots\ldots\ldots\ldots\ldots\ldots\ldots\ldots\ldots\ldots \quad (16)$$

to separate the contributions of P and M, Eqs. 15 can be expressed as:

$$(\sigma_x)_V = (\sigma_x)_{VP} + (\sigma_x)_{VM} \quad \ldots\ldots\ldots\ldots\ldots\ldots\ldots\ldots \quad (17a)$$

$$(\sigma_y)_V = (\sigma_y)_{VP} + (\sigma_y)_{VM} \quad \ldots\ldots\ldots\ldots\ldots\ldots\ldots\ldots \quad (17b)$$

$$(\tau_{xy})_V = (\tau_{xy})_{VP} + (\tau_{xy})_{VM} \quad \ldots\ldots\ldots\ldots\ldots\ldots\ldots\ldots \quad (17c)$$

in which, after some lengthly mathematical manipulations

$$(\sigma_x)_{VP} = \frac{\mu P}{2\pi b}\left\{\frac{4\,bxy^2}{[(x+b)^2+y^2]\,[(x-b)^2+y^2]} + \log\frac{(x-b)^2+y^2}{(x+b)^2+y^2}\right\} \quad (18a)$$

$$(\sigma_y)_{VP} = -\frac{\mu P y^2}{\pi b}\,\frac{2\,bx}{[(x+b)^2+y^2]\,[(x-b)^2+y^2]} \quad \ldots\ldots\ldots\ldots \quad (18b)$$

$$(\tau_{xy})_{VP} = \frac{\mu P y}{\pi b}\left\{\frac{b\,(b^2-x^2+y^2)}{[(x+b)^2+y^2]\,[(x-b)^2+y^2]}\right.$$

$$\left. -\frac{1}{2y}\left[\tan^{-1}\left(\frac{x+b}{y}\right) - \tan^{-1}\left(\frac{x-b}{y}\right)\right]\right\} \quad \ldots\ldots\ldots\ldots\ldots \quad (18c)$$

and $$(\sigma_x)_{VM} = \frac{3\,\mu^2 ph}{2\pi b^3}\left\{-2b + \frac{3y}{2}\left[\tan^{-1}\left(\frac{x+b}{y}\right) - \tan^{-1}\left(\frac{x-b}{y}\right)\right]\right.$$

$$\left. -\frac{by^2(x^2+y^2+b^2)}{[(x+b)^2+y^2]\,[(x-b)^2+y^2]} - \frac{x}{2}\log\frac{(x-b)^2+y^2}{(x+b)^2+y^2}\right\} \quad \ldots\ldots \quad (19a)$$

$$(\sigma_y)_{VM} = -\frac{3\,\mu^2 Phy^2}{2\pi b^3}\left\{\frac{b\,(x^2+y^2+b^2)}{[(x+b)^2+y^2]\,[(x-b)^2+y^2]}\right.$$

$$\left. -\frac{1}{2y}\left[\tan^{-1}\left(\frac{x+b}{y}\right) - \tan^{-1}\left(\frac{x-b}{y}\right)\right]\right\} \quad \ldots\ldots\ldots\ldots\ldots \quad (19b)$$

$$(\tau_{xy})_{VM} = \frac{3\mu^2 Phy}{2\pi b^3}\left\{\frac{xb\,(b^2 - x^2 - y^2)}{[(x+b)^2 + y^2]\,[(x-b)^2 + y^2]}\right.$$

$$\left. - \frac{x}{2y}\left[\tan^{-1}\left(\frac{x+b}{y}\right) - \tan^{-1}\left(\frac{x-b}{y}\right) - \frac{1}{2}\log\frac{(x-b)^2 + y^2}{(x+b)^2 + y^2}\right]\right\} \quad \ldots \quad (19c)$$

Summary of Stresses.—The stresses produced in the plate by P, M, and V decrease rapidly as the distance from the contact area increases. It follows that, in analyzing the stresses in the general vicinity of a particular fretting pad, the contribution of the other fretting pad can be neglected without introducing any substantial errors. The overall stresses at an arbitrary point of interest can thus be expressed as;

$$\sigma_x = (\sigma_x)_o + (\sigma_x)_P + (\sigma_x)_M + (\sigma_x)_V \quad \ldots \quad (20a)$$

$$\sigma_y = (\sigma_y)_o + (\sigma_y)_P + (\sigma_y)_M + (\sigma_y)_V \quad \ldots \quad (20b)$$

$$\tau_{xy} = (\tau_{xy})_o + (\tau_{xy})_P + (\tau_{xy})_M + (\tau_{xy})_V \quad \ldots \quad (20c)$$

in which $$(\sigma_x)_o = \frac{Q_o}{H_o} \quad \ldots \quad (21a)$$

$$(\sigma_y)_o = 0 \quad \ldots \quad (21b)$$

$$(\tau_{xy})_o = 0 \quad \ldots \quad (21c)$$

represent the stresses produced by the maximum tensile value of the cyclic load, Q_o.

Numerical Results

As was observed by various investigators (3,6,7), the friction coefficient, μ, appears to vary with the number of cycles during a fretting test. In the present study, numerical solutions were obtained for the following specific cases: $\mu = 0$, 0.2, 0.4, 0.6, and 0.8. The other major problem parameter that was varied in this study is

$$\alpha = \frac{\left(\frac{Q_o}{H_o}\right)}{\left(\frac{P}{b}\right)} \quad \ldots \quad (22)$$

in which (Q_o/H_o) = maximum value of axial cyclic stresses; and (P/b) = twice the average normal contact load under the fretting pad. Numerical solutions were obtained for $\alpha = 0$, 1, 5, and 10. The fretting pad height, h, was assumed to have a fixed value, $h = 0.2b$, in all cases that involved axial load, $Q_o \neq 0$, i.e., $\alpha \neq 0$. In the special use of $\alpha = 0$ (i.e., when the fretting pads themselves were considered to be moving), the ratio h/b was treated as a variable problem parameter, and numerical solutions were obtained for several different values of h/b in the range $0.2 < h/b < 3.0$. (Note that in this connection μ cannot exceed $2b/3h$ since otherwise the condition of no separation, i.e., Eq. 5, would not be satisfied.)

For each set of values of the problem parameters, the state of stress was determined numerically at a total number of 861 points in the general vicinity of each fretting pad, namely, at all points of a grid system defined by Δx,

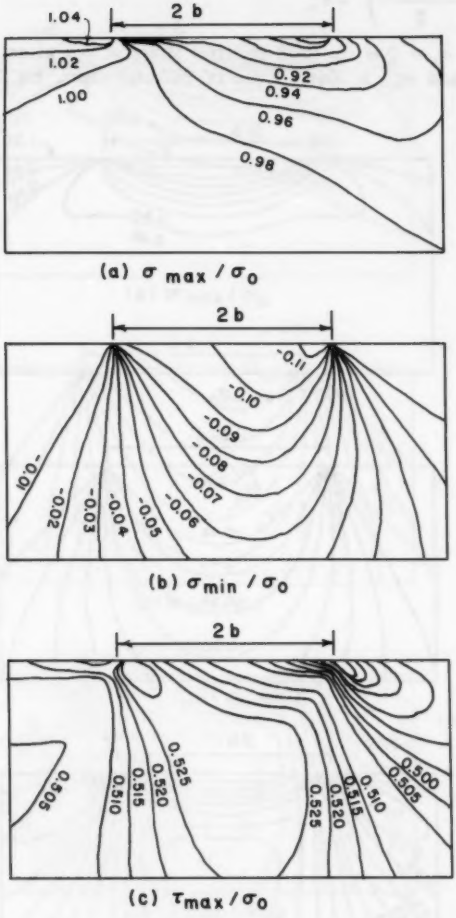

FIG. 6.—Stress Contour Lines ($\alpha = 5$; $\mu = 0.4$; $h/b = 0.2$)

$\Delta y = b/10$ in the region $-2b \leq x \leq 2b$, $0 \leq y \leq 2b$. The principal stresses and the maximum shear stress were then obtained at each point by treating the problem as a two-dimensional one, i.e., from the equations

$$\sigma_{max}, \sigma_{min} = \frac{\sigma_x + \sigma_y}{2} \pm \sqrt{\left(\frac{\sigma_x - \sigma_y}{2}\right)^2 + \tau_{xy}^2} \quad \ldots\ldots\ldots\ldots\ldots (23)$$

$$\tau_{max} = \sqrt{\left(\frac{\sigma_x - \sigma_y}{2}\right)^2 + \tau_{xy}^2} \quad \ldots\ldots\ldots\ldots\ldots\ldots\ldots\ldots (24)$$

Note that $\sigma_z = 0$ is the third principal stress in this plane stress problem. When σ_{max} and σ_{min} in Eqs. 23 are of different signs, Eq. 24 does indeed

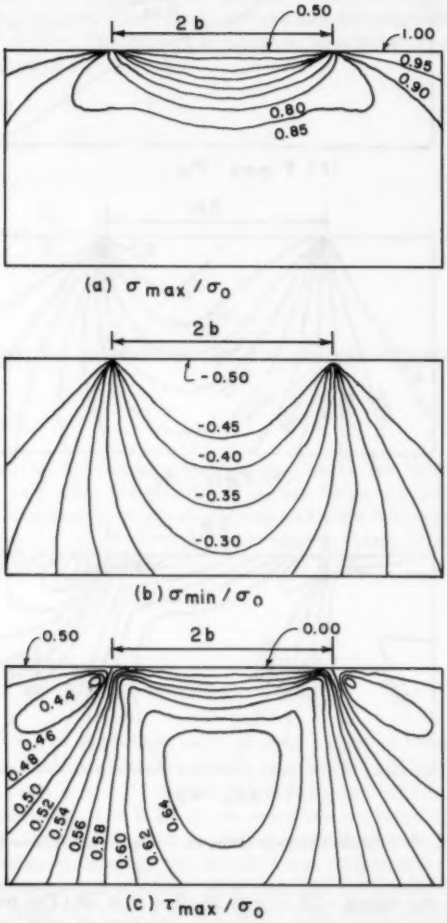

FIG. 7.—Stress Contour Lines ($\alpha = 1$; $\mu = 0$; $h/b = 0.2$)

define the maximum shear stress in a three-dimensional sense. When σ_{max} and σ_{min} have the same sign, however, τ_{max} would have to be calculated as one half the absolute value of σ_{max} or σ_{min}, whichever happens to be numerically larger.

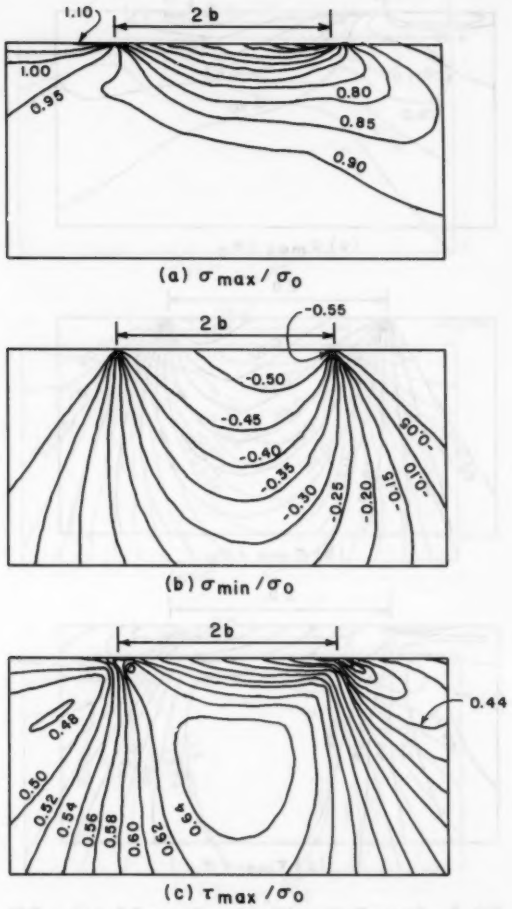

FIG. 8.—Stress Contour Lines ($\alpha = 1$; $\mu = 0.2$; $h/b = 0.2$)

In an effort to visually enhance the significance of the numerical results obtained in this study, stress contour diagrams were constructed for σ_{max}, σ_{min}, and τ_{max} for each set of values of the problem parameters considered. Due

to space limitations, however, only a small number of these graphs are presented in this paper.

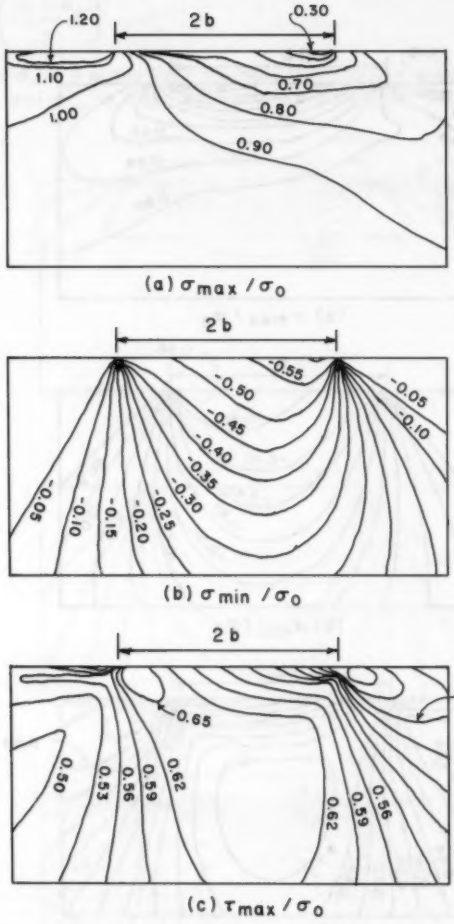

FIG. 9.—Stress Contour Lines ($\alpha = 1$; $\mu = 0.4$; $h/b = 0.2$)

Fig. 6 corresponds to a relatively large value of the axial cyclic stress ($\alpha = 5$), whereas Figs. 7–9 are for a relatively small value of that stress ($\alpha = 1$), with μ varying in the range 0–0.4. The numerical coefficients shown in these four figures are to be multiplied by $\sigma_o = Q_o/H_o$ to determine the actual

stresses. In an effort to illustrate the distribution of strains within the plate, the results corresponding to one particular case ($\alpha = 1$, $\mu = 0.4$), and obtained by using a value of $\nu = 0.34$ for Poisson's ratio are summarized in Fig. 10.

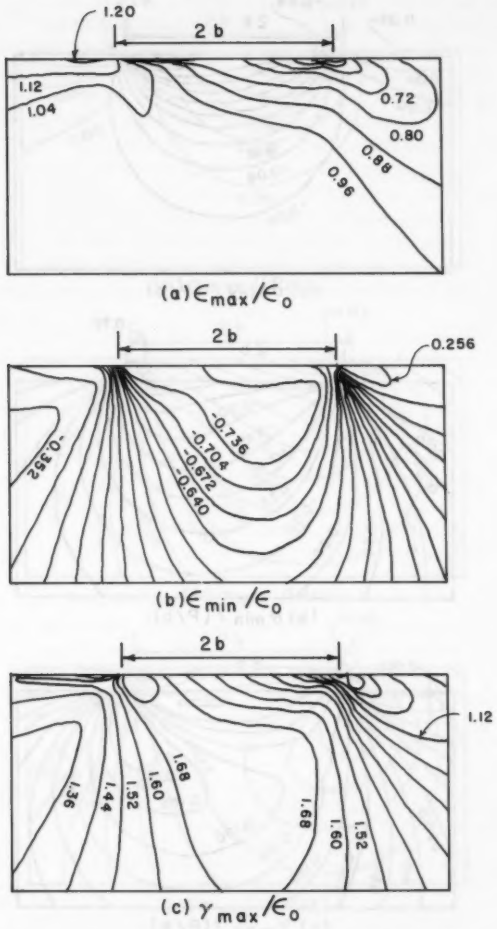

FIG. 10.—Stress Contour Lines ($\alpha = 1$; $\mu = 0.4$; $h/b = 0.2$)

The numerical coefficients in Fig. 10 are to be multiplied by $\epsilon_o = \sigma_o/E = Q/EH_o$ to determine the actual strains. Finally, Figs. 11 and 12 are for the special case of $\alpha = 0$ (i.e., no axial cyclic load) with $h/b = 0.2$ and $\mu =$

0.2, 0.4, respectively. Since $Q_o = 0$ in these two figures, the quantity $\sigma_o = Q_o/H_o$ can no longer be used as a common multiplying factor. Accordingly, the quantity (P/b) is used for this purpose.

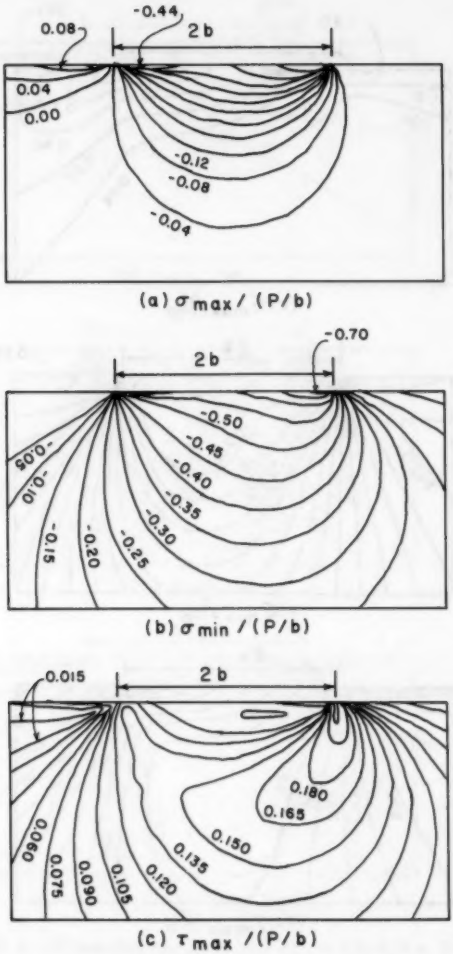

FIG. 11.—Stress Contour Lines ($\alpha = 0$; $\mu = 0.2$; $h/b = 0.2$)

It is seen from an examination of Figs. 6–12 that the stresses produced by the contact loads P, M, and V represent essentially a localized phenomenon, provided that $2b << L_o$ and $2b << H_o$, as previously indicated. In all the

cases considered, the maximum tensile stress occurs on the edge of the plate immediately outside the contact area, whereas the location of the maximum shear stress varies substantially from one case to another. In most cases, the

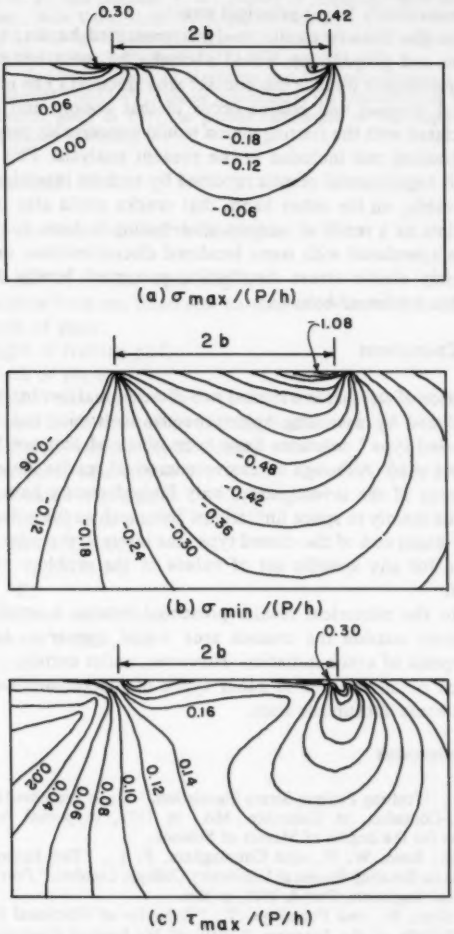

FIG. 12.—Stress Contour Lines ($\alpha = 0$; $\mu = 0.4$; $h/b = 0.2$)

shear stress reaches local maxima at several different points, some of which lie on the surface and some below it. In Fig. 8, e.g., there are a total number of five local maxima for the shear stress, the absolute maximum among them

occurring directly under the fretting pad at a depth of about $y \simeq b$. It is important to recall in this connection that τ_{max} in Figs. 6–12 refers to a maximum shear stress in the plane stress sense. When σ_{max} and σ_{min} have the same sign, τ_{max} in a three-dimensional sense would have to be obtained as one half the absolute value of the numerically larger principal stress.

According to the linearly elastic analysis presented herein, the question of crack initiation and propagation would normally be most critical on the edge of the plate immediately outside the contact area since: (1) The maximum values of the principal stresses and strains occur in that region; and (2) the surface abrasion associated with the fretting action would conceivably produce additional stress concentrations not included in the present analysis. This observation is consistent with experimental results reported by various investigators (4,9).

It is conceivable, on the other hand, that cracks could also initiate at some subsurface points as a result of various contributing factors, such as: (1) Stress concentrations associated with some localized discontinuities; or (2) deviations from the linearly elastic stress distribution presented herein due to residual stresses or other nonlinear behavior.

Summary and Conclusions

The distribution of stresses in a typical two-dimensional fretting-fatigue problem has been analyzed by assuming homogeneous, isotropic, and linearly elastic material. "Closed type" solutions have been obtained that are "exact" within the assumptions used. Although extensive numerical results have been obtained during the course of the investigation, only limited results have been included in this paper due mainly to space limitations. Inasmuch as the solutions presented are essentially exact and of the closed type, the interested reader could generate numerical data for any specific set of values of the problem parameters with minimal effort.

According to the numerical results presented herein, a small region of the plate immediately outside the contact area would appear to be most critical from the viewpoint of crack initiation. However, under certain conditions (e.g., in the presence of micropores or other types of discontinuities) cracks could also initiate at some subsurface sites.

Appendix I.—References

1. Chung, J. S., "Fretting Fatigue Stress Simulation," thesis presented to the University of Missouri-Columbia, at Columbia, Mo., in 1979, in partial fulfillment of the requirements for the degree of Master of Science.
2. Eden, E. M., Rose, W. N., and Cunningham, F. L., "The Endurance of Metals: Experiments on Rotating Beams at University College, London," *Proceedings*, Institute of Mechanical Engineers, Part 4, 1911, p. 839.
3. Endo, K., Goto, H., and Fukunage, T., "Behavior of Frictional Force in Fretting Fatigue," *Bulletin of the Japanese Society of Mechanical Engineers*, Vol. 17, No. 108, June, 1974.
4. Endo, K., and Goto, H., "Initiation and Propagation of Fretting Fatigue Cracks," *Wear*, Vol. 38, 1976, pp. 311–324.
5. Jordan, R. E., Jr., "The Effect of Surface Roughness on the Fretting Fatigue Behavior of 7475-T61 Aluminum," thesis presented to the University of Missouri-Columbia, at Columbia, Mo., in 1979, in partial fulfullment of the requirements for the degree of Master of Science.

6. Milestone, W. D., and Janeczko, J. T., "Friction Between Steel Surfaces During Fretting," *Wear*, Vol. 18, 1971, pp. 29–40.
7. Nishioka, and Hirakawa, K., "Fundamental Investigations of Fretting Fatigue," *Bulletin of the Japanese Society of Mechanical Engineers*, Vol. 12, No. 51, 1969, pp. 397–406.
8. Timoshenko, S. P., and Goodier, J. N., *Theory of Elasticity*, third ed., McGraw-Hill Book Co., Inc., New York, N.Y., 1970, pp. 97–100.
9. Waterhouse, R. B., and Taylor, D. E., "The Initiation of Fatigue Cracks in 0.7% Carbon Steel by Fretting," *Wear*, Vol. 17, 1971, pp. 139–147.
10. Watts, W. K., Jr., "The Effect of Hardness and Different Materials on the Fretting Fatigue Behavior of Ti-6A1-4V," thesis presented to the University of Missouri-Columbia, at Columbia, Mo., in 1977, in partial fulfillment of the requirements for the degree of Master of Science.

APPENDIX II.—NOTATION

The following symbols are used in this paper:

b = one half of contact area length;
c = distance between fixed and moving coordinate systems (see Eq. 11);
H_o = depth of plate;
h = height of fretting pad;
L_o = length of plate;
M = $Vh/2$ = moment;
P = normal force exerted by fretting pad;
Q_0 = maximum value of cyclic load;
$q_M(x)$ = distributed load due to M;
$q_P(x)$ = distributed load due to P;
$s(x)$ = distributed load due to V;
V = tangential force;
α = $(Q_o/H_o)/(P/b)$;
ϵ_o = σ_o/E;
μ = frictional coefficient;
ν = Poisson's ratio; and
σ_o = Q_o/H_o.

JOURNAL OF
THE ENGINEERING
MECHANICS DIVISION

DYNAMIC ANALYSIS OF UNBALANCED ANISOTROPIC SANDWICH PLATES

By Ibrahim M. Ibrahim,[1] Anis Farah,[2] and M. Nabil F. Rizk[3]

INTRODUCTION

Rigorous solutions for certain types of sandwich plates with unbalanced laminated faces have not been realized due to the existence of anisotropic coupling stiffnesses. Typical examples of such plates are those with unbalanced angle-ply faces. Neglecting the coupling action can result in appreciable errors in the deflection, stress, and frequency predictions.

Recently, a modified stiffness formulation was presented in Ref. 1, which allows the uncoupling of the bending and the membrane actions in sandwich plates. As a result, the analysis of unbalanced anisotropic sandwich plates under static loading that were not amenable to rigorous solutions has been realized.

The objectives of this paper are to extend the modified stiffness method to the dynamic analysis of anisotropic sandwich plates for which rigorous solutions are not available, and to demonstrate the effect of bending-membrane coupling in the static and dynamic structural responses of sandwich plates with unbalanced angle-ply laminated faces.

The modified formulation presented herein is independent of the boundary conditions of the plate and can be used in conjunction with a variety of analysis techniques. In order to demonstrate the potential of the formulation, solutions are generated herein for simply-supported sandwich plates using a double Fourier series procedure. The modified formulation yields solutions that are in complete agreement with those using the formulations presented in Refs. 2 and 3 for sandwich plates with unbalanced cross-ply faces. The method, therefore, should

[1]Assoc. Prof., Faculty of Engrg., Univ. of El-Zagazig, Egypt.
[2]Assoc. Prof., School of Engrg., Laurentian Univ., Sudbury, Ontario, Canada P3E 2C6.
[3]Assoc. Prof., Dept. of Mech. Engrg., El-Azher Univ., Cairo, Egypt.

Note.—Discussion open until September 1, 1981. To extend the closing date one month, a written request must be filed with the Manager of Technical and Professional Publications, ASCE. Manuscript was submitted for review for possible publication on September 7, 1978. This paper is part of the Journal of the Engineering Mechanics Division, Proceedings of the American Society of Civil Engineers, ©ASCE, Vol. 107, No. EM2, April, 1981. ISSN 0044-7951/81/0002-0405/$01.00.

be accurate for other sandwich plates, such as those with unbalanced angle-ply faces.

General Formulation

The sandwich plate shown in Fig. 1 consists of an orthotropic core with shear moduli G_x and G_y, and two unbalanced laminated face plates subscribing to the usual thin plate assumptions in which transverse shear deformations are neglected. It is assumed that the core is incompressible in the transverse direction and carries no longitudinal stresses, but that transverse shear strains are significant. The two unbalanced anisotropic laminated face plates are assumed to have the same thickness, number of plies, and material properties.

The uncoupled strain energy of the unbalanced anisotropic laminated face plates, U_f, can be expressed in terms of the modified stiffness matrices $[R^*]$,

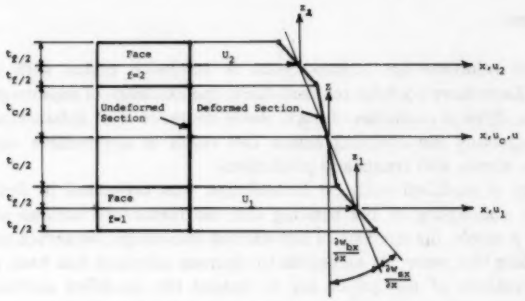

FIG. 1.—Sandwich Plates and Displacements

$[H^*]$, $[D^*]$, and the partial curvatures $\{\kappa_b\}$ and $\{\kappa_s\}$, by (1):

$$U_f = \frac{1}{2}\iint_A [\{\kappa_b\}^T[R^*]\{\kappa_b\} + 2\{\kappa_s\}^T[H^*]\{\kappa_b\} + \{\kappa_s\}^T[D^*]\{\kappa_s\}]\,dA \quad \ldots\ldots\ldots\ldots\ldots\ldots\ldots\ldots\ldots\ldots (1)$$

in which $$\{\kappa_b\} = \left\{-\frac{\partial^2 w_{bx}}{\partial x^2}, -\frac{\partial^2 w_{by}}{\partial y^2}, -\frac{\partial^2 (w_{bx} + w_{by})}{\partial x \partial y}\right\} \quad \ldots\ldots\ldots (2a)$$

$$\{\kappa_s\} = \left\{-\frac{\partial^2 w_{sx}}{\partial x^2}, -\frac{\partial^2 w_{sy}}{\partial y^2}, -\frac{\partial^2 (w_{sx} + w_{sy})}{\partial x \partial y}\right\} \quad \ldots\ldots\ldots\ldots\ldots (2b)$$

Also, (w_{bx}, w_{by}) and (w_{sx}, w_{sy}) are the partial deflections due to bending and transverse shear deformations, in the x and the y directions, respectively.

Kinetic Energy

The total kinetic energy of the sandwich plate considered is the sum of the kinetic energies of the core, T_c, and the face plates, T_f:

$$T = T_c + \sum_{f=1}^{2} T_f \ldots \ldots \ldots \ldots \ldots \ldots \ldots \ldots \ldots \ldots \ldots \ldots \ldots \ldots (3)$$

Based on the assumptions considered, that the faces of the sandwich plates have the same thickness, number of plies, and material properties, the centers of the mass of the sandwich plate in the x and y directions are located at the middle plane of the core, which in turn, coincides with the reference plane of the sandwich plate. Also, the centers of the mass of each face in the x and the y directions are located on the reference plane of the individual face plate, since the mass density of a ply is assumed to be independent of the orientation of the ply. As a result, for the sandwich plates considered in the work, the bending and membrane actions are not coupled in the kinetic energy expressions of the face plates and the core.

For the case of transverse vibration, the kinetic energy of the two face plates that includes both the translatory and rotary inertia terms can be expressed as follows:

$$\sum_{f=1}^{2} T_f = \frac{1}{2} \iint_A \left\{ 2Q_f \dot{w}^2 + 2\,[Q_f e^2 + I_f] \left[\left(\frac{\partial \dot{w}_{bx}}{\partial x} \right)^2 + \left(\frac{\partial \dot{w}_{by}}{\partial y} \right)^2 \right] \right.$$

$$\left. + 2I_f \left[\left(\frac{\partial \dot{w}_{sx}}{\partial x} \right)^2 + \left(\frac{\partial \dot{w}_{sy}}{\partial y} \right)^2 \right] + 2 \left(\frac{\partial \dot{w}_{bx}}{\partial x} \frac{\partial \dot{w}_{sx}}{\partial x} + \frac{\partial \dot{w}_{by}}{\partial y} \frac{\partial \dot{w}_{sy}}{\partial y} \right) \right\} dA \quad (4)$$

in which $e = \frac{1}{2}(t_c + t_f) \ldots \ldots \ldots \ldots \ldots \ldots \ldots \ldots \ldots \ldots (5a)$

$$Q_f = \int_{z_f} \rho_f dz_f; \quad I_f = \int_{z_f} \rho_f z_f^2 dz_f \ldots \ldots \ldots \ldots \ldots \ldots \ldots \ldots (5b)$$

and ρ_f = the mass density of the face plate.

The kinetic energy of the core that includes the rotary inertia terms can be expressed by

$$T_c = \frac{1}{2} \iint_A \left\{ Q_c \dot{w}^2 + I_c \left[\left(\frac{\partial \dot{w}_{bx}}{\partial x} \right)^2 + \left(\frac{\partial \dot{w}_{by}}{\partial y} \right)^2 \right] + \frac{I_c t_f^2}{t_c^2} \left[\left(\frac{\partial \dot{w}_{sx}}{\partial x} \right)^2 \right. \right.$$

$$\left. \left. + \left(\frac{\partial \dot{w}_{sy}}{\partial y} \right)^2 \right] + 2 \frac{I_c t_f}{t_c} \left[\frac{\partial \dot{w}_{bx}}{\partial x} \frac{\partial \dot{w}_{sx}}{\partial x} + \frac{\partial \dot{w}_{by}}{\partial y} \frac{\partial \dot{w}_{sy}}{\partial y} \right] \right\} dA \ldots \ldots \ldots (6)$$

In the preceding equation

$$Q_c = \int_{z_c} \rho_c dz_c; \quad I_c = \int_{z_c} \rho_c z_c^2 dz_c \ldots \ldots \ldots \ldots \ldots \ldots \ldots \ldots (7)$$

in which ρ_c = the mass density of the core.

Note that both the modified strain energy expression (Eq. 1) and the kinetic energy expression (Eq. 3) are functions of the partial deflections only. The governing differential equations of motion generated from the application of the variational principle can be expressed by the following:

$$\frac{\partial^2 \bar{N}_x}{\partial x^2} + \frac{\partial^2 \bar{N}_{xy}}{\partial x \partial y} - \frac{2e}{t_c}\frac{\partial Q_x}{\partial x} + \eta_1 = 0 \quad \ldots \quad (8a)$$

$$\frac{\partial^2 \bar{N}_{xy}}{\partial x \partial y} + \frac{\partial^2 \bar{N}_y}{\partial y^2} - \frac{2e}{t_c}\frac{\partial Q_y}{\partial y} + \eta_2 = 0 \quad \ldots \quad (8b)$$

$$\frac{2e}{t_c}\left[\frac{\partial Q_x}{\partial x} + \frac{\partial Q_y}{\partial y}\right] + \frac{\partial^2 M_x}{\partial x^2} + \frac{2\partial^2 M_{xy}}{\partial x \partial y} + \frac{\partial^2 M_y}{\partial y^2} + \eta_3 = 0 \quad \ldots \quad (8c)$$

In the preceding equations, Q_x and Q_y = the transverse shear forces in the orthotropic core (1); and

$$\begin{Bmatrix} \{\bar{N}\} \\ \{M\} \end{Bmatrix} = \left[\begin{array}{c|c} [\bar{C}^*] & [\bar{B}^*] \\ \hline [H^*] & [D^*] \end{array}\right] \begin{Bmatrix} \{\kappa_b\} \\ \{\kappa_s\} \end{Bmatrix} \quad \ldots \quad (9)$$

in which $[\bar{C}^*] = [R^*] - [H^*]$ . . . . . (10a)

$[\bar{B}^*] = [H^*] - [D^*]$ . . . . . (10b)

$\{\bar{N}\}^T \{\bar{N}_x, \bar{N}_y, \bar{N}_{xy}\}$ . . . . . (10c)

$\{M\}^T = \{M_x, M_y, M_{xy}\}$ . . . . . (10d)

Also $\eta_1 = [\alpha_2 - \alpha_4]\dfrac{\partial^2 \ddot{w}_{bx}}{\partial x^2} + [\alpha_4 - \alpha_3]\dfrac{\partial^2 \ddot{w}_{sx}}{\partial x^2}$ . . . . . (11a)

$$\eta_2 = [\alpha_4 - \alpha_3]\frac{\partial^2 (\ddot{w}_{bx} + \ddot{w}_{sx})}{\partial y^2} + [\alpha_2 + \alpha_3 - 2\alpha_4]\frac{\partial^2 \ddot{w}_{by}}{\partial y^2} \quad \ldots \quad (11b)$$

$$\eta_3 = -\alpha_1(\ddot{w}_{bx} + \ddot{w}_{sx}) + \alpha_3 \frac{\partial^2 (\ddot{w}_{bx} + \ddot{w}_{sx})}{\partial y^2} + \alpha_3 \frac{\partial^2 \ddot{w}_{sx}}{\partial x^2}$$

$$+ \alpha_4 \frac{\partial^2 \ddot{w}_{bx}}{\partial x^2} + [\alpha_4 - \alpha_3]\frac{\partial^2 \ddot{w}_{by}}{\partial y^2} \quad \ldots \quad (11c)$$

and $\alpha_1 = 2Q_f + Q_c$ . . . . . (12a)

$\alpha_2 = 2Q_f e^2 + 2I_f + I_c$ . . . . . (12b)

$\alpha_3 = 2I_f + I_c \dfrac{t_f^2}{t_c^2}$ . . . . . (12c)

$\alpha_4 = 2I_f - I_c \dfrac{t_f^2}{t_c^2}$ . . . . . (12d)

It is pointed out that the difficulty associated with the anisotropic coupling stiffnesses in the governing differential equations (Eq. 8) has been totally eliminated, since in addition to the uncoupling of the energy expressions, all the anisotropic stiffnesses vanish in Eq. 9 (1).

Numerical Evaluation

Note that the formulation is independent of the boundary conditions of the plate, and that the governing differential equations are a function of the partial

deflection only. As such, a variety of analysis procedures may be applied. Herein, in order to demonstrate the potential, and assess the accuracy of the formulation, a Fourier series approach is applied to the prediction of the dynamic response of rectangular simply-supported sandwich plates.

The boundary conditions for a rectangular ($L \times B$) simply-supported plate are as follows (1):

$$w_{bx} = w_{by} = w_{sx} = M_x = \bar{N}_x = 0 \quad \text{for} \quad x = 0, L \quad \ldots\ldots\ldots\ldots \quad (13a)$$

$$w_{bx} = w_{by} = w_{sx} = M_y = \bar{N}_y = 0 \quad \text{for} \quad y = 0, B \quad \ldots\ldots\ldots\ldots \quad (13b)$$

The boundary conditions (Eq. 13) and the differential equations (Eq. 8) are satisfied by the following series expansion:

$$(w_{bx}, w_{by}, w_{sx}) = \sum_{m=1}^{\infty} \sum_{n=1}^{\infty} (w_{bxmn}, w_{bymn}, w_{sxmn}) \sin \frac{m\pi x}{L} \sin \frac{n\pi y}{B} e^{i\omega t} \qquad (14)$$

in which w_{bxmn}, w_{bymn}, and w_{sxmn} = undetermined coefficients. Substitution of Eqs. 9 and 14 into the governing differential equations (Eq. 8) yields the following system of equations:

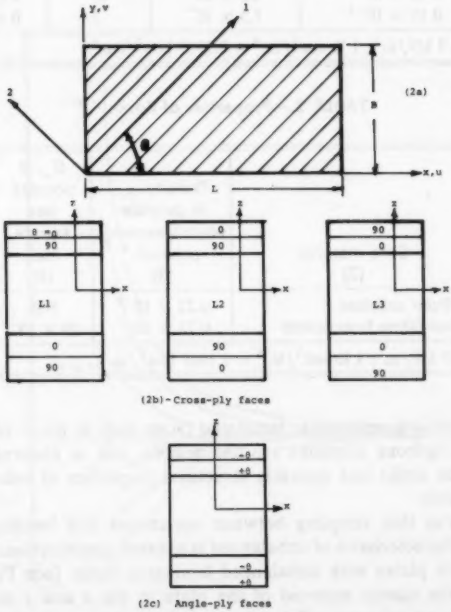

FIG. 2.—Sandwich Plate and Ply Lay-Up Configuration

$$\begin{bmatrix} g_{11} & g_{12} & g_{13} \\ g_{21} & g_{22} & g_{23} \\ g_{31} & g_{32} & g_{33} \end{bmatrix} - \omega_{mn}^2 \begin{bmatrix} m_{11} & m_{12} & m_{13} \\ m_{21} & m_{22} & m_{23} \\ m_{31} & m_{32} & m_{33} \end{bmatrix} \begin{Bmatrix} w_{bxmn} \\ w_{bymn} \\ w_{zxmn} \end{Bmatrix} = 0 \quad \ldots\ldots\ldots \quad (15)$$

in which the expressions for m_{ij} and $g_{ij}(i, j = 1, 2, 3)$ are given in Appendix I. Solutions of Eq. 15 yield the frequencies ω_{mn} of the structure for each combination of m and n.

Results and Analysis

The analysis in this section is focused on demonstrating the potential, and assessing the accuracy of the formulation in predicting the frequencies of sandwich plates with unbalanced anisotropic laminated faces such as those with angle-ply faces for which rigorous solutions are unavailable, and to illustrate the effect of coupling in the static and dynamic structural responses of sandwich plates with angle-ply faces.

TABLE 1.—Properties of Face Laminates

Face material (1)	Density, ρ_f in pounds-square seconds per inch^4 (2)	E_{11}, in pounds per square inch (3)	E_{11}/E_{22} (4)	G_{12}/E_{22} (5)	ν_{12} (6)
GR	0.15×10^{-3}	30×10^6	40	1.0	0.25
GL	0.15×10^{-3}	7.5×10^6	3	0.4	0.25

Note: 1 psi = 6.9 kN/m^2; 1 lb-sec^2/in.^{4} = 0.1069 N-s^2/cm^4.

TABLE 2.—Properties of Cores

Core designation (1)	Core material (2)	Density, ρ_c, in pounds-square seconds per inch^4 (3)	G_x, in pounds per square inch (4)	G_y, in pounds per square inch (5)
WC	Cellular cellulose	0.22×10^{-3}	500	500
SC	Glass-fabric honeycomb	0.22×10^{-3}	30×10^3	30×10^3

Note: 1 psi = 6.9 kN/m^2; 1 lb-sec^2/in.^{4} = 0.1069 N-s^2/in.^{4}.

The analysis in this section is focused on demonstrating the potential, and assessing the accuracy of the formulation in predicting the frequencies of sandwich plates with unbalanced anisotropic laminated faces such as those with angle-ply faces for which rigorous solutions are unavailable, and to illustrate the effect of coupling in the static and dynamic structural responses of sandwich plates with angle-ply faces.

It is pointed out that coupling between membrane and bending actions is one of the main characteristics of unbalanced laminated constructions. For certain types of sandwich plates with unbalanced laminated faces [see Fig. 2(*b*), L1, and Fig. 2(*c*)], the elastic centroid of the plate in the x and y directions are not located on the same plane parallel to the face plates. As a result, the formulation for such plates are derived with respect to a reference plane, Z (Fig. 1), which

does not contain the elastic centroids in all directions. The coupling stiffnesses, $[C]$ (1), accounts for the difference in locations of the elastic centroids of the plate and the difference plane chosen. Coupling stiffness, $[B_f]$ (1), also exists when the reference plane of a face plate, z_f (Fig. 1), does not contain the elastic centroids of the face plate in the x and the y directions [see Fig. 2(b), L1, L2, and L3, and Fig. 2(c)]. For unbalanced cross-ply laminated faces [Fig. 2(b)], the resulting coupling stiffnesses do not alter the orthotropic nature of the sandwich plate. However, for unbalanced angle-ply laminated faces [Fig. 2(c)], the resulting coupling stiffnesses are anisotropic, which has made solutions for such plates inherently abstruse. Note that neglecting the anisotropic coupling stiffnesses, $B_{16}^{(f)}$ and $B_{26}^{(f)}$ (1), can result in appreciable errors in the deflection and frequency predictions, the magnitude of which depends on several factors related to the elastic properties of the face plates and the core and the geometry of the sandwich plate.

In order to establish the magnitude of the coupling effect on the deflection and natural frequencies of unbalanced angle-ply sandwich plates, the center deflection, w_c, of the sandwich plate subjected to a uniform transverse load of 1 lb/sq in. (6.9 kN/m^2), and the natural frequency, ω_{11}, of the plate are compared with the results for the center deflection, w_0, and the natural frequency, w_{11}^0, respectively, of an equivalent sandwich plate with the anisotropic coupling stiffnesses $B_{16}^{(f)} = B_{26}^{(f)} = 0$.

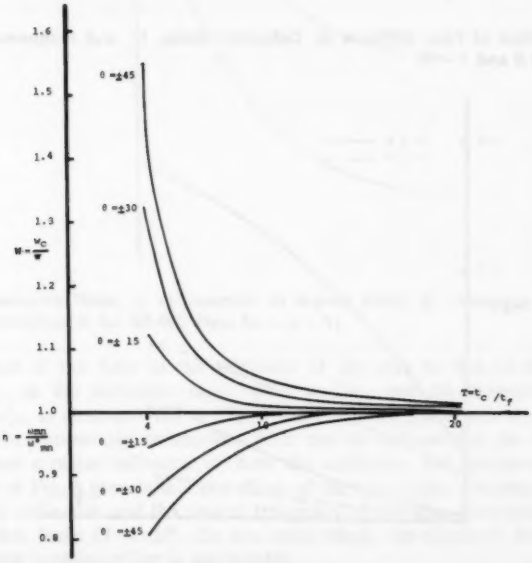

FIG. 3.—Deflection Ratio, W, and Frequency Ratio, η, as Function of Thickness Ratio, T, and Ply Orientation, θ, for GR-WC Plate (R = 2.5)

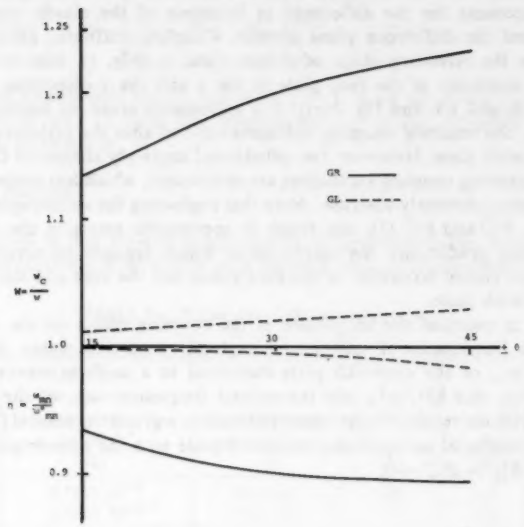

FIG. 4.—Effect of Face Stiffness on Deflection Ratio, W, and Frequency Ratio, η (WC, R = 1.0 and $T = 4$)

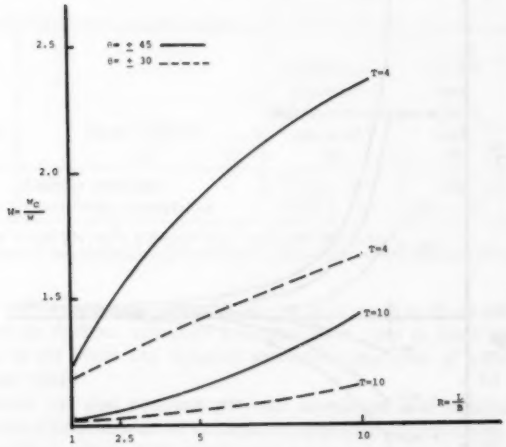

FIG. 5.—Deflection Ratio, W, as Function of Aspect Ratio, R, Thickness Ratio, T, and Ply Orientation, θ, for GR-WC Plate

In this study, the face plates are constructed of either graphite-epoxy (GR) or glass-epoxy (GL) angle-ply composites, having the properties listed in Table 1. The cores considered include a weak core (WC) and a relatively stiff core (SC), with the properties given in Table 2. In all the cases considered, the core thickness is taken as 1 in. (25.4 mm), while the thickness of the face plates vary from 0.01 in.–0.25 in. (0.254 mm–6.35 mm). As in the case of thin angle-ply plates (5), the influence of bending-membrane coupling diminishes rapidly with an increase in the number of plies. Therefore, in order to generate extreme coupling, each face is considered to consist of only two equal thickness plies (see Fig. 2).

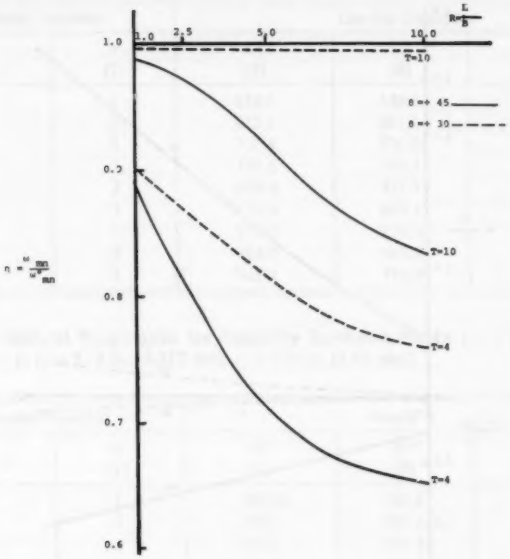

FIG. 6.—Frequency Ratio, η, as Function of Aspect Ratio, R, Thickness Ratio, T, and Ply Orientation, θ, for GR-WC Plate ($m = n = 1$)

The effect of the ratio of the thickness of the core to that of the faces, $T = t_c/t_f$, on the deflection ratio, $W = w_c/w_0$, and the frequency ratio, $\eta = \omega_{11}/\omega_{11}^0$, is demonstrated in Fig. 3 for a GR-WC plate with aspect ratio R = 2.5, for various ply orientation, θ. It can be realized that the thickness ratio, T, has a major influence on both the deflection and frequency ratios. Inspection of Fig. 3 reveals that the effect of the anisotropic coupling stiffness on both the deflection and the natural frequency of the plate practically vanish for very thin faces ($T < 20$). On the other hand, for relatively thick faces ($T < 10$), the coupling effect is appreciable.

It is pointed out that coupling always reduces the stiffness of the angle-ply sandwich plate considered herein. That is, neglecting the anisotropic coupling

stiffnesses can generate errors in the deflection and frequency results which can reach as high as 150% for the deflection and 50% for the frequency predictions (Figs. 3–7). In general, the effect of coupling on the deflection response is always higher than its effect on the frequency response of angle-ply sandwich plates.

Note that, since the magnitude of the anisotropic coupling stiffnesses increase with an increase in the face elastic moduli as well as in the ply orientation, θ, the effect of coupling on the deflection and the frequency, always increases with an increase in the elastic moduli (Fig. 4) and the angle $\theta (0 < \theta < 45)$ (Figs. 3, 5, 6, and 7).

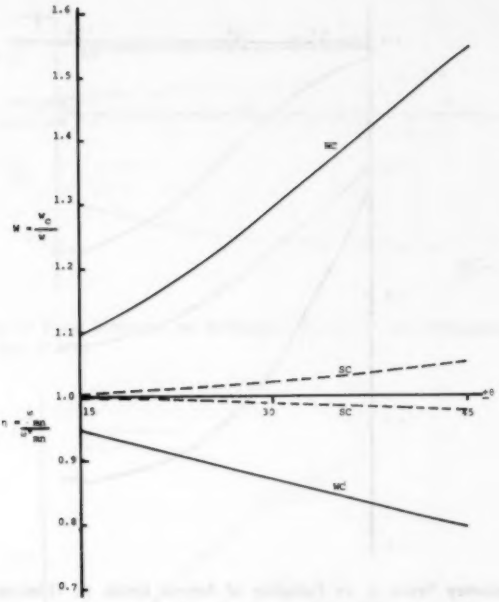

FIG. 7.—Effect of Core Stiffness on Deflection Ratio, W, and Frequency Ratio, η (GR, R = 2.5 and $T = 4$)

The effect of the aspect ratio of the plate, $R = L/B$, on the deflection ratio, W, and the frequency ratio, η, are presented in Figs. 5 and 6, respectively. It can be realized that the effect of anisotropic coupling stiffnesses on both the deflection and the frequency responses increase with an increase in the aspect ratio.

The effects of the core shear stiffness on the deflection and the frequency ratios are presented in Fig. 7, from which it can be noted that the coupling effect is increased with a decrease in the core shear stiffness.

In general, it can be stated that the effect of the anisotropic coupling stiffnesses

on the deflection and the frequency responses depends mainly upon the relative thickness of the core and the faces (T), and that the effect is magnified with an increase in the aspect ratio, the stiffness of the face plates and ply orientation, and/or a decrease in the core shear stiffness. Numerous numerical results in this study verify that the effect shown in Figs. 3–7 is typical.

In order to quantify the previous analysis, results for the natural frequencies of sandwich plates with unbalanced GR cross-ply and angle-ply faces are presented

TABLE 3.—Natural Frequencies for Cross-Ply Sandwich Plates [L = 50 in. (127.0 cm), L/B = 2, t_f = 1/8 in. (0.318 cm), t_c = 1.0 in. (2.54 cm)]

Model Number		Lay-Up Design		
m (1)	n (2)	L1 (3)	L2 (4)	L3 (5)
1	1	152.6	146.0	159.3
1	2	422.7	401.1	444.3
1	3	707.4	670.8	744.1
2	1	197.6	196.4	199.2
2	2	442.4	423.7	461.5
2	3	720.0	685.3	754.9
3	1	273.7	279.5	268.7
3	2	482.0	468.8	496.2
3	3	745.1	714.2	776.7

TABLE 4.—Natural Frequencies for Angle-Ply Sandwich Plates [L = 50 in. (127.0 cm), L/B = 2, t_f = 1/8 in. (0.318 cm), t_c = 1.0 in. (2.54 cm)]

Model Number		Angle θ		
m (1)	n (2)	15° (3)	30° (4)	45° (5)
1	1	90.60	122.6	152.9
1	2	199.9	283.3	382.1
1	3	371.0	519.5	658.7
2	1	179.4	209.2	227.3
2	2	275.0	344.2	422.9
2	3	423.2	542.1	678.4
3	1	276.1	300.4	308.6
3	2	365.2	428.7	484.4
3	3	499.7	591.1	711.6

in Tables 3 and 4, respectively. The core considered is orthotropic with shear moduli $G_x = 17 \times 10^3$ psi (117.3 kN/m^2), $G_y = 35 \times 10^3$ psi (241.5 kN/m^2), and density $\rho = 0.22 \times 10^{-3}$ lb-sec^2/in.^{4} (0.235×10^{-4} N-s^2/cm^4). For the cross-ply cases, solutions are generated for the ply lay-ups L1, L2, and L3 shown in Fig. 2. The results presented in Table 3 are in excellent agreement with those obtained using the formulations presented in Refs. 2 and 3. For the angle-ply cases, the results obtained were not verified, since to the writer's knowledge, rigorous solutions are unavailable for such plates. It is expected,

however, that the degree of accuracy of the results of the angle-ply cases is the same as those for the cross-ply cases.

Conclusion

The modified stiffness formulation is extended to the dynamic analysis of sandwich plates with anisotropic unbalanced laminated faces, such as those with unbalanced angle-ply faces, which were not amenable to rigorous solutions. The formulation is independent of the boundary conditions and can be used in conjunction with a variety of analysis techniques, such as the finite element method. Using a double Fourier series solution, the method has been applied to the analysis of sandwich plates with unbalanced cross-ply and unbalanced angle-ply faces. The results for the cross-ply cases are in complete agreement with those obtained using other analysis techniques. It is expected, therefore, that the solutions for the angle-ply cases have the same degree of accuracy as those with cross-ply faces.

It was pointed out that the difficulty associated with the analysis of sandwich plates with unbalanced angle-ply faces is due to the existence of anisotropic coupling stiffness in the formulation. The study of the effect of anisotropic coupling stiffnesses on the deflection and natural frequency of sandwich plates with unbalanced angle-ply faces reveals that for certain types of sandwich plates, the effect of coupling is significant. For such plates, neglecting coupling can result in appreciable errors which can reach as high as 150% for the deflection results, and 50% in the frequency prediction. It can be concluded, in general, that the overall influence of the anisotropic coupling stiffnesses on the behavior of unbalanced angle-ply sandwich plates is governed mainly by the thickness ratio (T). It was found that for relatively thin faces ($T > 20$), the coupling phenomenon practically vanishes; however for relatively thick faces ($T < 10$), the coupling effect is appreciable and it was found that the effect of coupling is magnified with an increase in the aspect ratio of the plate, the stiffness of the faces, and the angle of orientation of the plies, and/or a decrease in core shear stiffnesses. Finally, since the effects of factors which influence coupling are interdependent, the anisotropic coupling stiffnesses should always be considered in the analysis of sandwich plates with unbalanced angle-ply faces.

Acknowledgment

This research was sponsored by the Natural Science and Engineering Research Council of Canada under grants No. A0859 and No. A0858.

Appendix I.—Coefficients m_{ij} and g_{ij}

Coefficients g_{ij}

$$g_{11} = -(\beta^4 \bar{C}^*_{11} + \eta^2 \beta^2 \bar{C}^*_{66}) \quad \ldots \quad (16a)$$

$$g_{12} = -\beta^2 \eta^2 (\bar{C}^*_{12} + \bar{C}^*_{66}) \quad \ldots \quad (16b)$$

$$g_{13} = -\beta^4 \bar{B}^*_{11} + \beta^2 G_x \frac{4e^2}{t_c} \quad \ldots \quad (16c)$$

$$g_{21} = \eta^2 \frac{4e^3}{t_c} G_y - \eta^4 \bar{B}^*_{22} - \eta^2 \beta^2 (\bar{C}^*_{21} + \bar{C}^*_{66}) \quad (16d)$$

$$g_{22} = -\eta^2 \frac{4e^2}{t_c} G_y - \eta^2 \beta^2 \bar{C}^*_{66} + \eta^4 [\bar{B}^*_{22} - \bar{C}^*_{22}] \quad (16e)$$

$$g_{23} = \frac{4e^2}{t_c} G_y \eta^2 - \eta^4 \bar{B}^*_{22} \quad (16f)$$

$$g_{31} = -\left[\frac{4e^2}{t_c} \eta^2 G_y + \beta^4 H^*_{11} + \eta^4 D^*_{22} + \eta^2 \beta^2 (D^*_{12} + 2D^*_{66} + H^*_{12} + 2H^*_{66})\right] \quad (16g)$$

$$g_{32} = \frac{4e^3}{t_c} G_y \eta^2 - \eta^4 (H^*_{22} - D^*_{22}) - \eta^2 \beta^2 (H^*_{12} + 2H^*_{66} - D^*_{12} - 2D^*_{66}) \quad (16h)$$

$$g_{33} = -\left[\frac{4e^2}{t_c} (\beta^2 G_x + \eta^2 G_y) + \beta^4 D^*_{11} + \eta^4 D^*_{22} + 2\eta^2 \beta^2 (D^*_{12} + 2D^*_{66})\right] \quad (16i)$$

in which $[\bar{B}^*] = [H^*] - [D^*]$ (17a)

$[\bar{C}^*] = [R^*] - [H^*]$ (17b)

Coefficients m_{ij}

$m_{11} = \beta^2 [\alpha_4 - \alpha_2]$ (18a)

$m_{12} = 0$ (18b)

$m_{13} = \beta^2 [\alpha_3 - \alpha_4]$ (18c)

$m_{21} = \eta^2 [\alpha_3 - \alpha_4]$ (18d)

$m_{22} = \eta^2 [2\alpha_4 - \alpha_3 - \alpha_2]$ (18e)

$m_{23} = m_{21}$ (18f)

$m_{31} = -[\alpha_1 + \beta^2 \alpha_4 + \eta^2 \alpha_3]$ (18g)

$m_{32} = m_{21}$ (18h)

$m_{33} = -[\alpha_1 + \alpha_3 (\beta^2 + \eta^2)]$ (18i)

in which $\beta = \frac{m\pi}{L}$ and $\eta = \frac{n\pi}{B}$ (19)

Appendix II.—References

1. Monforton, G. R., and Ibrahim, I. M., "Modified Stiffness Formulation of Unbalanced Anisotropic Sandwich Plates," *International Journal of Mechanical Sciences*, Vol. 19, 1977, pp. 335–343.
2. Monforton, G. R., and Ibrahim, I. M., "Analysis of Sandwich Plates with Unbalanced Cross-Ply Faces," *International Journal of Mechanical Sciences*, Vol. 17, 1975, pp. 227–238.
3. Monforton, G. R., and Schmit, L. A., Jr., "Finite Element Analysis of Sandwich

Plates and Cylindrical Shells with Laminated Faces," *Proceedings of the Conference on Matrix Methods in Structural Mechanics, AFFDL-TR-68-150,* Air Force Flight Dynamics Laboratory, 1968, pp. 573–616.
4. Plantena, F. J., *Sandwich Construction,* John Wiley and Sons, Inc., New York, N.Y., 1966.
5. Whitney, J. M., "Bending-Extensional Coupling in Laminated Plates under Transverse Loading," *Journal of Composite Materials,* Vol. 3, Jan., 1969, pp. 20–28.

Appendix III.—Notation

The following symbols are used in this paper:

A = surface area of plate;
$[A], [B], [C], [D], [H]$ = matrices containing sum of stiffnesses;
$[A_f], [B_f], [C_f], [D_f], [H_f]$ = membrane, coupling, and bending stiffnesses;
B = width of plate;
$[D^*], [H^*], [R^*]$ = modified stiffness matrices;
G_x, G_y = shear moduli of orthotropic core;
I_c, I_f = inertia constants associated with rotary inertia of core and faces, respectively;
L = length of plate;
L1, L2, L3 = lay-up design;
$\{M\}$ = vector containing sum of moment resultants in two-face plate;
$M_x^{(f)}, M_y^{(f)}, M_{xy}^{(f)}$ = moment resultants of face plate, f;
Q_c, Q_f = inertia constants associated with translatory inertia of core and faces, respectively;
Q_x, Q_y = transverse shear forces in core;
T = total kinetic energy;
T_c, T_f = kinetic energies of core and faces, respectively;
t_c, t_f = thickness of core and face plates, respectively;
U_f = strain energy of two plates;
$w = w_{bx} + w_{by} = w_{sx} + w_{sy}$ = total transverse deflection;
w_{bx}, w_{by} = partial transverse deflection in x and y directions due to bending, respectively;
w_{sx}, w_{sy} = partial transverse deflection in x and y directions due to shear, respectively;
$w_{bxmn}, w_{bymn}, w_{sxmn}$ = undetermined displacement coefficients;
x, y, z = rectangular coordinate system;
θ = angle between principal axes of lamina and reference axes;
$\{\kappa_b\}, \{\kappa_s\}$ = vector of partial curvatures;
ρ_c, ρ_f = densities of core and faces, respectively; and
ω = frequencies.

Superscripts and Subscripts

c = core of sandwich plate; and
f = face of sandwich plate.

JOURNAL OF
THE ENGINEERING
MECHANICS DIVISION

TECHNICAL NOTES

Note.—Discussion open until September 1, 1981. To extend the closing date one month, a written request must be filed with the Manager of Technical and Professional Publications, ASCE. This paper is part of the Journal of the Engineering Mechanics Division, Proceedings of the American Society of Civil Engineers, ©ASCE, Vol. 107, No. EM2, April, 1981.

Technical Notes

To provide a place within ASCE for publication of technical ideas that have not advanced, as yet, to the point where they warrant publication as a Proceedings paper in a *Journal*, the publication of Technical Notes was authorized by the Board of Direction on October 16–18, 1967, under the following guidelines:

1. An original manuscript and two copies are to be submitted to the Manager of Technical and Professional Publications, ASCE, 345 East 47th Street, New York, N.Y., 10017, along with a request by the author that it be considered as a Technical Note.
2. The two copies will be sent to an appropriate Technical Division or Council for review.
3. If the Division or Council approves the contribution for publication, it shall be returned to Society Headquarters with appropriate comments.
4. The technical publications staff will prepare the material for use in the earliest possible issue of the *Journal*, after proper coordination with the author.
5. Each Technical Note is not to exceed 4 pages in the *Journal*. As an approximation, each full manuscript page of text, tables, or figures is the equivalent of one-half a *Journal* page.
6. The Technical Notes will be grouped in a special section of each *Journal*.
7. Information retrieval abstracts and key words will be unnecessary for Technical Notes.
8. The final date on which a Discussion should reach the Society is given as a footnote with each Technical Note.
9. Technical Notes will not be included in *Transactions*.
10. Technical Notes will be included in ASCE's annual and cumulative subject and author indexes.

The manuscripts for Technical Notes must meet the following requirements:

1. Titles must have a length not exceeding 50 characters and spaces.
2. The author's full name, Society membership grade, and a footnote reference stating present employment must appear on the first page of the manuscript. Authors need not be Society members.
3. The manuscript is to be submitted as an original copy (with two duplicates) that is typed double-spaced on one side of 8-1/2-in. (220-mm) by 11-in. (280-mm) white bond paper.
4. All mathematics must be typewritten and special symbols must be properly identified. The letter symbols used must be defined where they first appear, in figures or text, and arranged alphabetically in an Appendix.—Notation.
5. Standard definitions and symbols must be used. Reference must be made to the lists published by the American National Standards Institute and to the *Authors' Guide to the Publications of ASCE*.
6. Tables must be typed double-spaced (an original ribbon copy and two duplicate copies) on one side of 8-1/2-in. (220-mm) by 11-in. (280-mm) paper. An explanation of each table must appear in the text.
7. Figures must be drawn in black ink on one side of 8-1/2-in. (220-mm) by 11-in. (280-mm) paper. Because figures will be reproduced with a width of between 3 in. (76 mm) to 4-1/2 in. (110 mm), the lettering must be large enough to be legible at this width. Photographs must be submitted as glossy prints. Explanations and descriptions must be made within the text for each figure.
8. References cited in text must be typed at the end of the Technical Note in alphabetical order in an Appendix.—References.
9. Dual units, i.e., U.S. Customary followed by SI (International System) units in parentheses, should be used throughout the paper.

Buckling of Rings Subjected to Interacting Loads

By Robert Schmidt,[1] M. ASCE

Introduction

This technical note deals with the interaction effects of multiple external and internal pressure loads, e.g., normal gas pressure, centrally directed pressure, etc., acting on a circular elastic ring buckling in its own plane. Several simple formulas for the critical load are derived and a number of unusual phenomena are discovered. Moreover, a misconception concerning the buckling of a ring subjected to the constant-directional pressure load is clarified.

Heretofore, the extensive technical literature on the stability of rings has dealt only with a single distributed pressure load or multiple point loads.

Analysis

It is possible to imagine several different ways of applying a fairly uniform external or internal pressure load to a ring. The most common way—at least in the published literature—is to subject the ring to a gas or hydrostatic pressure that remains normal to the ring as it buckles. Pressure loads with non-normal directions during buckling can be produced by attaching strings to the ring at closely spaced equidistant points; placing the ring horizontally on a smooth table; drilling a concentric circle of holes, corresponding in number to the strings, through the table; passing the strings through these holes; and then attaching weights to the free ends of the strings, thus obtaining an essentially conservative load system. By drilling more than one circle of holes, and passing strings through each of them, multiple interacting pressure load systems can be obtained.

Herein, in order to save space, all steps in the derivation of the governing equation will be omitted, as these are elementary, and can be found in many publications, e.g., in Refs. 2, 3, 4, 6. The derived governing equation is

$$u^{vi} + (k+2)u^{iv} + (2k+1-k_n)u'' + u\sum_{i=1}^{N} k_i\left(1-\frac{a}{h_i}\right) = 0 \quad \ldots\ldots\ldots (1)$$

in which u = circumferential (tangential) displacement of a point of the centroidal

[1]Prof. of Engrg. Mechanics, Dept. of Civ. Engrg., Univ. of Detroit, Detroit, Mich. 48221.

Note.—Discussion open until September 1, 1981. To extend the closing date one month, a written request must be filed with the Manager of Technical and Professional Publications, ASCE. Manuscript was submitted for review for possible publication on July 31, 1980. This paper is part of the Journal of the Engineering Mechanics Division, Proceedings of the American Society of Civil Engineers, ©ASCE, Vol. 107, No. EM2, April, 1981. ISSN 0044-7951/81/0002-0421/$01.00.

line; a = radius of the circular centroidal line of the ring; $u^{vi} = d^6u/d\phi^6$, ϕ being the position angle measured from any reference radius, $u^{iv} = d^4u/d\phi^4$, etc.; $k_n = a^3p_n/EI$, $k_i = a^3p_i/EI$, $k = k_n + \Sigma k_i$, where E = modulus of elasticity, I = centroidal moment of inertia of the cross-sectional area, p_n = external gas (normal) pressure load per unit length, and p_i = inward (initially radial and normal) pressure load exerted by the strings passing through a given circle of holes; h_i = distance measured inward along a diameter from the ring's centroidal line to a point on the given circle of holes; and Σ indicates summation of all pressure loads p_i produced by the strings passing through the holes of the several circles of holes (each p_i will be characterized by a different direction after buckling).

Since the solution of Eq. 1 for a closed ring must be periodic, posses a certain symmetry, and be devoid of rigid-body displacements

$$u = C \sin m\phi \quad (m = 2, 3, 4, \ldots) \ldots\ldots\ldots\ldots\ldots\ldots\ldots\ldots (2)$$

Substitution of Eq. 2 in Eq. 1 results in the algebraic equation

$$-m^2(m^2 - 1)^2 + km^2(m^2 - 2) + k_n m^2 + \Sigma k_i\left(1 - \frac{a}{h_i}\right) = 0 \ldots\ldots\ldots (3)$$

With the notation

$$k_n = n_n k,\ k_i = n_i k,\ n_n + \sum_{i=1}^{N} n_i = 1 \ldots\ldots\ldots\ldots\ldots\ldots\ldots (4)$$

$$R_i = 1 - \frac{a}{h_i} \quad (i = 1, 2, \ldots, N) \ldots\ldots\ldots\ldots\ldots\ldots\ldots (5)$$

Eq. 3 can be rewritten in the form

$$k[m^2(m^2 - 2 + n_n) + \Sigma n_i R_i] = m^2(m^2 - 1)^2 \ldots\ldots\ldots\ldots\ldots (6)$$

which can be easily solved for the dimensionless critical pressure load k in terms of the parameters m, n_n, n_i, and R_i.

If the ring is subjected to an external gas pressure only, $k_i = 0$, $k_n = a^3p_n/EI = k = a^3p/EI = m^2 - 1$, and the critical pressure load is found to be $p_{cr} = 3EI/a^3$, for $m = 2$. If $k_n = k_2 = k_3 = \ldots = k_N = 0$, $k_1 = k$, $R_1 = 0$, i.e., when the ring is subjected to an external pressure always directed to the original center of the ring, $k_1 = k = a^3p/EI = (m^2 - 1)^2/(m^2 - 2)$, from which $p_{cr} = 4.5EI/a^3$, for $m = 2$. If $k_n = k_2 = k_3 = \ldots = k_N = 0$, $k_1 = k$, $R_1 = 1$, i.e., when the ring is subjected to an external constant-directional pressure ($h_1/a \to \infty$), $k_1 = k = a^3p/EI = m^2$, from which $p_{cr} = 4EI/a^3$, for $m = 2$. The three different critical values calculated agree with those frequently quoted in the technical literature, e.g., in Refs. 1, 5–7.

Problem 1

Consider a circular ring subjected to two interacting pressures p_n and p_1, $p_n + p_1 = p$, and assume that $R_1 = 1$, i.e., p_1 = constant-directional pressure. Then, from Eq. 6, for $m = 2$

$$(8 + 4n_n + n_1)k = 36 \quad (7)$$

or, since $n_n + n_1 = 1$

$$(3 + n_n)k = 12; \quad n_1 = 1 - n_n \quad (8)$$

Equation 8 indicates that the ring under this combination of loads can "buckle" while being in tension if $n_1 > 4$, i.e., $k_1 > -\infty$—a somewhat unexpected result. It is also observed that for $n_1 < 4$, the dimensionless critical net pressure load is positive (compression) and decreases with increasing n_n and k_n. (The stability boundaries consist of straight line segments and do not violate any of the known theorems on their properties.)

Problem 2

Consider a circular ring subjected to two interacting pressure loads p_1 and p_2, $p_1 + p_2 = p$ = net pressure, and assume that $R_1 = 1$ and $R_2 = 0$, i.e., p_1 = constant-directional pressure and p_2 = centrally directed (polar) pressure. Then, from Eq. 6, for $m = 2$

$$(8 + n_1)k = 36, \quad n_2 = 1 - n_1 \quad (9)$$

Equation 9 indicates that the ring subjected to this combination of loads can again "buckle" while in tension if $n_2 > 9$.

Problem 3

Consider a circular ring subjected to only one pressure load, say $p_3 = p$, exerted by the strings passing through the holes of the circle of holes characterized by $R_3 = -13/3$, i.e., $h_3 = 3a/16$. In this case, Eq. 6 reduces to

$$\left[m^2(m^2 - 2) - \frac{13}{3}\right]k = m^2(m^2 - 1)^2 \quad (10)$$

and yields $k = 108/11$ for $m = 2$, and exactly the same value $k = 108/11$ for $m = 3$. This result implies that for $h_i < 3a/16$, such a string-loaded ring will buckle in a higher mode than the first. (It should be noted at this point that, for very small values of the ratio a/h_i, the ring's buckling behavior will be similar to that of shallow arches for which the assumptions made in this communication are invalid.)

Remarks

The foregoing three problems obviously do not exhaust all the possibilities of combining different pressure loads on a ring; they merely serve as illustrative examples.

Now, if the ring that is subjected to the constant-directional pressure is not free, but hinged at two diametrally opposite points, its critical buckling pressure is not $k = a^3p_{cr}/EI = 4$ as before, but $k = 3.265$, according to Ref. 3 and Ref. 7. However, even this critical value, obtained via the general solution of Eq. 1 and the appropriate boundary conditions, is not the lowest. A careful analysis of hingeless circular arches by means of Eq. 1 indicates that when

the ring is fixed at one point against both rotation and translation, $k = 0.7014$, in the case of constant-directional pressure—a truly surprising result.

Acknowledgment

The results presented in this paper were obtained in the course of research supported by the United States National Science Foundation Grant ENG76-11521 to the University of Detroit. Barbara Etheridge's help is also appreciated.

Appendix.—References

1. Albano, E. D., and Seide, P., "Bifurcation of Rings Under Concentrated Centrally Directed Loads," *Journal of Applied Mechanics*, Vol. 40, No. 2, June, 1973, pp. 553–558.
2. Brush, D. O., and Almroth, B. O., *Buckling of Bars, Plates, and Shells*, McGraw-Hill Book Co., Inc., New York, N.Y., 1975.
3. Chwalla, E., and Kollbrunner, C. F., "Beiträge zum Knickproblem des Bogenträgers und des Rahmens," *Der Stahlbau*, Vol. 11, No. 10, May, 1938, pp. 73–78.
4. Schmidt, R., "Buckling of Rings Subjected to Unconventional Loads," Industrial Mathematics, Vol. 30, Part 2, 1980, pp. 135–142.
5. Seide, P., and Albano, E. D., "Bifurcation of Rings Under Concentrated Normal Loads," *Journal of Applied Mechanics*, Vol. 40, No. 1, Mar., 1973, pp. 233–238.
6. Simitses, G. J., *An Introduction to the Elastic Stability of Structures*, Prentice-Hall, Inc., Englewood Cliffs, N.J., 1976.
7. Singer, J., and Babcock, C. D., "On the Buckling of Rings Under Constant Directional and Centrally Directed Pressure," *Journal of Applied Mechanics*, Vol. 37, No. 1, Mar., 1970, pp. 215–218.

Method of Direct Solution To Inverse Problems

By Morteza A. M. Torkamani,[1] M. ASCE

Introduction

Many problems in engineering and science are converted to a system of linear simultaneous equations, i.e.:

$$[A]\{x\} = \{y\} \qquad (1)$$

[1] Asst. Prof. of Civ. Engrg., Univ. of Pittsburgh, Pittsburgh, Pa. 15261.

Note.—Discussion open until September 1, 1981. To extend the closing date one month, a written request must be filed with the Manager of Technical and Professional Publications, ASCE. Manuscript was submitted for review for possible publication on February 14, 1980. This paper is part of the Journal of the Engineering Mechanics Division, Proceedings of the American Society of Civil Engineers, ©ASCE, Vol. 107, No. EM2, April, 1981. ISSN 0044-7951/81/0002-0424/$01.00.

Such a set of equations may arise by approximation of a continuous relationship, $y(t) = A\,[t, \tau, x(\tau)]$, by a discrete representation, letting $y_i = y(t_i)$, $x_j = x(\tau_j)$; or by expansion of the continuous functions $y(t)$ and $x(\tau)$ in terms of appropriate sets of orthogonal functions, in which case y_i and x_j represent expansion coefficients.

If the functions $A_i(x_j)$ are linear in x_j, we may write the problem in the form

$$y_i = \sum_{j=1}^{m} A_{ij} x_j, \quad i = 1, 2, \ldots n \quad \ldots\ldots\ldots\ldots\ldots\ldots\ldots\ldots\ldots\ldots (2)$$

or in the matrix form as Eq. 1. If the functions $A_i(x_j)$ are not strictly linear, but vary smoothly enough, they may be expanded in a Taylor series about some set of initial values of the x_j say x_j^o

$$y_i = A_i(x_j^o) + \sum_{j=1}^{m} \left.\frac{\partial A_i}{\partial x_j}\right|_{x_j^o} \Delta x_j + \ldots \quad \ldots\ldots\ldots\ldots\ldots\ldots\ldots\ldots\ldots\ldots (3)$$

Defining $\Delta y_i = y_i - A_i(x_j^o)$ and ignoring second and higher order terms in Eq. 3, we have

$$\Delta y_i = \left.\frac{\partial A_i}{\partial x_j}\right|_{x_j^o} \Delta x_j$$

This is the same form as Eq. 2, with the substitution of Δy_i for y_i; Δx_j for x_j; and

$$\left.\frac{\partial A_i}{\partial x_j}\right|_{x_j^o} = A_{ij}$$

For simplicity, we shall proceed using the notation of Eq. 1 with the understanding that the aforementioned substitution can be made at any stage of the calculations for a system which results from the perturbation of a quasilinear problem (3).

If Eq. 1 is a well-posed problem, the solution to this system of simultaneous equations is obtained by any of the wellknown existing techniques (1). However, in many circumstances Eq. 1 cannot be solved directly. This occurs when matrix A is ill conditioned or is a rectangular matrix. There are methods available to handle this situation, such as Orthogonal Decomposition Methods (4), and Natural Inverse of a Matrix (5); but in any event, the solution obtained for Eq. 1 by any direct method is often not acceptable. This is due to the fact that the error introduced in the conversion from a continuous system to a discrete system has not been considered in the solution.

The objective of this paper is to present a method of solution which will account for the discretization errors in the solution. The technique will be compared to the present method of solution which has been used in many cases for an acceptable solution of Eq. 1.

Consider the following optimization problem:

Minimize $\{x\}^T [c] \{x\}$

subject to $([A]\{x\} - \{y\})^T ([A]\{x\} - \{y\}) \leq e^2$

such that $\{\epsilon\} = [A]\{x\} - \{y\}$

$$e^2 = \{e\}^T\{e\}$$

and $\{\epsilon\} \le \{e\}$ . . . . (4)

in which $[c]$ is banded positive definite square matrix, varies from problem to problem, and in the limit it might be an identity matrix; and $\{e\}$ = vector of upper bound on acceptable error.

Equation 4 may be obtained from a continuous minimization problem after discretization. The Lagrangian function to Eq. 4 is

$$L(x,\gamma) = \{x\}^T[c]\{x\} + \gamma^{-1}\{([A]\{x\} - \{y\})^T([A]\{x\} - \{y\}) - e^2\} \quad \text{. . . (5)}$$

and with the gradient of this Lagrangian function set to zero

$$\nabla L(x,\gamma) = 0 \quad \text{. . . (6)}$$

will give $\{x\} = ([A]^T[A] + \gamma[c])^{-1}[A]^T\{y\}$ . . . . (7)

in which γ^{-1} = Lagrangian multiplier. If the Lagrangian Multiplier γ^{-1} is known, by substituting γ into Eq. 7 and solving for $\{x\}$, one will obtain the optimal solution to the optimization problem (Eq. 4). However, the Lagrangian multiplier is not known, and the known quantities are the upper bound on acceptable error vector $\{e\}$ or $e^2 = \{e\}^T\{e\}$.

Therefore, there is need for a method of solution to the primal optimization problems (Eq. 4). The following algorithm is a technique for finding optimal solution to Eq. 4. This algorithm has the advantage of solving a convex nonlinear optimization problem by a series of linear programming optimizations.

Algorithm to Solve Convex Minimization Problems

It can be shown that the optimization problem (Eq. 4) is a convex minimization problem, (2,6). Any convex minimization problem has a unique solution. A solution algorithm to solve convex minimization problems is as follows. Consider the general convex minimization problem:

Minimize $f(x)$

Subject to $g(x) \ge 0; \quad x \in R^n; \quad x \in X$ . . . . (8)

in which $f(x)$ = a convex function; $g(x)$ = m vectors of concave functions; and X = a set of all feasible solutions:

1. Pick a feasible solution x^1 such that $g(x^1) > 0$, $x^1 \in X$.
2. Construct linear programming problem:

Minimize $\lambda_1 f(x^1)$

Subject to $\lambda_1 g(x^1) \ge 0; \quad \lambda_1 = 1; \quad \lambda_1 \ge 0$ . . . . (9)

Solve this linear programming problem for primal solution λ_1 and dual solution π, η. Let us say these solutions are $(\lambda_1^0, \pi^0, \eta^0)$.

3. Construct minimization problem:

Minimize $f(x) - \pi^0 g(x) - \eta^0$

Subject to $x \in X$ . . . . . (10)

Let us say x^2 is the optimal solution of Eq. 10.

4. If $f(x^2) - \pi^0 g(x^2) - \eta^0 \geq 0$, stop $\bar{x} = \lambda_1^0 x^1$ is the optimal solution to Eq. 8. If $f(x^2) - \pi^0 g(x^2) - \eta^0 < 0$, add a new column to the linear programming problem (Eq. 9).

Minimize $\lambda_1 f(x^1) + \lambda_2 f(x^2)$

Subject to $\lambda_1 g(x^1) + \lambda_2 g(x^2) \geq 0; \quad \lambda_1 + \lambda_2 = 1; \quad \lambda_i \geq 0 \quad i = 1, 2$ (11)

Let us say that $(\lambda_1^1, \lambda_2^1, \pi^1 \eta^1)$ are primal and dual optimal solutions to Eq. 11.

5. Construct minimization problem

Minimize $f(x) - \pi^1 g(x) - \eta^1$

Subject to $x \in X$ . . . . . (12)

with new Lagrangian multiplier (π^1, η^1) and solve the problem. Let us say x^3 is the answer to this minimization problem.

6. If $f(x^3) - \pi^1 g(x^3) - \eta^1 \geq 0$ stop, $\bar{x} = \lambda_1^1 x^1 + \lambda_2^1 x^2$ is the optimal solution to Eq. 8. If $f(x^3) - \pi^1 g(x^3) - \eta^1 < 0$ add a new column to linear programming problem (Eq. 11) and continue. For proof and convergence of algorithm see Refs. 2 and 6. This algorithm will give the optimal solutions to the primal problem (Eq. 8) and the dual system (Eq. 10) simultaneously.

There are several important technical cases where the objective is to solve

$$[A]\{x\} = \{Y\} + \{\epsilon\} \quad \text{. . . . . (13)}$$

and a least square error procedure was used.

$$\{x\} = ([A]^T [A])^{-1} [A]^T \{y\} \quad \text{. . . . . (14)}$$

In order to obtain an acceptable smooth solution, a positive definite banded symmetric matrix is added to the matrix $([A]^T [A])$ such that

$$\{x\} = ([A]^T [A] + \gamma [c])^{-1} [A]\{y\} \quad \text{. . . . . (15)}$$

in which $[c]$ = a banded positive definite symmetric matrix; and γ = a small positive number. By applying this technique the intention is to include some error in the solution, but the result is not always satisfactory. In this method it is not possible to control the contribution of the error to the problem in a direct way, trial and error method should be used to obtain the desired solution. Of course the solution to Eq. 15 depends on parameter γ and by varying γ one would have a set of solutions, which may or may not be feasible solutions and none of them are the optimal solution to Eq. 4.

Example

The two-story frame structure of Fig. 1 with element properties $m_1 = m_2 = 1$, $k_1 = k_2 = 4\pi^2$ and $k_3 = k_4 = 6\pi^2$ are subjected to ground excitation $A(t) = 100 \sin(4\pi t)$.

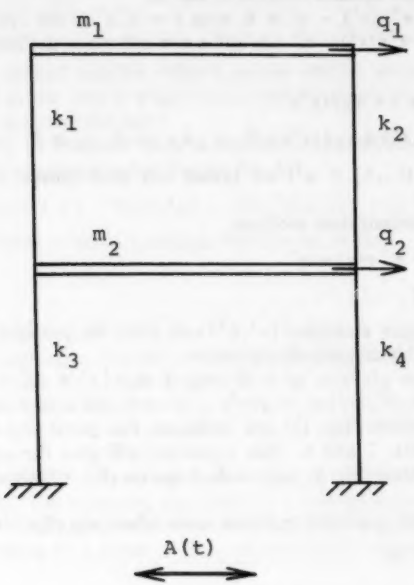

FIG. 1.—Two-Story Frame Structure Subject to Harmonic Ground Excitation $A(t)$

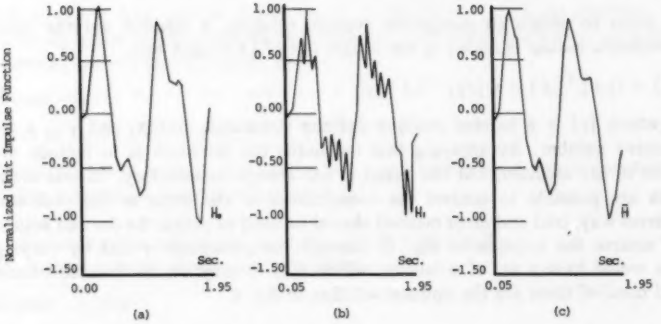

FIG. 2.—Unit Impulse Response Function: (*a*) Exact Solution; (*b*) Direct Solution; and (*c*) Optimal Solution to Integral Eq. 16

The absolute acceleration $y(t)$ on the roof level is related to the ground acceleration $A(t)$ by

$$y(t) = \int_0^t A(t-\tau)\, x(\tau)\, d\tau \quad \ldots \quad (16)$$

in which $y(t) = 80 \sin(2\pi t) - 100 \sin(4\pi t) + 20 \sin(2\pi \sqrt{6t})$. In order to calculate $x(\tau)$, it is assumed that $t_i = i\Delta t$ and $\tau_j = j\Delta\tau$, in which $\Delta t = \Delta\tau = 0.05$ and integral Eq. 16 is discretized:

$$y(t_i) = \sum_{j=1}^{t_i} W_j A(t_i - \tau_j)\, x(\tau_j)\, \Delta\tau \quad i = 1, 2 \ldots \quad \ldots \quad (17)$$

in which w_j depends on the numerical integration scheme used in discretization. In this example, a 40-points time increment was considered. Equation 17 resulted in a 40×40 simultaneous system of equations. A direct solution to this system of simultaneous equations is shown in Fig. 2(*b*), where the exact answer is shown in Figure 2(*a*). The optimization technique applied to this problem and further details of each step are given in Ref. 6. The optimal solution is shown in the Fig. 2(*c*).

Conclusion

A method of solution and an algorithm were presented in this paper for the solution of many converted problems in engineering and science to a system of linear simultaneous equations. The method is based on minimizing an objective function subjected to the upper bound of the error on the constrained equations. The optimization problem is one of convex minimization, and a unique solution to the problem exists. The method is applied to a two-story frame structure subjected to harmonic ground excitation and the optimal solution is in good agreement to the exact solution.

Acknowledgment

The writer wishes to express his appreciation to Joel I. Abrams, University of Pittsburgh, for reading the text of this paper.

Appendix.—References

1. Bathe, K. J., and Wilson, E. L., *Numerical Methods for Finite Element Analysis*, Prentice-Hall, Inc., Englewood Cliffs, N.J., 1976.
2. Dantzig, G. G., *Linear Programming and Extensions*, Princeton University Press, Princeton, N.J., 1963.
3. Jackson, D. D., "Interpretation of Inaccurate, Insufficient and Inconsistent Data," *Geophysics Journal of the Royal Astronomical Society*, Vol. 28, No. 2, June, 1972, pp. 97–110.
4. Jennings, A., *Matrix Computation for Engineers and Scientists*, John Wiley and Sons, Inc., New York, N.Y., 1977.
5. Lanczos, C., *Linear Differential Operators*, D. Van Nostrand Co., Inc., London, England, 1961.
6. Torkamani, M. A. M., and Hart, G. C., "Building System Identification Using Earthquake Data," *ENG-7507*, Mechanics and Structures Department, University of California, Los Angeles, Calif., Jan., 1975.

JOURNAL OF
THE ENGINEERING
MECHANICS DIVISION

DISCUSSION

Note.—This paper is part of the Journal of the Engineering Mechanics Division, Proceedings of the American Society of Civil Engineers, ©ASCE, Vol. 107, No. EM2, April, 1981. ISSN 0044-7951/81/0002-0433/$01.00.

Discussions

Discussions may be submitted on any Proceedings paper or technical note published in any *Journal* or on any paper presented at any Specialty Conference or other meeting, the *Proceedings* of which have been published by ASCE. Discussion of a paper/technical note is open to anyone who has significant comments or questions regarding the content of the paper/technical note. Discussions are accepted for a period of 4 months following the date of publication of a paper/technical note and they should be sent to the Manager of Technical and Professional Publications, ASCE, 345 East 47th Street, New York, N.Y. 10017. The discussion period may be extended by a written request from a discusser.

The original and three copies of the Discussion should be submitted on 8-1/2-in. (220-mm) by 11-in. (280-mm) white bond paper, typed double-spaced with wide margins. The length of a Discussion is restricted to two *Journal* pages (about four typewritten double-spaced pages of manuscript including figures and tables); the editors will delete matter extraneous to the subject under discussion. If a Discussion is over two pages long it will be returned for shortening. All Discussions will be reviewed by the editors and the Division's or Council's Publications Committees. In some cases, Discussions will be returned to discussers for rewriting, or they may be encouraged to submit a paper or technical note rather than a Discussion.

Standards for Discussions are the same as those for Proceedings Papers. A Discussion is subject to rejection if it contains matter readily found elsewhere, advocates special interests, is carelessly prepared, controverts established fact, is purely speculative, introduces personalities, or is foreign to the purposes of the Society. All Discussions should be written in the third person, and the discusser should use the term "the writer" when referring to himself. The author of the original paper/technical note is referred to as "the author."

Discussions have a specific format. The title of the original paper/technical note appears at the top of the first page with a superscript that corresponds to a footnote indicating the month, year, author(s), and number of the original paper/technical note. The discusser's full name should be indicated below the title (see Discussions herein as an example) together with his ASCE membership grade (if applicable).

The discusser's title, company affiliation, and business address should appear on the first page of the manuscript, along with the *Proceedings* paper number of the original paper/technical note, the date and name of the *Journal* in which it appeared, and the original author's name.

Note that the discusser's identification footnote should follow consecutively from the original paper/technical note. If the paper/technical note under discussion contained footnote numbers 1 and 2, the first Discussion would begin with footnote 3, and subsequent Discussions would continue in sequence.

Figures supplied by the discusser should be designated by letters, starting with A. This also applies separately to tables and references. In referring to a figure, table, or reference that appeared in the original paper/technical note use the same number used in the original.

It is suggested that potential discussers request a copy of the *ASCE Authors' Guide to the Publications of ASCE* for more detailed information on preparation and submission of manuscripts.

Pressures on Curtain Wall with External Mullions[a]

Closure by Bernard M. Leadon[4] and Michael L. Kownacki[5]

The writer appreciates the comments by T. Stathopoulos and will endeavor to clarify our presentation of the results of the study, hopefully to his satisfaction. He and other readers should refer at once to the "Errata" section of this Closure for correction of several numerical errors which unfortunately appeared in the original paper for which the writer is sincerely apologetic.

The flows discussed are parallel to the face of the building, as indicated in the Introduction, and are treated in terms of two components: one parallel to the vertical mullions; and the other horizontal. The component normal to the building surface and away from mullion influence is zero. Thus, if the flow is at 90° to the mullions, it is a purely horizontal flow parallel to the building face while, if the flow is at 45° to the mullions, its vertical and horizontal components are of equal magnitude. The appropriate model orientation then is with plate parallel to the tunnel center line and mullions either transverse to or at 45° to the tunnel center line. In actuality the plates used were plywood boards 8 ft × 3 ft × 3/4 in. (2.44 m × 91.4 cm × 1.9 cm) mounted slightly above the tunnel floor and spanning its 3-ft (91.4-cm) width with streamwise slope adjusted for constant static pressure along the tunnel roof. Upon one plate were mounted six 1/4-scale I-beams 2 in. (5.08 cm) high and set at 90° to the tunnel center line. Upon the second plate were mounted six 1/4-scale mullions but at 45° to the tunnel center line. Upon a third plate were mounted 12 1/10-scale mullions at 45° to the center line.

For the 1/4-scale, $\theta = 45°$ model the ratio of mullion spacing, L, to tunnel width, W, was 0.417. This value of L/W was shown to be too large for free lateral adjustment of the flow to the disturbing influence of the mullions by the observation that the pressures measured on the plate were nearly the same as those which had been measured on the 1/4-scale, $\theta = 90°$ model.

For the 1/10-scale, $\theta = 45°$ model the value of L/W was 0.167, and the differential pressures measured were less than half of those measured on the 1/4-scale, $\theta = 90°$ model. This was attributed to the freedom of the streamlines near the plate to deflect in the direction of the mullions and to exert pressure on the mullions only in proportion to the square of the normal component of velocity. When pressure coefficients were calculated in this way, agreement was within 0.03 at all points excepting that at $X/L = 1.0$. It is not reasonable to speak of the discrepancy relative to local pressure coefficients which range

[a]August, 1979, by Bernard M. Leadon and Michael L. Kownacki (Proc. Paper 14732).

[4]Prof. of Engrg. Sci., Univ. of Florida, 231 Aerospace Engrg. Bldg., Gainesville, Fla. 32611.

[5]Staff Engr., Goodyear Atomic, Piketon, Ohio.

from negative to positive unless possibly in comparison with the whole range which is 0.26; thus the discrepancy is only 11% except, again at $X/L = 1.0$, where it is 35%. Put another way, the mean slope of the C_p versus X/L distribution for the 1/4-scale, $\theta = 90°$ model was approx 0.27 over X/L from 0–0.917. For the 1/10-scale, $\theta = 45°$ model it was approx 0.24 when the normal component of velocity was used to compute the dynamic pressure. This slope would have been approx 0.10 if the full free stream dynamic pressure were used. In these terms then we stated that the $C_{p_\perp}$ distributions for the 1/10-scale, $\theta = 45°$ model "agreed fairly well" with the C_p distribution for the 1/4-scale, $\theta = 90°$ model, and "at $L/W = 0.167$ the independence principle appears to hold." In an extended study, of course, one might test additional scales of model to ascertain with greater precision the effect of L/W upon measured pressures.

From the results just discussed, however, the ratio L/W is clearly shown to be an important parameter in wind tunnel testing of two-dimensional planar geometries, much as for three-dimensional bluff bodies the model to tunnel cross-sectional area ratio is an important parameter. In either case the parameter only indicates a maximum value which must must not be exceeded if the test is to simulate full-scale conditions properly. We do not treat L/W as a critical similarity parameter which must be held constant as between model and prototype. On the other hand it is taken for granted that the geometries of model and prototype, including the ratio of mullion spacing to mullion height, must be identical for geometrical similarity.

As to the numbers of mullions in the two models, we filled the available model length with mullions which resulted in twice as many for the smaller scale model. There is no reason to hold this number constant since after four mullions the turbulent boundary layer and separated flow zones between the next two will be very little affected by adding more mullions forward. As to testing a smaller model in a proportionately smaller tunnel, one would certainly expect to duplicate results already obtained if both tests were done with comparable accuracy.

Data on extreme pressure coefficients were not recorded, but it is agreed that such measurements could be interesting.

With regard to the effects of turbulence in the free stream we were convinced that four or more upstream mullions would generate enough turbulence in the boundary layer to render mean surface pressures independent of free stream conditions, but we were perhaps negligent in not explaining this point. It has long been known, e.g., that heat transfer in a turbulent boundary layer on a plate exposed to a nonaccelerating freestream is quite insensitive to freestream turbulence level (3). We have recently had occasion to verify this point and have reported elsewhere (4) that the change from a 0.05% to a 4.5% turbulence level makes no difference whatsoever in the pressure coefficients measured on the 1/4-scale, $\theta = 90°$ model.

We are grateful for the opportunity to present this closure. We also note that the National Science Foundation has supported this work under Grant No. PFR-7726391.

Appendix.—References

3. Kestin, J., Maeder, P. F., and Wang, H. E., "Influence of Turbulence on the Transfer of Heat from Plates with and without a Pressure Gradient," *International Journal*

of Heat and Mass Transfer, Vol. 3, No. 2, Sept., 1961, pp. 133–154.
4. Leadon, B. M. and Jenkins, D. A., "Pressures on a Curtain Wall, Full Scale and Model Results," presented at the October 27–30, 1980, ASCE Fall Convention and Exhibit, held at Hollywood, Fla.

Errata.—The following corrections should be made to the original paper:

Page 515, paragraph 2, line 8: Should read "may be modeled in a wind tunnel." instead of "may be molded in a wind tunnel."
Page 517, paragraph 2, line 2: Should read "The tap locations were at $x/L = 0$, 0.038, 0.25, 0.417, 0.583, 0.75, 0.917, and 1.00." instead of "The tap locations were at $x/L = 0$, 0.083, 0.25, 0.417, 0.50, 0.583, 0.75, 0.917, and 1.00."
Page 517, Fig. 2(*b*): delete points plotted at $X/L = 0.083$ and 0.417 for 90° 1/4-scale model. These points are correctly plotted in Fig. 2(*a*) and in Fig. 3(*a*).
Page 519, paragraph 5, line 3: Should read "C_p calculated as if θ was 90°" instead of "C_p calculated as if θ was zero"
Page 519, paragraph 5, line 4: Should read "(whereas in one case it was 90° while in the other it was 45°)" instead of "(Whereas in one case it was zero while in the other it was 45°)"
Page 520, line 1: Should read "x/L for the 1/4-scale model" instead of "x/L for the 1/10-scale model"

A 3D Hypoelastic Constitutive Relationship[a]

Closure by Alaa E. Elwi[4] and David W. Murray,[5] M. ASCE

The writers would like to thank Bazant for his interest in, and discussion of, their paper. While they agree that orthotropic models may eventually be shown to be inadequate to represent the complexities of concrete behavior, they believe that the arguments advanced by Bazant as a basis for rejecting all orthotropic and hypoelastic models are fallacious.

Bazant's arguments appear to arise out of a lack of appreciation of a number of fundamental characteristics of the nonlinear hypoelastic orthotropic models that are currently being used to simulate concrete behavior. Some of these characteristics may be itemized as:

1. For any orthotropic relationship normal and shearing stresses and strains are coupled except in the principal directions of orthotropy.

---

[a]August, 1979, by Alaa E. Elwi and David W. Murray (Proc. Paper 14746).
[4]Structural Engr., Civ. and Structural Dept., associated with Pullman-Kellog Ltd., Edmonton, Alberta, Canada, T6G 2G7.
[5]Prof. of Civ. Engrg., Univ. of Alberta, Edmonton, Alberta, Canada, T6G 2G7.

2. Orthotropic behavior is assumed only in an incremental sense which does not imply an orthotropic relationship between total stresses and total strains.

3. The principal directions of orthotropy are assumed to rotate as loading progresses. The direction of incremental orthotropy is an independent assumption of the model.

The arguments and illustrative example presented by Bazant to demonstrate lack of invariance are fallacious because they do not recognize these characteristics. Given any assumed directions of incremental orthotropy, increments of stresses and strains and the incremental constitutive coefficients are tensor quantities and there is no lack of invariance. If one can categorically reject all incremental hypoelastic relationships how can one then accept incremental plasticity relationships which are special cases of (irreversible) hypoelastic relationships (20,21).

The writers have arbitrarily chosen the directions of incremental orthotropy to be the principal directions of total stress. This appears to work reasonably well for the test data available to them. Whether or not this assumption will prove acceptable to simulate data from tests in which the principal axes rotate can only be verified after reliable data of this type are experimentally produced. In the meantime the writers maintain that choosing the principal stress directions to be the directions of orthotropy imposes a condition on the material law which, rather than limiting the capability of the model, stabilizes it. There is no implied coincidence between the principal directions of total stresses and total strains nor between the principal directions of incremental stresses and incremental strains. In a general finite element formulation the increments of equivalent uniaxial strains are accumulated but the increments of stress are not. Rather a stress point which satisfies the stress-equivalent uniaxial strain curve is found, and equilibrium is established in an iterative manner. The instantaneous incremental constitutive matrix depends upon the entire history at the material point, since it is a function of the equivalent uniaxial strains. Therefore induced damage affects the current as well as future values of strains and also the orientation of principal stresses.

In his fourth paragraph Bazant makes a number of statements regarding nonvanishing shear stresses and isotropy. The writers cannot accept these statements. They believe he has misinterpreted this model, as well as other hypoelastic models (2,4,5).

The writers also believe that dilatancy has little direct structural significance. When dilatancy is suppressed by confinement, the resulting behavior can be observed directly in biaxial and triaxial tests and this behavior is represented in the stress-equivalent uniaxial strain curve, in the ultimate surfaces, and in the representation of Poisson's ratio.

The writers agree with Bazant that more basic experimentation including shear components is necessary. However the writers believe that results from biaxial and triaxial tests form the only reliable data upon which to base general constitutive models at the present time.

The writers also wish to point out that endochronic and plasticity theories, regardless of their success in representing concrete behavior, do not preclude other lines of investigation.

Finally the writers wish to admit an inaccuracy in referring to their type

of ultimate surfaces as "Argyris" surfaces. These surfaces would be more properly referred to as "Willam-Warnke" surfaces (17).

Appendix.—References

19. Elwi, A. E., and Murray, D. W., "Nonlinear Analysis of Axisymmetric Reinforced Concrete Structures," *Structural Engineering Report No. 87*, University of Alberta, May, 1980.
20. Eringen, A. C., *Nonlinear Theory of Continuous Media*, McGraw-Hill Book Co., Inc., New York, N.Y., 1962.
21. Green, A. E., "Hypoelasticity and Plasticity II," *Journal of Rational Mechanics and Analysis*, Vol. 5, 1956, pp. 725–734.

Errata.—The following corrections should be made to the original paper:

Page 624, Eq. 3: Should read

$$\begin{Bmatrix} d\epsilon_1 \\ d\epsilon_2 \\ d\epsilon_3 \\ d\gamma_{12} \end{Bmatrix} = \begin{bmatrix} \frac{1}{E_1} & \frac{-\mu_{12}}{\sqrt{E_1 E_2}} & \frac{-\mu_{13}}{\sqrt{E_1 E_3}} & 0 \\ & \frac{1}{E_2} & \frac{-\mu_{23}}{\sqrt{E_2 E_3}} & 0 \\ & & \frac{1}{E_3} & 0 \\ \text{symmetrical} & & & \frac{1}{G_{12}} \end{bmatrix} \begin{Bmatrix} d\sigma_1 \\ d\sigma_2 \\ d\sigma_3 \\ d\tau_{12} \end{Bmatrix} \quad \text{instead of}$$

$$\begin{Bmatrix} d\epsilon_1 \\ d\epsilon_2 \\ d\epsilon_3 \\ d\gamma_{12} \end{Bmatrix} = \begin{bmatrix} \frac{1}{E_1} & \frac{-\mu_{12}}{E_1 E_2} & \frac{-\mu_{13}}{E_1 E_3} & 0 \\ & \frac{1}{E_2} & \frac{-\mu_{23}}{E_2 E_3} & 0 \\ & & \frac{1}{E_3} & 0 \\ \text{symmetrical} & & & \frac{1}{G_{12}} \end{bmatrix} \begin{Bmatrix} d\sigma_1 \\ d\sigma_2 \\ d\sigma_3 \\ d\tau_{12} \end{Bmatrix}$$

Page 637, paragraph 3, line 2: Should read "and Willam, et al. (17)," instead of "and William, et al. (17),"

Page 638, Ref. 1: Should read "Argyris, J. H., Krempl, E., and Willam, K. J." instead of "Argyris, J. H., Krempl, E., and William, K. J."

Page 639, Ref. 17: Should read "Willam, K. J., and Warnke, E. P." instead of "William, K. J., and Warnke, E. P."

Probability of Response To Evolutionary Process[a]

Discussion by Jorge D. Riera,[3] M. ASCE

The importance of expedient procedures to determine the probability distribution of the response of lightly damped systems subjected to nonstationary random excitation is unquestionable. In this context, Spanos and Lutes present in their paper very interesting results, which may become valuable in applications of random vibration methods to many engineering problems.

The writer believes, however, that some clarifications are necessary. Moreover, comments by Spanos and Lutes on some suggestions presented herein may enhance the value of their results.

In first place, it appears that Eqs. 6 and 7 hold only approximately, provided that both $a(t)$ and $\phi(t)$ are slowly varying functions of time. Since such assumption is introduced later in the paper, the question remains whether that is indeed the case.

Also note that if $S(t, \omega_0) = S(\omega_0)$, as indicated by Eq. 21, the process is a white noise process, and not a more general type of stationary process. In such case, the variance of the response is approximately given by Eq. 23. The writer showed in Ref. 25 that if the excitation $w(t)$ is an amplitude modulated white noise with spectral density function S_0, then the variance of the response $x(t)$ is given by:

$$\sigma^2(t) = \frac{\pi S_0}{2(1-\zeta^2)\omega_0^2} \int_0^t \exp\left[-2\zeta\omega_0(t-s)\right]$$

$$[1 - \cos 2p_0(t-s)]\, f(s)\, ds \quad \ldots\ldots\ldots\ldots\ldots\ldots\ldots\ldots\ldots\ldots\ldots\ldots \quad (62)$$

in which $f(t)$ = the modulating function; and $\omega_d = \omega_0\sqrt{1-\zeta^2}$. When $f(s)$ is a unit step function at the origin, Eq. 48 results:

$$\sigma^2(t) = \frac{\pi S_0}{2\zeta\omega_0^3}\left[1 - \frac{\exp(-2\zeta\omega_0 t)}{1-\zeta^2}(1 - \zeta^2\cos 2\omega_d t\right.$$

$$\left. + \zeta\sqrt{1-\zeta^2}\sin 2\omega_d t)\right] \quad \ldots\ldots\ldots\ldots\ldots\ldots\ldots\ldots\ldots\ldots\ldots\ldots \quad (63)$$

which, upon assuming that $\zeta << 1$, reduces to Eq. 23.

Formally, for a slowly varying modulating function, Eq. 29 can be directly obtained from Eq. 62 by dropping the term $[1 - \cos 2\omega_d(t-s)]$. This suggests

[a]April, 1980, by Polichronis-Thomas D. Spanos and Loren D. Lutes (Proc. Paper 15313).

[3]Prof. of Civ. Engrg., Curso de Pós-Graduação em Engenharia Civ., Universidade Federal do Rio Grande do Sul, Porto Alegre, Brasil.

that the expression:

$$c(t) = \frac{\pi \exp(-2\zeta\omega_0 t)}{(1-\zeta^2)\omega_0^2} \int_0^t \exp(2\zeta\omega_0 s)\,[1-\cos 2p_0(t-s)]\,S(s,\omega_0)\,ds$$

$$+ c(o)\exp(-2\zeta\omega_0 t) \quad \ldots\ldots\ldots\ldots\ldots\ldots\ldots\ldots\ldots\ldots\ldots\ldots \quad (64)$$

may be more accuracte than Eq. 29. In fact, if Eq. 64 was valid, the assumptions that $\zeta << 1$ and that $f(t)$ is a slowly varying function of time might be relaxed. It must be kept in mind, however, that the results apply to modulated white noise, and therefore constitute only approximations for other nonstationary excitations.

Finally, it should be pointed out that there is an error in Eq. 29, in which the argument of the factor $\exp(2\zeta\omega_0 t)$ is negative.

Appendix.—Reference

25. Riera, J. D., "Aplicacão do Método das Variáveis de Estado ao Estudo de Sistemas Dinâmicos sob Excitacões Aleatórias Não-Estacio-nárias," *Paper No. A-22, Anais do IV Congresso Brasileiro de Eng. Mecânica*, Florianópolis, Brasil, 1977, pp. 255–268.

Concrete Strength Prediction by the Maturity Method[a]

Discussion by Luke M. Snell,[2] M. ASCE

One of the major problems in concrete construction is to determine when the in-place concrete has reached sufficient strength so that the formwork and shoring can be safely removed. In the past, contractors have used a "field maturity concept" to aid them. When the weather is warm, the formwork and shorings are removed early; when the weather is cool, they are removed later than normal.

Although this field method is similar to the maturity concept, some differences are obvious. The method just described uses the ambient temperature surrounding the forms. Casual acknowledgment of the temperatures cannot provide accurate data. The definitions of warm, cool, early, and late are also left to the individual contractor. Thus, the contractors remove the formwork and shoring when they feel that they can safely do so. The removals are not based on a minimum maturity factor but on a rule of thumb or past experiences, or both. Normally this method is adequate, however, several recent failures have been attributed to early removal of formwork and shoring when the in-place concrete was of insufficient strength. Applications of an exact maturity method appears to be needed within the construction industry.

---

[a]June, 1980, by Tarun R. Naik (Proc. Paper 15453).

[2]Assoc. Prof. of Construction, Dept. of Engrg. and Tech., Rm. 0332, Science Building, Southern Illinois Univ. at Edwardsville, Edwardsville, Ill. 62026.

The maturity method as presented by the author can provide an accurate estimate of the in-place concrete strength provided it is used correctly. The user of this method must be aware of the limitations associated with the method. Unlike other nondestructive testing methods mentioned by the author, the maturity method does not measure any of the physical properties of the concrete (e.g., the Swiss hammer measures surface hardness, the Windsor probe measures penetration resistance, pull-out test measures a pull-out stress, pulse velocity measures the velocity of a transmitted low frequency ultrasonic sound wave). The maturity method presents a time-temperature history of the in-place concrete. This time-temperature history presented as a maturity number can be used to estimate strength provided expected concrete strength ($f'c$) or the exact mix design is known. This is shown by the author in Fig. 8. Each mix design provides a different maturity-compressive strength curve. When the design strengths or the mix designs are unknown, the maturity concept would be inaccurate. In concrete construction, misbatched concrete (such as concrete with a lower cement factor than specified by the design mix), misplaced concrete (placement of a concrete with a design strength of 3,000 psi where a concrete with a design strength of 5,000 psi was specified) or mishandling of the concrete (poor vibration, segregation, adding excess water, etc.) are not uncommon. In these particular instances mentioned, the maturity method would indicate a higher strength than the in-place concrete had achieved. Thus, basing decisions for removal of formwork or shoring only on a maturity method could result in failure.

To safely use the maturity method, some method of documenting the design strength or the mix design of the concrete must be incorporated into the test plan. Use of other nondestructive tests along with the maturity method would appear to hold promise of providing an accurate estimate of in-place concrete strength at a designated time.

The writer shares the author's opinion that the maturity method has great potential. It is also the writer's opinion that the user must realize the limitations of this method and use the maturity method only when the mix design of the concrete is known or can be determined by other test methods.

Discussion by Owen Richards[3]

The author has done what is too rare today: reported on an extraordinarily precise study of methods of determining in-place concrete strengths. The issue is critical for construction safety, as the strength of little rapid highrise concrete is officially recognized until 28-day cylinders are broken and several floors in use.

The earliest age 4-in. × 8-in. cores, drilled at 7 days and dried for 24 hr before testing, are said to be some 6% higher in strength (based on maturity and other test relationships) than the actual core indications. D. L. Bloem (9) reported a similar finding for cast-in-place [American Society of Testing and Materials (ASTM) Method C 873] pushout cylinders. If the latter C 873 pushout molds had been used, compressive tests might have been conducted at 1-day

[3]Principal, Owen Richards Testing Equipment, R.D. 2, Box 156, The Plains, Va. 22171.

or earlier ages—when constructors most need significant strength test data to aid in judgements for curing requirements.

A further advantage of the C 873 pushouts (aside from cost, a small fraction of that for drilled cores) is that they are already in the as-cured condition, thus needing no drying out, as for a wet-drilled core. Early age cores are especially subject to aggregate-cement paste bond damage and low strength indications, as witnessed by ASTM C 42 advising that "concrete shall be 14 days old" before drilling.

An especial problem with me is an evident difference in logical approach inherent in T. R. Naik's Table 6 and in what this writer considers significant for evaluating probable in-place concrete performance. The writer consider the ASTM C 39 "standard cure cylinder" to be a test for potential strength of an artificial concrete of purely contractual interest between concrete seller and buyer: it enables one to judge as to whether concrete ingredients, mixing and handling up to the point of the buyer's becoming owner are acceptable. The C 39 potential strength should not, in my mind, be used to calculate a novel potential strength (as in Col. 3, Table 6) based on correlation with core strength of what is in effect a different concrete.

If any such correlation is made (and it may have significance in evaluating the buyer's handling, placement and curing efforts), it would in my mind best be in the direction of calculating in-place core strengths on potential strength.

Conducting such an in-place core on potential strength calculation (which, as noted, the writer depreciates), one gets a regression equation, for mixes No. 5 and 6, of f_{cc} (i.e., compressive strength of cores on potential strength) $= 0.853\, f_c + 317$; the indicated estimated strengths are naturally lower than those developed in Col. 3 of Table 6. Since they are lower, they may qualify as more conservative, and therefore desirable, in judging potential in-place strength performance and interim load-bearing capacity of the concrete involved.

The author has presented a most interesting and informative presentation of a formal approach to in-place strength evaluation. As one somewhat familiar with the general outlines of his active testing program at the University of Wisconsin in Milwaukee, this writer looks forward to his publication of similar work at more significant and earlier test ages, especially that based on his pullout strength (ASTM C 900) work.

A technique of evaluating in-place strength development has been developed by this writer in the course of comparing various methods of testing concrete for strength, with emphasis on the pullout. As is well known, concrete strength tends to increase in strength when tested at various points starting at the top and moving toward the bottom of a specimen or structure. The writer hypothesizes this trend is systematic, as confirmed by the technique; and that the same technique is helpful in evaluating strength gain versus time and maturity indications.

The technique arose out of pullout tests of 2-in. square, 5-in. high mortar specimens or "columns" in a program for ASTM CO1.27 subcommittee on strength of cement. The writer tested each column at five equally spaced elevations: at the top (designated level T), middle (M), bottom (B), and at upper levels (U) and lower (L) levels, midway between M and T and B elevations, respectively. Straight-line regression calculations of pullout strength at U on T, M on U, and so on, confirmed the obvious: increasing strengths at the

approach to the B could not reach infinity; i.e., the pullout strength, f_p, at successively lower levels, $L + 1$, was $f_p = aL + b$, where a was less than 1 and b, positive.

The same applies to strength on time: measured at successive and about equally spaced time intervals, concrete strength gain increments taper off, and, naturally, peak out.

To return to T. R. Naik's report, all but one of the lab cured cylinder lots' strengths conformed to the hypothesis. The sole exception was the weakest mix, No. 6, in which the $L + 1$ age formula was $f_c = 1.05L + 291$, with the 655-psi incremental strength increase in the 14-day–28-day period exceeding all others, the next highest gain period (usually the highest) being the earliest, 2 days–5 days.

By contrast, none of the core lots really met the requirements of the hypothesis within the usual range, where in $f_c = aL + b$, a varies from 0.8–0.9. The cores of mix No. 1 gave $f_{cc} = 0.47L + 2940$, paralleled by the same mix's $f_c = 0.64L + 2{,}270$, with relatively low slope and high gain rate.

This is the pattern which early-age maturity-strength investigations may clarify, if, as hoped, they are successful. At very early ages of strength development, in which C 873 pushout cylinders and C 900 pullouts may prove most helpful, the slope a in the formula for strength after successive time periods will exceed 1.0, reverting to the 0.6–0.9 range when the later ages of 1 day–91 days, with which we are traditionally familiar, are reached.

The author is congratulated on his most informative work. Further publication on strength development during the period of several hours to 1 week is eagerly anticipated.

Appendix.—Reference

9. Bloem, D. L., "Concrete Strength in Structures," *Journal of the American Concrete Institute*, National Ready Mixed Concrete Association Report, Vol. 65, No. 3, Mar., 1968, pp. 176–187.

Technical Papers

Original papers should be submitted in triplicate to the Manager of Technical and Professional Publications, ASCE, 345 East 47th Street, New York, N.Y. 10017. Authors must indicate the Technical Division or Council, Technical Committee, Subcommittee, and Task Committee (if any) to which the paper should be referred. Those who are planning to submit material will expedite the review and publication procedures by complying with the following basic requirements:

1. Titles must have a length not exceeding 50 characters and spaces.

2. The manuscript (an original ribbon copy and two duplicate copies) should be double-spaced on one side of 8-1/2-in. (220-mm) by 11-in. (280-mm) paper. Three copies of all figures and tables must be included.

3. Generally, the maximum length of a paper is 10,000 word-equivalents. As an *approximation*, each full manuscript page of text, tables or figures is the equivalent of 300 words. If a particular subject cannot be adequately presented within the 10,000-word limit, the paper should be accompanied by a rationale for the overlength. This will permit rapid review and approval by the Division or Council Publications and Executive Committees and the Society's Committee on Publications. Valuable contributions to the Society's publications are not intended to be discouraged by this procedure.

4. The author's full name, Society membership grade, and a footnote stating present employment must appear on the first page of the paper. Authors need not be Society members.

5. All mathematics must be typewritten and special symbols must be identified properly. The letter symbols used should be defined where they first appear, in figures, tables, or text, and arranged alphabetically in an appendix at the end of the paper titled Appendix.—Notation.

6. Standard definitions and symbols should be used. Reference should be made to the lists published by the American National Standards Institute and to the *Authors' Guide to the Publications of ASCE*.

7. Figures should be drawn in black ink, at a size that, with a 50% reduction, would have a published width in the *Journals* of from 3 in. (76 mm) to 4-1/2 in. (110 mm). The lettering must be legible at the reduced size. Photographs should be submitted as glossy prints. Explanations and descriptions must be placed in text rather than within the figure.

8. Tables should be typed (an original ribbon copy and two duplicates) on one side of 8-1/2-in. (220-mm) by 11-in. (280-mm) paper. An explanation of each table must appear in the text.

9. References cited in text should be arranged in alphabetical order in an appendix at the end of the paper, or preceding the Appendix.—Notation, as an Appendix.—References.

10. A list of key words and an information retrieval abstract of 175 words should be provided with each paper.

11. A summary of approximately 40 words must accompany the paper.

12. A set of conclusions must end the paper.

13. Dual units, i.e., U.S. Customary followed by SI (International System) units in parentheses, should be used throughout the paper.

14. A practical applications section should be included also, if appropriate.